Vapour Phase Mass Transfer Coefficients in Structured Packing

by

Francois Erasmus van der Westhuizen

Thesis submitted in partial fulfilment of the requirements for the degree

Master of Science in Engineering
(Chemical Engineering)

in the Department of Process Engineering
at Stellenbosch University

Supervised by
Prof. A.J. Burger
Prof. J.H. Knoetze

December 2008

Declaration

By submitting this thesis electronically, I declare that the entirety of the work contained therein is my own, original work, that I am the owner of the copyright thereof (unless to the extent explicitly otherwise stated) and that I have not previously in its entirety or in part submitted it for obtaining any qualification.

Date: 18 November 2008

Copyright © 2008 Stellenbosch University

All rights reserved

Synopsis

An abundance of correlations for the prediction of the vapour phase mass transfer coefficient (k_G) in structured packing were found in literature. Most of these correlations used one of two dependencies for the vapour phase mass transfer coefficient on the diffusion coefficient (D_G), namely $k_G \propto D_G^{0.67}$ or $k_G \propto D_G^{0.5}$. The main objective of this study was to test the validity of these assumed dependencies by sublimating naphthalene in various gases and to propose a new correlation for the prediction of the vapour phase mass transfer coefficient.

To create the proposed correlation diffusion coefficient data were required for the systems investigated. The first part of the study therefore dealt with the measurement of the diffusion coefficient for the systems investigated. The measurement technique used was the open Stefan tube method. In this method various gases were passed over a tube containing naphthalene and the subsequent naphthalene mass loss was related to a diffusion coefficient. After a sensitivity analysis the optimum parameters (tube diameter, diffusion path length and gas sweep velocity) were determined for each system. Results indicated that the diffusion rate increased with decreasing carrier gas density. This increase in the diffusion coefficient was also observed for decreasing tube diameters, which was most likely as a result of viscous shear effects. These shear effects negate certain central prerequisites in using the Stefan tube method and experiments were therefore conducted in the region where shear effects were considered negligible. A correlation was subsequently proposed for the prediction of the diffusion coefficient of naphthalene in the gases investigated:

$$D = 1.034 \times 10^{-3} . \frac{T^{0.0986} \cdot M_G^{2.24} \cdot \mu_G^{0.261}}{\rho_G^{2.86} \cdot p_{Naph}^{0.0731}} \qquad [\mathrm{cm^2/s}] \qquad (R^2 = 0.9997)$$

It is, however, recommended that the experiments be repeated for larger tube diameters, which will verify the accuracy of the proposed correlation.

In the second part of the study a small-scale test column was constructed to measure the vapour phase mass transfer coefficient of naphthalene in the various gases investigated. A naphthalene-coated packing sheet was inserted into the column, gas flow was initiated and the naphthalene mass loss was related to a mass transfer coefficient.

The results indicated that the vapour phase mass transfer coefficient dependency of $k_G \propto D_G^{0.5}$ tended to supply more accurate predictions than the $k_G \propto D_G^{0.67}$ dependency. A potential flaw in the correlations from literature was also identified, namely that most correlations did not take mass transfer in the laminar flow regime into consideration. An additional term, $\left(\rho_G / \rho_{G,Naph}\right)^c$, accounting for laminar conditions, was therefore added in the correlation created from the experimental results. The proposed correlation for the prediction of the vapour phase mass transfer coefficient was as follows:

$$Sh_G = \left(0.167\,\mathrm{Re}_{G,e}^{0.650} + \left(\rho_G / \rho_{G,Naph}\right)^{0.349}\right) Sc_G^{0.545} \qquad (3.27)$$

It is also recommended that the accuracy of the correlation be tested for gas densities outside the scope of this investigation.

Opsomming

Verskeie korrelasies vir die voorspelling van die gasfase massa-oordragkoëfisiënt (k_G) in gestruktureerde pakking is beskikbaar in die literatuur. Meeste van hierdie korrelasie gebruik een van twee afhanklihede van die gasfase massa-oordragkoëfisiënt op die diffusie koëfisiënt (D_G), naamlik $k_G \propto D_G^{0.67}$ of $k_G \propto D_G^{0.5}$. Die hoofdoel van die studie was om die betroubaarheid van hierdie afhanklikhede te toets deur naftaleen te sublimeer in verskeie gasse en ‘n korrelasie op te stel vir die voorspelling van die gasfase massa-oordragkoëfisiënt..

Om die voorgestelde korrelasie op te stel was diffusie-koëfisiënt data benodig vir die sisteme wat ondersoek was. Die eerste afdeling van hierdie studie het dus gefokus op die meting van die diffusie-koëfisiënt. Die meet-tegniek gebruik was die Stefan-buis metode. In die metode was verskeie gasse oor n buis, bevattende naftaleen, geblaas en die naftaleen massaverlies was omgeskakel tot ‘n diffusie-koëfisiënt. Die optimum buisdeursnee, diffusiepadlengte en gasvloeitempo was bepaal deur n sensitiwiteits analise op elke sisteem uit te voer. Resultate het aangedui dat die diffusietempo toeneem met afnemende gas digtheid. Hierdie toename in die diffusietempo was ook gevind vir afnemende buisdeursnee en was waarskynlik die gevolg van skuifwerking. Die teenwoordigheid van skuifwerking veroorsaak onakkuraathede in die metingsproses van die Stefan-buis metode. ‘n Korrelasie, vir die voorspelling van die gasfase massa-oordragkoëfisiënt van naftaleen in die gasse behandel, was opgestel en was soos volg:

$$D = 1.034 \times 10^{-3} . \frac{T^{0.0986} \cdot M_G^{2.24} \cdot \mu_G^{0.261}}{\rho_G^{2.86} \cdot p_{Naph}^{0.0731}} \qquad [\mathrm{cm^2/s}] \qquad (R^2 = 0.9997)$$

In die tweede afdeling van hierdie studie was ‘n kleinskaalse toetskolom gebou om die massa-oordragkoëfisiënt van naftaleen in die gasse wat behandel was te meet. Die naftaleenbedekte pakkingsvel was geplaas in die kolom, gasvloei is begin en die naftaleen massaverlies was omgeskakel tot ‘n massa-oordragkoëfisiënt.

Die resultate het aangedui dat die gasfase massa-oordragkoëfisiënt afhanklikheid van $k_G \propto D_G^{0.5}$ beter voorspellings verskaf as die afhanklikheid van $k_G \propto D_G^{0.67}$. ‘n Potensiële fout in die korrelasies vanaf literatuur was dat die meeste korrelasies nie massa-oordrag in die laminêre vloeigebied in ag neem nie. Die korrelasie opgestel vanaf die eksperimentele data bevat dus ‘n addisionele term, $\left(\rho_G / \rho_{G,Naph} \right)^c$, wat die laminêre kondisies in aanmerking neem. Hierdie korrelasie is soos volg:

$$Sh_G = \left(0.167\,\mathrm{Re}_{G,e}^{0.650} + \left(\rho_G / \rho_{G,Naph} \right)^{0.349} \right) Sc_G^{0.545} \qquad (3.27)$$

Dit word voorgestel dat die akkuraatheid van die korrelasie getoets word met ‘n gas wat nie in hierdie studie behandel was nie.

Acknowledgements

I would like to thank the following people and institutions for their contributions towards this study:

Sasol for providing financial support and Koch-Glitsch for providing the structured packing used in this study.

Prof. André Burger, Prof. Hansie Knoetze, Prof. Izak Nieuwoudt and Dr. André Erasmus for their support and guidance over the last two years, as well as the time Prof. Burger and Prof. Knoetze spent proof reading this thesis.

Cara Schwarz for all her guidance and the free time she expended in proof reading this thesis.

The workshop personnel, Anton Cordier and Jannie Barnard, for their timely help in constructing the apparatuses.

Juliana Steyl, who went out of her way in making sure the orders for the equipment were placed and following up on late deliveries.

My fiancée, Wilma Bester, for always being there for me and my family for their love and support.

My friends for supporting me through all the tough times, especially Gareth, Maggie and Liesl.

Lastly, I dedicate this thesis to my mother, Sarie van der Westhuizen, who always supported me. I wish you could have been here at the completion of my study.

Table of Contents

Page

CHAPTER 1. Introduction

1.1 Brief Background on Distillation…….1
1.2 Column Internals in Distillation……...2
1.3 Mass Transfer in Structured Packing…..…….3
1.4 Objective and Hypothesis……...…….…… 4
1.5 Scope and Project Outline……....5

CHAPTER 2. Vapour Diffusion Coefficient

2.1 Introduction……..……7
2.2 Literature Review…….…7
2.2.1 Experimental techniques in determining the vapour diffusion coefficient……..……...….7
2.2.2 Theoretical techniques in determining the vapour diffusion coefficient……..……...….16
2.3 Theory……..……....20
2.3.1 Diffusion through a stagnant gas (Fick's law) as applied to the Stefan tube…….. 20
2.3.2 Establishment of steady state (Fick's second law)……... 25
2.3.3 Determination of the vapour pressure of naphthalene…….. 26
2.4 Experimental…….....….27
2.4.1 Apparatus…….....…… 27
2.4.2 Experimental procedure…….....….32
2.4.3 Chemicals and gases used……... 33
2.5 Comparison between Correlations and Measurements of previous Investigators for the Naphthalene/Air system……..34
2.6 Results and Discussion…… 37
2.6.1 Verification of the accuracy of the experimental technique with the naphthalene/air system…….....…. 38

2.6.2 The diffusion of naphthalene in carbon dioxide (CO_2)……..…48
2.6.3 The diffusion of naphthalene in helium……..... 51
2.6.4 Investigating the effect of changes in the tube diameter……...55
2.6.5 Correlating the results……... 57
2.7 Concluding Remarks……..…..60

CHAPTER 3. Mass Transfer in Structured Packing

3.1 Introduction……..……64
3.2 Literature Review……..…65
3.3 Theory…….. 76
3.3.1 Diffusion through a stagnant gas…….. 76
3.3.2 Naphthalene sublimation in structured packing……....78
3.4 Experimental…….....…79
3.4.1 Apparatus…….....…… 79
3.4.2 Naphthalene coating procedure…….82
3.4.3 Experimental procedure…….....…84
3.5 Results and Discussion…… 85
3.5.1 Experimental calculations…….85
3.5.2 Verification of the accuracy of the experimental setup: *Sublimation of naphthalene in air at atmospheric pressure*….87
3.5.3 Sublimation of naphthalene in air for a system pressure above atmospheric conditions……..… 91
3.5.4 Sublimation of naphthalene in CO_2 at atmospheric pressure…93
3.5.5 Sublimation of naphthalene in helium at atmospheric Pressure…….95
3.5.6 Correlating the experimental results……..... 96
3.6 Concluding Remarks…….. 98

CHAPTER 4. Conclusions and Recommendations…….. 102

References……..…107

APPENDIX 1. Stefan Tube Experimental Setup

A1.1 Gas Flow Chamber Design……... 115
A1.2 Piping and Instrumentation Specification……..… 120
A1.3 Experimental Setup within Fume Cabinet…… 122

APPENDIX 2. Experimental Results for the Diffusion Coefficient Measurements

A2.1 Experimental Results for the Naphthalene/Air System……..…….. 124
A2.2 Experimental Results for the Naphthalene/CO_2 System……..…….127
A2.3 Experimental Results for the Naphthalene/Helium System……..128
A2.4 Sample Calculations……..…130
A2.5 Account of Error Analysis……..... 132

APPENDIX 3. Test Column Experimental Setup

A3.1 Test Column Design……..135
A3.2 Piping and Instrumentation Diagram…… 136
A3.3 Calibration Certificate for the PT100 Temperature Probes…….. 138
A3.4 Calibration Certificate for the Mass Flow Controller……... 140

APPENDIX 4. Experimental Results for the Mass Transfer Coefficient Determination on Structured Packing

A4.1 Experimental Results for the Naphthalene/Air System (Atmospheric pressure)……..…141
A4.2 Experimental Results for the Naphthalene/Air System (System pressure above atmospheric pressure)……..... 142
A4.3 Experimental Results for the Naphthalene/CO_2 System (Atmospheric pressure)……..…143
A4.4 Experimental Results for the Naphthalene/Helium System (Atmospheric pressure)……143
A4.5 Sample Calculations……..…144

Nomenclature…….147
List of Relevant Correlations from Literature…..…….. 150

List of Figures

Page

CHAPTER 2. Vapour Diffusion Coefficient

Figure 2.1: *Simplified schematic representation of the two bulb apparatus*……9

Figure 2.2: *Simplified schematic representation of the gas chromatography method*……..……... 10

Figure 2.3: *Simplified schematic representation of the classic Stefan tube*…..… 12

Figure 2.4: *Simplified schematic representation of the closed Stefan tube*…..…14

Figure 2.5: *Schematic representation of the diffusion of substance A through a non-diffusing gas B* ……..…….. 21

Figure 2.6: *Flow diagram of experimental apparatus*……..…28

Figure 2.7: *Simplified illustration of the diffusion unit (a) Side view, (b) Top view*……... 29

Figure 2.8: *Schematic representation of (a) the inner diffusion tube and (b) outer casing*……..30

Figure 2.9: *Proper fitting of the inner tube within the outer casing*……..…….. 31

Figure 2.10: *Experimental diffusion coefficient data from previous investigators on the naphthalene/air system*……..35

Figure 2.11: *Maximum error (%) in diffusion coefficient determination versus error in the temperature measurement (at the lowest system temperature of 26 ^{o}C)*……... 39

Figure 2.12: *Diffusion coefficient at various gas linear sweep velocities (Tube specifications: (a) Diffusion path length = 62 mm, (b) Tube diameter = 15.2 mm)*…….. 40

Figure 2.13: *The effect of an increase in the diffusion path length (L) on the experimentally determined diffusion coefficient (d_{tube} constant at 15.2 mm)*…… 41

Figure 2.14: *The effect of decreasing the diffusion tube diameter on the experimentally determined diffusion coefficient (L constant at 62 mm)*…… 43

Figure 2.15: *The effect of increasing the ratio of the inner wall area along the diffusion path length to the naphthalene surface area on the experimentally determined diffusion coefficient*…… 43
Figure 2.16: *Diffusion mass flux at various tube diameters (Experimental conditions: (a) Diffusion path length = 62 mm, (b) Temperature = 47 ^{o}C)*…….. 44
Figure 2.17: *Time to reach steady state for the naphthalene/air system*……45
Figure 2.18: *Diffusion coefficient results for the naphthalene/air system compared with previous investigators and empirical correlations*……...…….46
Figure 2.19: *Experimental diffusion coefficient results for the naphthalene/CO_2 system*……..….. 48
Figure 2.20: *Time to reach steady state for the naphthalene/CO_2 system*……. 50
Figure 2.21: *Results obtained for the naphthalene/CO_2 system at 200 kPa absolute pressure*…….... 51
Figure 2.22: *Experimental diffusion coefficient results for the naphthalene/helium system*……..…….. 52
Figure 2.23: *Time to reach steady state for the naphthalene/helium system*.....53
Figure 2.24: *Results obtained for the naphthalene/helium system at 200 kPa absolute pressure*….……... 54
Figure 2.25: *Deviation of the diffusion coefficient versus tube diameter for the three systems investigated*……..… 56
Figure 2.26: *Comparison between the experimentally obtained diffusion coefficient data for each system investigated*…….……58
Figure 2.27: *Parity plot between the correlated and experimental results for the diffusion coefficient of naphthalene in air, helium and CO_2*……..59
Figure 2.28: *Deviation (%) between the correlated and experimental results*…...60

CHAPTER 3. Mass Transfer in Structured Packing

Figure 3.1: *Simplified schematic representation of the penetration theory*……. 67

Figure 3.2: *Geometry of a structured packing sheet with (a) the arrangement and (b) the geometry of the triangular cross section of the flow channel*……..…….69
Figure 3.3: *Flow diagram of small-scale test* column…….…….80
Figure 3.4: *Simplified schematic representation of the test column (a) Side view and (b) Front* view……... 82
Figure 3.5: *Top view of the placement of the packing sheets within the test* column……... 84
Figure 3.6: *Experimental results for the naphthalene sublimation in air (atmospheric pressure) compared to the experimental results from the study performed by Erasmus* [3] $Sc_G \approx 1.95$……..... 87
Figure 3.7: *Experimental results for the naphthalene sublimation in air (atmospheric pressure) compared to* k_G *correlations from literature.* $Sc_G \approx 1.95$…….….. 89
Figure 3.8: *Parity plot of the values predicted by equation 3.24 versus the experimental* results……..90
Figure 3.9: *Experimental results for the naphthalene sublimation in air (system pressure above atmospheric conditions) compared to* k_G *correlations.* $Sc_G \approx 2.01$…….. 92
Figure 3.10: *Experimental results for the naphthalene sublimation in* CO_2 *(atmospheric pressure) compared to* k_G *correlations.* $Sc_G \approx 1.39$……. 93
Figure 3.11: *Comparison between the experimental results for the smaller and larger cross sectional area tests.* $Sc_G \approx 1.39$……..……...…. 94
Figure 3.12: *Experimental results for the naphthalene sublimation in helium (atmospheric pressure) compared to* k_G *correlations.* $Sc_G \approx 4.30$……. 95
Figure 3.13: *Parity plot of the values predicted by equation 3.27 versus the experimental* results……..98

APPENDIX 1. Stefan Tube Experimental Setup

Figure A1.1: *Chamber Top and Bottom Plates (a) Top view, (b) Side view*……...115

Figure A1.2: *Chamber Side Plates (a) Top view, (b) Side view*……. 116
Figure A1.3: *Chamber Straightening Vanes (a) Side view, (b) Top view*……... 117
Figure A1.4: *Dimensions of the Stainless Steel Buss for the Topside Circular Opening in the Gas Flow Chamber* ……... 118
Figure A1.5: *Stainless Steel Screw Lid to fit into the Buss Illustrated in Figure A1.*4…… 118
Figure A1.6: *Dimensions of the Stainless Steel Buss for the Bottom-side Circular Opening in the Gas Flow Chamber*…… 119
Figure A1.7: *Illustration of the experimental setup within the fume cabinet (dimensions included)*……...… 122

APPENDIX 3. Test Column Experimental Setup

Figure A3.1: *Schematic representation of the test column (a) Side view and (b) Front view* ……... 135

List of Tables

Page

CHAPTER 2. Vapour Diffusion Coefficient

Table 2.1: *Comparison between the various methods for the determination of the diffusion coefficient*……. 15

Table 2.2: *Chemicals and gases used in experiments*…….....34

Table 2.3: *Previous investigators on the determination of the diffusion coefficient of the naphthalene/air system (experimental technique included)*…… 34

CHAPTER 3. Mass Transfer in Structured Packing

Table 3.1: *Dimensions of structured packing for current investigation*……. 86

APPENDIX 1. Stefan Tube Experimental Setup

Table A1.1: *Instrumentation for Stefan tube experiment*…….……. 120

Table A1.2: *Piping specification for Stefan tube experiment*…… 121

APPENDIX 2. Experimental Results for the Diffusion Coefficient Measurements

Table A2.1: *Experimental results for the naphthalene/air system at various gas flow rates (tests for turbulence)*…….. 124

Table A2.2: *Experimental results for the naphthalene/air system at various tube diameters (tests for wall adsorption)*……. 125

Table A2.3: *Experimental results for the naphthalene/air system at various diffusion path lengths (tests for wall adsorption)*…….. 125

Table A2.4: *Experimental results for the naphthalene/air system at the optimal* parameters…….126

Table A2.5: *Experimental results for the naphthalene/CO_2 system (includes variations of gas flow rate, tube diameter and diffusion path length)*……..... 127
Table A2.6: *Experimental results for the naphthalene/helium system (includes variations of gas flow rate, tube diameter and diffusion path length)*……. 128

APPENDIX 3. Test Column Experimental Setup

Table A3.1: *Instrumentation for the test column*……... 136
Table A3.2: *Piping specification for the test column*…… 137

APPENDIX 4. Experimental Results for the Mass Transfer Coefficient Determination

Table A4.1: *Experimental results for the naphthalene/air system at atmospheric pressure*……. 141
Table A4.2: *Experimental results for the naphthalene/air system for a system pressure of above atmospheric pressure*…… 142
Table A4.3: *Experimental results for the naphthalene/CO_2 system at* atmospheric pressure……. 143
Table A4.4: *Experimental results for the naphthalene/helium system at atmospheric pressure*…… 143

CHAPTER **1**

Introduction

1.1 Brief Background on Distillation

The separation of liquid mixtures into their components, by means of distillation, has been accomplished for centuries [1]. By the year 1100, distillation was already being used in the production of alcoholic beverages [1]. The first vertical column continuous distillation still, as it is known today, was developed in France in 1813 by Jean Baptiste Cellier-Blumenthal [2]. Packing, as a column internal, was used as far back as 1820 when a technologist, named Clement, used glass balls in an alcohol still, while the first sieve tray column was developed by Aenneas Coffey in 1830 [2].

In the first quarter of the twentieth century the application of distillation spread quickly from being used almost exclusively in the alcoholic beverage industry, into becoming the main separation technique of liquid mixtures in the chemical industry. This swift expansion accelerated even more when distillation was discovered to be an effective means by which crude oil could be separated into its various products [2].

Throughout the remainder of the twentieth century to the present day, the preferred and most widely used method for the separation of liquid mixtures into their chemical components was, and still is, multistage distillation. Unfortunately, the distillation process is very energy intensive [1].

The continuous improvement, referring to the efficiency and energy consumption of known distillation applications are therefore of utmost importance.

1.2 Column Internals in Distillation

Column internals can be separated into two main types: *trays* and *packing*. The main task of both the trays and the packing is to facilitate good contact between the vapour- and liquid phases. With trays, the vapour is bubbled through the liquid phase, thereby providing the necessary contact between the liquid and vapour phases. In the case of packed columns a much larger surface area is provided for the liquid to wet, while liquid films and drops supply the area between the liquid and vapour phases. A comparison between the two column internals therefore show that for packed columns the liquid is the dispersed phase and the vapour the continuous phase, while the opposite is true for columns using trays [2].

Since the late 1970's, with the introduction of the sheet metal structured packing by Sulzer, distillation at low pressure has been revolutionised. This more affordable structured packing offered significant capacity and efficiency advantages over the conventional column internals, namely trays and random packings, thereby making it more competitive.

The following list of factors indicates where the use of structured packing is favoured above that of trays [2]:

- Low liquid hold-up essential
- Foaming systems
- Vacuum systems
- Systems where low pressure-drop is required
- Small diameter columns

The use of structured packing therefore becomes an attractive alternative for distillation systems where high efficiency, high capacity and low pressure-drop are required.

1.3 Mass Transfer in Structured Packing

The use of structured packing as a column internal exhibits improved mass transfer characteristics in comparison to trays and random packing [1, 3]. Due to structured packing's energy intensive nature and overall importance in the industry, the creation of reliable models to describe its mass transfer characteristics becomes paramount. In order to determine the efficiency of column packing, accurate mass transfer models and correlations are required [3, 4].

Since it is generally acknowledged that resistance in the vapour phase determines the overall mass transfer rate in distillation processes, the vapour phase mass transfer rate becomes the issue under investigation [3, 5]. The main difficulty in setting up correlations for the determination of the mass transfer coefficient is that in most experimental procedures the volumetric gas phase mass transfer coefficient ($k_G a_e$) is measured.

A relatively novel concept is to separate the volumetric vapour phase mass transfer coefficient into a vapour phase mass transfer coefficient (k_G) and an effective surface area (a_e) [3]. The vapour phase mass transfer coefficient can then be correlated in terms of the gas phase flow rate and transport properties. Most correlations for the vapour phase mass transfer coefficient stem from the wetted-wall theory and are set up with a power law series, which has the following basic form:

$$Sh_G = a\,\mathrm{Re}_G^b\,Sc_G^c \tag{1.1}$$

where: $$Sh_G = \frac{k_G d_h}{D_G} \tag{1.2}$$

$$Sc_G = \frac{\mu_G}{D_G \rho_G} \tag{1.3}$$

$$\mathrm{Re}_G = \frac{\rho_G u_G d_h}{\mu_G} \tag{1.4}$$

In equation 1.1 the Reynolds number (Re_G) takes the flow properties into account and the Schmidt number (Sc_G) takes the transport properties into account.

1.4 Objective and Hypothesis

Erasmus [3] experimentally determined the vapour phase mass transfer coefficient for a naphthalene/air system in a column containing structured packing. The experimental data were then correlated and tested against wetted wall experimental data.

However, only air was used as the carrier gas in the experiments performed by Erasmus [3], resulting in a constant Schmidt number for all the experimental runs. Certain assumptions were therefore made regarding the reliance of the mass transfer coefficient on the Schmidt number (Sc_G). Since the Schmidt number is a function of the diffusion coefficient (D_G), this assumed dependency also extended towards the diffusion coefficient. Erasmus [3] raised the Schmidt number in the correlation (equation 1.1) to the power of 0.33 and 0.5 (denoted by c in equation 1.1), seeing as most existing mass transfer correlations exhibit Schmidt number dependencies that are in that area [6-10]. This made it possible to extrapolate the correlation to systems other than naphthalene/air. The proposed dependency of the vapour phase mass transfer coefficient is as follows:

$$Sh_G \propto Sc_G^{0.33} \; or \; k_G \propto D_G^{0.67} \tag{1.5}$$

$$Sh_G \propto Sc_G^{0.5} \; or \; k_G \propto D_G^{0.5} \tag{1.6}$$

For correlations proposed from wetted-wall experimental data the accuracies of the correlations are slightly improved by using the dependency described by equation 1.6 [6, 10]. Various correlations, specifically aimed at predicting gas phase mass transfer in structured packing, however, makes use of the dependency described by equation 1.5 [7-9]. In distillation operations the gas phase Schmidt number is not considerably larger or smaller than unity (ranges from 0.5 to 5) [3]. The theory is therefore that

choosing either of the dependencies depicted in equations 1.5 and 1.6 will not significantly influence the calculation of the vapour phase mass transfer coefficient [3].

The aim of this study is to test this assumed dependency of the mass transfer coefficient on the Schmidt number and diffusion coefficient. The hypothesis is that the correlation set up by Erasmus [3] will not necessarily predict the mass transfer coefficient satisfactorily for systems other than naphthalene/air. If not, a new and improved correlation, incorporating the information gathered in this study, will be proposed. A secondary aim is to test the theory that using either of the dependencies (from equations 1.5 and 1.6) will give similar predictions or if one of the dependencies will provide more accurate predictions.

1.5 Scope and Project Outline

The aim of this investigation is achieved by varying the Schmidt number in sublimation experiments. In order to do this, the sublimation of *naphthalene* is performed in different carrier gasses with significantly differing densities. Three carrier gases are used, namely air, carbon dioxide and helium.

The scope of this investigation is therefore sub-divided into the following phases:

1. Design and construction of an experimental set-up to measure the vapour diffusion coefficient of naphthalene in the various carrier gases. This phase is necessary, since diffusion coefficient data is needed in order to correlate the mass transfer coefficient.
2. Assess the accuracy of the diffusion coefficient apparatus by comparing the experimental results with results from previous studies. This is followed by the physical measurement of the diffusion coefficient in the various carrier gases.
3. Propose correlation for the prediction of the vapour diffusion coefficient.
4. Design and construction of the apparatus to determine the vapour phase mass transfer coefficient in the Flexipac 350Y structured packing (manufactured by Koch-Glitsch).

5. Physical measurement of the vapour phase mass transfer coefficient.
6. Compare the experimental results with the predictions from the correlation proposed by Erasmus [3], as well as the other correlations found in literature.
7. Propose improved correlation for the prediction of the vapour phase mass transfer coefficient, utilising the sum of the experimental results.

The present study therefore consists of two main experimental sections. The first section (measurement and correlation of the vapour diffusion coefficient) is represented by phases 1 to 3 in the project outline. This section will be addressed in Chapter 2. Phases 1 to 3 are of utmost importance, since the diffusion coefficient data gathered from this section is necessary in creating the proposed correlation for the prediction of the vapour phase mass transfer coefficient. The second section (measurement and correlation of the vapour phase mass transfer coefficient) is represented by phases 4 to 7 in the project outline. This section will be addressed in Chapter 3.

CHAPTER **2**

Vapour Diffusion Coefficient

2.1 Introduction

Molecular diffusion is an extremely important concept since it is the rate determining step in most mass transfer operations [11]. In all the published correlations for the determination of the mass transfer rate, the diffusion coefficient is a parameter that is required in order to employ the correlations. Consequently, the accurate measurement of the diffusion coefficient becomes extremely important.

For the naphthalene/air system, as used by Erasmus [3], diffusion coefficient data was readily available. Consequently it was possible to immediately determine the Schmidt number for the gas flow in the packed column experiments he performed. Diffusion coefficient data for naphthalene in systems other than air are, however, less readily available. In the present study the vapour phase mass transfer coefficient of naphthalene in air, CO_2 and helium were measured. In order to correlate the experimental results diffusion coefficient data on the naphthalene/CO_2 and naphthalene/helium system were therefore required. The incorporation of an experimental procedure, where the vapour diffusion coefficient was physically measured, therefore became necessary.

2.2 Literature Review

2.2.1 Experimental techniques in determining the vapour diffusion coefficient

Numerous experimental methods are available for the measurement of the diffusion coefficient [12, 13]. Only a limited number of these methods are, however, applicable to

systems where the diffusing component is in the solid state [14]. The following section only focuses on those methods applicable to the measurement of the vapour phase diffusion coefficient for naphthalene that are reasonably accurate, that are easy to use, or that have some special advantage. The main methods are [13]:

- The two-bulb apparatus (Stokes diaphragm cell)
- The gas chromatography method
- The Stefan tube evaporation method

Two-bulb apparatus

The two-bulb apparatus (Stokes diaphragm cell) can be used in researching the diffusion of gases or liquids across membranes and usually consists of two compartments. These compartments are separated by a connecting tube containing a glass frit or porous membrane. The two compartments are stirred, usually by means of a magnet rotating around the cell. Initially the two compartments are filled with solutions of different concentrations. After completion of the experiment the two compartments are emptied and the concentrations of both solutions are measured. The diffusion coefficient can then be determined using an equation specifically developed for use in this method [13].

This method involves the following assumptions:

- The flux of a component remains constant along the connecting tube.
- The composition gradient of the species is entirely contained within the connecting tube.
- The volume of the connecting tube is smaller than the volume of either bulb.

The advantages of this method are its ease of construction, as well as the fact that the lack of moving parts makes this a convenient measuring technique at elevated temperatures. The calculation of the diffusion coefficient by means of this method, however, requires accurate knowledge of the concentration difference between the two species. Accurate analyses are therefore required. When dealing with two

species with large saturated vapour pressures this method can be very reliable, since their concentrations are easily measured. When dealing with species with very low saturated vapour pressures, such as naphthalene, this measuring technique can, however, prove problematic. This is due to the difficulties in accurately measuring the concentrations. Furthermore, the inaccuracies of this method are reported to be between 1 and 3.5 % [13]. A schematic representation of this apparatus is shown in Figure 2.1.

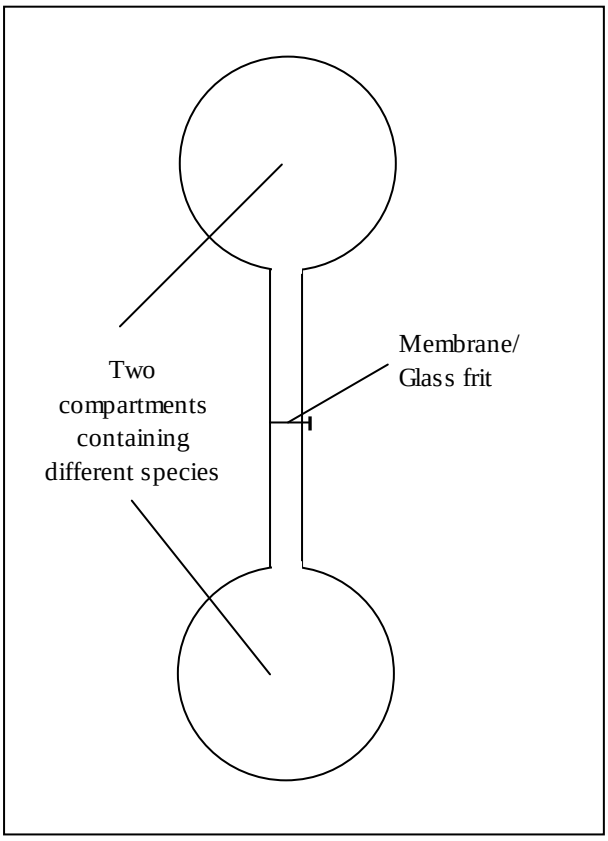

Figure 2.1: *Simplified schematic representation of the two bulb apparatus*

Gas chromatography

This flow method consists of a long hollow tube with a carrier gas flowing through it. A trace amount of gas is then injected, as a pulse, into the carrier gas. The dispersion of the pulse is caused by the combined action of two factors, namely molecular diffusion and the parabolic velocity profile of the carrier gas. Measurements of the dispersion as the pulse exits the tube (characterised by a Gaussian distribution function) lead to values for the diffusion coefficient [13].

As mentioned previously, the dispersion of the gas is not due to molecular diffusion alone, but is also as a result of the velocity profile of the carrier gas. The arrested flow elution method improves the original gas chromatography method by removing the velocity factor of the carrier gas. This is done by stopping the flow through the tube for a certain period of time, allowing the pulse to disperse through molecular diffusion alone [15-18]. A schematic representation of the gas chromatography method is shown in Figure 2.2.

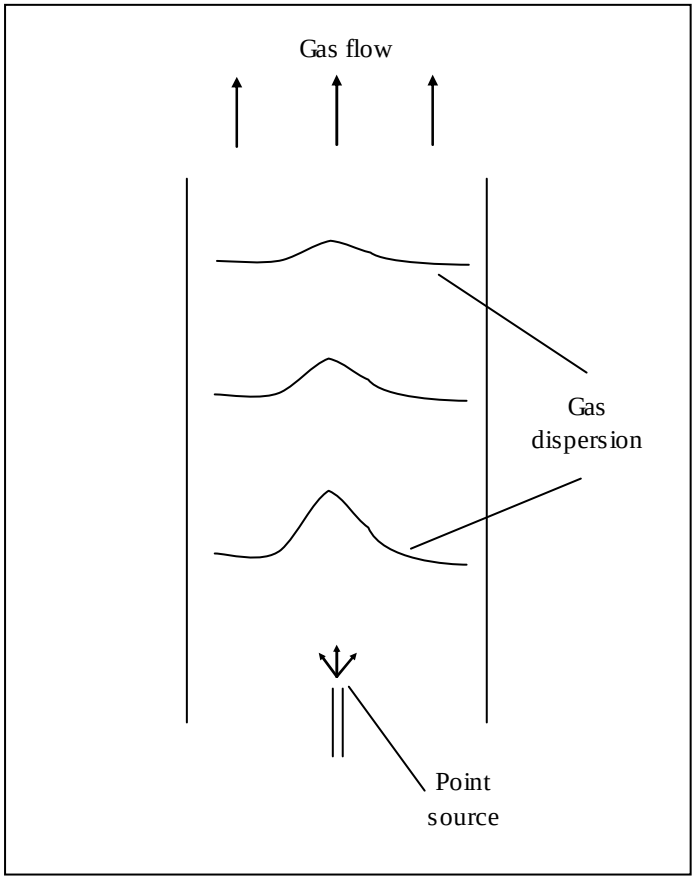

Figure 2.2: *Simplified schematic representation of the gas chromatography method*

The advantages of this method are as follows [13]:

- Determination of the diffusion coefficient can be completed in a minimum amount of time (a matter of minutes).
- The injection of more than one sample pulse into the gas is possible. Multiple dispersion readings can therefore be taken per experiment.
- A small amount of sample is needed to create the pulse.

A possible source of error for this method is the entrance effect caused by the injection of the pulse sample. End effects, caused by the detector element, may also cause disturbances in the concentration profile [13]. Overall, this method is reasonably accurate, with inaccuracies in the determination of the diffusion coefficient through gas chromatography being reported in the region of 1 to 3.6% [13, 15].

Stefan tube

The use of the Stefan tube for the measurement of the vapour diffusion coefficient was originated by Stefan [19] in the latter part of the 19th century. Since then the method has also been used extensively by other investigators [11, 19-33].

Since the conception of the Stefan tube method several modifications have been added to the design of the former apparatus, depending on the particular use of the device. These modifications have predominantly been in the design of the diffusion cell and the flow control as well as the improvement of the thermostatic conditions[25]. These improvements ensure that the evaporation of the liquid (or sublimation of the solid) in the vertical tube occurs via molecular diffusion alone.

The application of the Stefan tube entails the use of a vertical tube, with one of the components (in the solid or liquid state) placed in the bottom of the tube [12, 19-21]. The second component, in the gaseous state, is then passed over the top of the tube [12]. The gas therefore fills the tube and provides the medium through which the solute diffuses from the bottom of the tube into the pure gas that is flowing over the top of the tube. The change in the solute concentration, or mass, is the parameter that needs

to be measured in order to calculate the diffusion coefficient [12, 19, 22]. However, it should be noted that, if the mass loss is physically measured, experiments will be of long duration, especially when working with a solute with low vapour pressure [22]. The long experimental run therefore results in a conveniently weighable mass loss [11, 19, 22]. A schematic representation of the classic Stefan tube is depicted in Figure 2.3.

Correct application of the apparatus requires the entire system to be maintained at isobaric and isothermal conditions, thus necessitating the experiment to be set up in a temperature-controlled environment. The simplest method to achieve this is to submerge the Stefan tube in a water or oil bath.

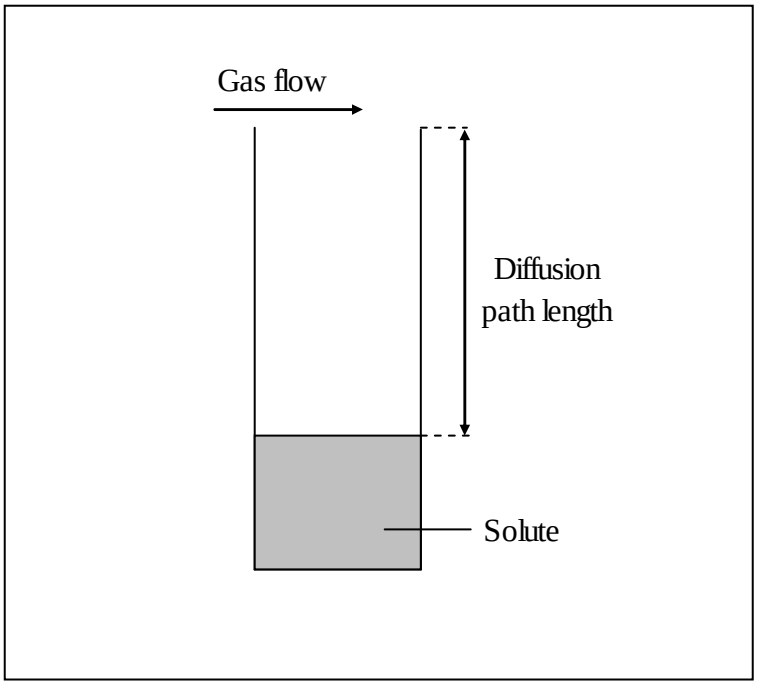

Figure 2.3: *Simplified schematic representation of the classic Stefan tube*

The Stefan tube appears to be the method of choice for the determination of vapour diffusion coefficients, especially when dealing with solid to gas systems. Most of the experimental procedures found in literature use some variation of this method [11, 14, 19-33]. The main reason for the popularity of this method, when working with solid to gas systems, is the fact that solid substances generally have substantially lower saturated vapour pressures than liquids and gases. The assumption of a constant diffusion path length is therefore more valid than when working with liquid to gas systems. One of its main advantages is its adaptability and ease of construction. The

main disadvantage, when dealing with solid to gas systems, is the long experimental durations required when using this technique. This is to obtain the conveniently weighable mass losses necessary in determining the diffusion coefficient. The accuracy of this measuring technique depends on the particular adaptation employed, with stated inaccuracies ranging from 1 to 4.1% [22]. A few of this method's variations for determining the diffusion coefficient are briefly summarised as follows:

- Nirdosh *et al.* [11] made use of glass as construction material for the Stefan tube. This was done for the evaporation of a liquid, where it is important to measure the drop in the liquid level and the transparent nature of the glass tube made it easy to measure the level drop. The experiments by Nirdosh *et al.* [11] were also performed at near ambient conditions, making the low heat conductance of the glass a minor issue.

- Tashiro *et al.* [23] made use of a technique where they continuously measured the solute concentration in the gas stream passing over the tube. This measurement is, however, very difficult when sublimating solids. This is due to the low vapour pressure of solids, resulting in a very low diffusion flux. The concentration of the solute in the gas stream therefore has to be of sufficient magnitude for continuous measurements. Caldwell [14] also measured the concentration of a solute (naphthalene) in the gas stream, but the difficulty with the low concentration was solved by using a much larger naphthalene pellet with numerous diffusion tubes extending upwards toward the gas stream. A larger concentration of the solute in the gas was therefore achieved, making continuous concentration measurements possible.

- Lee *et al.* [19] physically weighed the tube after each experimental run in order to obtain the total mass of solute that was evaporated or sublimated. This method, as stated previously, is time consuming in systems with low diffusion fluxes (e.g.: the sublimation of naphthalene). Longer experimental runs are necessary to obtain the weighable mass loss.

- Cho *et al.* [27] and Mack [31] also physically measured the mass loss of solid naphthalene, but adapted the conventional open tube Stefan method to a closed tube method. Diffusion, however, occurs along a concentration gradient and with a closed system this gradient decreases with time. In order to get accurate diffusion coefficient measurements this concentration gradient needs to be maintained at a known constant level. Cho *et al.* [27] and Mack [31] solved this problem by placing activated charcoal at the opposite end of the diffusion tube. It was assumed that the evaporating/sublimating substance would diffuse through the carrier gas along the tube and be absorbed by the activated charcoal, thus maintaining a zero concentration of naphthalene at the opposite end of the tube. A simplified representation of the apparatus used by Cho *et al.* [27] is shown in Figure 2.4.

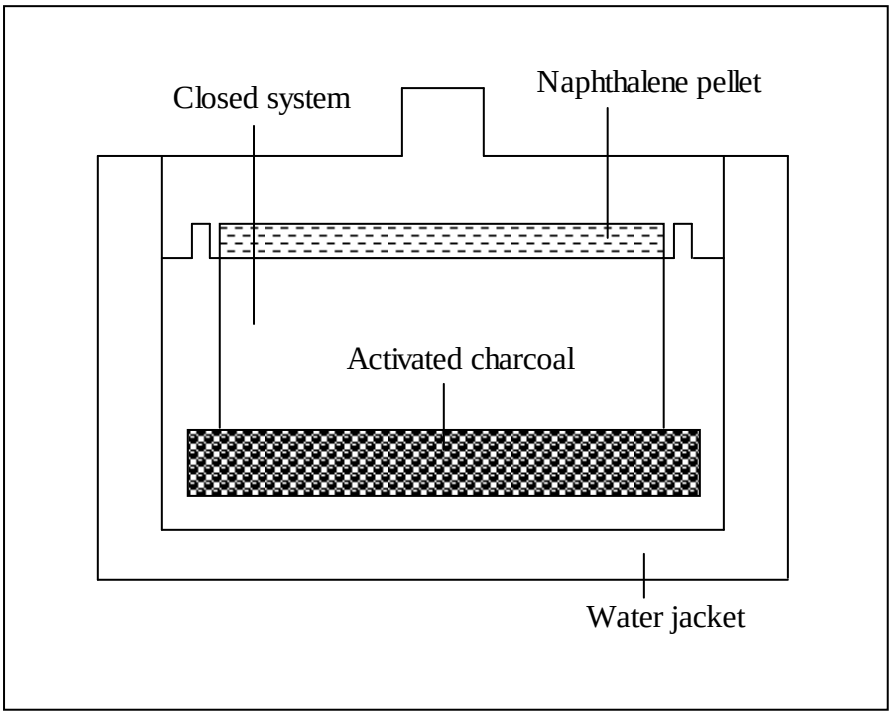

Figure 2.4: *Simplified schematic representation of the closed Stefan tube*

- Pieterse *et al.* [32], Tesconi *et al.* [30], Da Siva *et al.* [29], Siddiqi *et al.* [28] and Pichon *et al.* [33] made use of thermo-gravimetric analysis. In this novel method the mass loss is continuously monitored during the experiment. This method has the added benefit of being able to conduct experiments at elevated

temperatures (above 400 K) and also at different system pressures (both below and above atmospheric pressure). This method, however, requires very accurate and continuous calibration of the balance, since the effects of temperature on the balance reading needs to be included in the calculation of the mass loss.

A comparison between the various experimental methods is represented in Table 2.1. From Table 2.1 it is clear that the reported inaccuracies for all three experimental techniques are similar, with the Two-bulb method giving marginally more accurate results. The Two-bulb method, however, can prove problematic when measuring the diffusion coefficient of naphthalene (as discussed in section 2.2.1). Both the gas chromatography method and the Stefan tube method give accurate results, with the gas chromatography method reported to be slightly more accurate. It should, however, be noted that the stated accuracy of the Stefan tube method improves for solid/gas systems [14]. This improvement is due to the constant diffusion path length observed for solid/gas systems. The Stefan tube method, therefore, appears to be more suited to solid to gas systems. Numerous investigators have employed this method successfully and the limitations and shortcomings of the Stefan tube method are therefore well documented. The Stefan tube method was therefore chosen as the diffusion coefficient measuring technique in this study.

Table 2.1: *Comparison between the various methods for the determination of the diffusion coefficient*

Method	**Advantages**	**Disadvantages**	**Inaccuracy**
Two-bulb	Easy to build; Convenient measuring technique for elevated temperatures	Difficulties in measuring the concentrations of low saturated vapour species (e.g. naphthalene)	1 to 3.5 %
Gas chromatography	Short experimental durations; Small quantities of sample required	Entrance effects from injection of pulse	1 to 3.6 %
Stefan tube	Adaptable; Easily constructed	Long experimental duration to obtain weighable mass loss	1 to 4.1%

2.2.2 Theoretical techniques in determining the vapour diffusion coefficient

Knowledge of vapour-phase diffusion coefficients is crucial in the understanding of countless physical and chemical processes [34]. Several correlations for the prediction of molecular diffusion coefficients have been cited in the literature [19, 22, 34, 35-36], of which the empirical correlation by Fuller *et al.* [36] is recommended for supplying the most accurate predictions of molecular diffusivities in air [7]. In the following section the correlations from literature are discussed in more detail.

Most of the empirical correlations for the estimation of diffusion coefficients can be traced back to the Chapman-Enskog empirical correlation and the kinetic theory of gases [36, 37]. The theory assumes that the gas consists of rigid spherical particles that are entirely elastic upon collision with other molecules. This implies that momentum is conserved. The theory also takes into account the intermolecular forces of repulsion and attraction between molecules, as well as the difference in sizes between the molecules. The Chapman-Enskog empirical correlation for the prediction of the diffusion coefficient (D_{AB}) has the following form [37]:

$$D_{AB} = \frac{1.8583\times10^{-7}T^{3/2}}{P\sigma^2\Omega}\left(\frac{1}{M_A}+\frac{1}{M_B}\right)^{\frac{1}{2}} \qquad [\mathrm{m^2/s}] \qquad (2.1)$$

where: P is absolute pressure [atm]

σ is the collision diameter [Å]

Ω is the collision integral based on the Lenard-Jones potential [-]

T is temperature [K]

M_A, M_B is molecular mass [g/mol]

The collision diameter (σ) refers to the distance between molecule centres (of unlike pairs) upon collision. The collision integral (Ω) is a ratio describing the deviation of a gas with interactions compared to a gas with rigid, elastic spheres. According to Fuller *et al.* [36] the Chapman-Enskog empirical correlation suffers from two major limitations. The first limitation is the 3/2 power dependency of the temperature term.

According to experimental data this dependency is in the range of 1.6 to 1.8 [36]. The second limitation is the limited availability of collision diameter (σ) and collision integral (Ω) data from literature. Fuller *et al.* [36] therefore modified the theoretically derived Chapman-Enskog equation and proposed the following correlation:

$$D_{AB} = \frac{1.00\times10^{-3}.T^{1.75}\left(1/M_A + 1/M_B\right)^{1/2}}{P\left[\left(\sum_A v_i\right)^{1/3} + \left(\sum_B v_i\right)^{1/3}\right]^2} \qquad [\mathrm{cm^2/s}] \qquad (2.2)$$

where: T is temperature [K]

M_A, M_B is molecular mass [g/mol]

P is absolute pressure [atm]

v_i is special atomic diffusion volumes [m^3/mol]

The correlation by Fuller *et al.* [36] has an average absolute inaccuracy of 4.3 % and can be applied to a wide range of substances through the application of the special atomic diffusion volumes (v_i). Fuller *et al.* [36] estimated the special diffusion volumes in a least squares analysis for all the major elements in the periodic table, as well as for most of the simple gases (such as oxygen, nitrogen, etc.). The special diffusion volumes in equation 2.2 can therefore be estimated for a wide range of substances. The main disadvantage of the correlation by Fuller *et al.* [36] is, however, an oversimplification of the predicted temperature dependence [34].

The correlation proposed by Fuller *et al.* [36] can be simplified as follows for the naphthalene/air system [22]:

$$D_{AB} = 3.0933\times10^{-6}.T^{1.75} \qquad [\mathrm{m^2/s}] \qquad (2.3)$$

where: T is temperature [K]

Arnold [35] set up a correlation using the Stefan-Maxwell-Sutherland expression, from the kinetic theory of gases. The proposed equation is as follows:

$$D_{AB} = \frac{0.00837\sqrt{\frac{1}{M_A}+\frac{1}{M_B}}}{\left(V_A^{1/3}+V_B^{1/3}\right)^2}.\left(\frac{T^{5/2}}{T+C}\right) \qquad [\text{cm}^2/\text{s}] \qquad (2.4)$$

where: V is molar volume [m^3/mol]

C is the Sutherland constant [-]

T is temperature [K]

M_A, M_B is molecular mass [g/mol]

Arnold [35] made two important contributions aimed at overcoming the two limitations of the Chapman-Enskog empirical correlation (as discussed previously). The first contribution by Arnold [35] was the introduction of a Sutherland temperature correction factor, which was aimed at improving the temperature dependency. The second contribution was aimed at solving the problem of the scarcity of the collision diameter (σ) data. This was accomplished by estimating the collision diameter from Le Bas atomic volume parameters, making it possible to predict the diffusion coefficient for virtually any binary gas system [36]. The average inaccuracy of this correlation, specifically for the prediction of the diffusion coefficient in air, is approximately 5% [36].

Marrero *et al.* [34, 38] set up a correlation based on the Chapman-Enskog kinetic theory of gases, describing the temperature dependence of the diffusion coefficient, as follows:

$$D_{AB} = \left(\frac{M_A+M_B}{2M_AM_B}\right)^{1/2}.\left(\frac{T^{3/2}}{P}\right).\left(\frac{1}{\omega\Omega}\right) \qquad [\text{cm}^2/\text{s}] \qquad (2.5)$$

with: $$\Omega = 17.54\left[\ln\left(\frac{T/\theta}{4.10\times10^7}\right)\right]^2.\exp\left[16.61\left(\frac{\theta}{T}\right)+35.87\left(\frac{\theta}{T}\right)^2\right] \qquad (2.6)$$

for: $\frac{T}{\theta} \geq 36.6$

and: $\Omega = 1.83\times10^{4}\left(\frac{\theta}{T}\right)^{1/3}$ (2.7)

for: $\frac{T}{\theta} < 36.6$

where: Ω is the collision integral [-]

ω is the scale factor for the collision integral [-]

θ is the scale factor for temperature [-]

T is temperature [K]

M_A, M_B is molecular mass [g/mol]

P is absolute pressure [atm]

For equation 2.5 the two scale factors (ω and θ) are adjustable. Referring to the Chapman-Enskog empirical correlation (equation 2.1) the two scale factors in the correlation by Marrero *et al.* [34, 38] are simply two terms into which the numerical constants in equation 2.1 have been absorbed. This was done in order to write the Chapman-Enskog into a more practical form. The collision integral (Ω) now depends solely on temperature through the ratio T/θ. The inaccuracy of this correlation is stated as being less than 12 % for all systems investigated [34].

Cho *et al.* [27] and Chen *et al.* [22] set up correlations from experiments performed on the naphthalene/air system with the closed Stefan tube method (as mentioned in section 2.2.1). Both correlations are functions of temperature and are only applicable to the determination of the diffusion coefficient of naphthalene in air. The correlations are as follows:

Cho *et al.* [27]: $D_{AB} = 8.1771\times10^{-7}T^{1.983}$ [cm^2/s] (2.8)

Chen *et al.* [22]: $D_{AB} = 1.495\times10^{-6}T^{1.888}$ [cm^2/s] (2.9)

where: T is temperature [K]

The correlation by Cho *et al.* [27] is applicable over the temperature range 287.66-327.12 K (14.5-53.96 ^{o}C) and has an average absolute inaccuracy of 3 %. The

correlation by Chen *et al.* [22] is valid over the temperature range 295.16-302.16 K (22-29 ^{o}C) and has an average absolute inaccuracy of 4.1 %.

Gustafson *et al.* [15] set up a correlation that is only applicable to the determination of the diffusion coefficient of polycyclic aromatic hydrocarbons (such as naphthalene, anthracene, benzene etc.) in air. This correlation was formed through gas chromatography experiments that were performed with the arrested flow elution method (as mentioned in section 2.2.1) and has an absolute error between predicted and measured values of 9.1 %. The equation proposed by Gustafson *et al.* [15] is as follows:

$$D_{AB} = \frac{\left(0.186 \times 10^{0.00283T}\right)}{V^{0.213}} \qquad [\text{cm}^2/\text{s}] \qquad (2.10)$$

where: V is the molar volume at the system temperature [cm^3/mol]

From the preceding investigators on the naphthalene/air system [14, 15, 22, 27, 28, 31] it is clear that the correlation by Fuller *et al.* [36] is the *empirical* correlation that gives the most accurate predictions for the naphthalene/air system. The power dependency of the temperature term in the correlations proposed by Cho *et al.* [27] and Chen *et al.* [22] is 1.983 and 1.888 respectively, which was obtained through experimentation. The dependency of the temperature term in the empirical correlation by Fuller *et al.*[36] is therefore closer to the experimentally obtained power dependency than those empirical correlations using the dependency of the Chapman-Enskog correlation.

2.3 Theory

2.3.1 Diffusion through a stagnant gas (Fick's law) as applied to the Stefan tube

The theory behind the diffusion of a species A (solid or liquid phase) through a non-diffusing or stagnant species B (vapour phase), at steady state, is investigated in this section. This process, which is described by Fick's law, can be applied to the diffusion process that occurs in the Stefan tube [19, 27].

The system being explored is the passing of a non-diffusing gas (B) over a tube, which facilitates the sublimation/evaporation of a solute (A) placed at the bottom of the tube. From Figure 2.5 it can be seen that the end of the diffusion path (point 1) is impermeable to the gas (B), thus stopping it from passing through. The vapour from the solute therefore diffuses upwards through the gas in the tube [11, 19, 37].

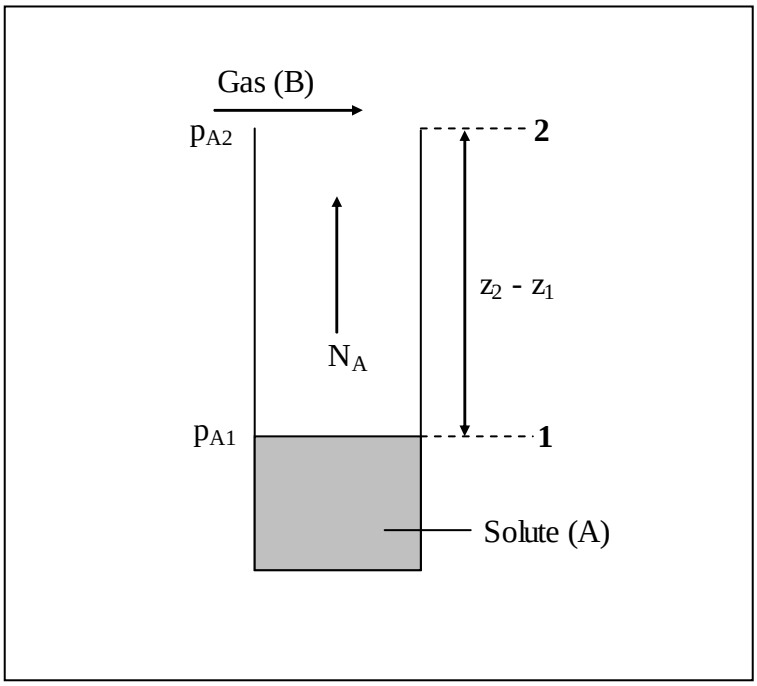

Figure 2.5: *Schematic representation of the diffusion of substance A through a non-diffusing gas B*

Referring to Figure 2.5, it can be seen that the boundary at the solid surface (point 1) is impermeable to the gas (B) since the gas is usually insoluble in the solid substance. The gas (B) is therefore unable to diffuse into or away from the solid surface. For a binary mixture of A and B, when the bulk fluid is stationary, the diffusion of molecules is represented by the general Fick's law equation. This equation is written as follows and, as can be seen, the diffusion of the molecules is solely the product of the existence of a concentration gradient [37]:

$$J_A = -c_T D_{AB} \frac{dx_A}{dz} \tag{2.11}$$

where: J_A is the molar flux of component A [kmol/s.m^2]

c_T is the total concentration of A and B [kmol/m^3]

x_A is the mol fraction A

D_{AB} is the molecular diffusivity of A in B [m^2/s]

z is the length along the diffusion path [m]

The diffusion flux can now be converted to a diffusion velocity of A as follows:

$$J_A = v_{Ad} . c_A \tag{2.12}$$

where: v_{Ad} is the diffusion velocity of A [m/s]

c_A is the concentration of A in the mixture [kmol/m^3]

However, equation 2.11 can only be applied to diffusion in a stationary fluid; i.e., no net movement of the binary mixture of A and B has occurred. When the whole fluid is moving in bulk or convective flow a term needs to be added to equation 2.11 in order to calculate the true diffusion flux of component A. With convective flow, assuming that component A is still diffusing in the same direction, the diffusion velocity (v_{Ad}) is now measured relative to the moving fluid. The velocity of component A relative to a stationary point (v_A) can now be expressed as follows:

$$v_A = v_{Ad} + v_M \tag{2.13}$$

where: v_M is the molar average velocity of the whole fluid relative to a stationary point [m/s]

To a stationary observer component A would be moving faster than the bulk of the fluid, seeing as the diffusion velocity (v_{Ad}) is added to that of the bulk phase (v_M).

Multiplying equation 2.13 by c_A now gives:

$$c_A v_A = c_A v_{Ad} + c_A v_M \tag{2.14}$$

Each of the three terms in equation 2.14 now represents a flux. The first term ($c_A v_A$) can be represented by N_A, which is the total flux of A relative to the stationary point (in kmol/s.m^2). The second term ($c_A v_{Ad}$) is the diffusion flux relative to the moving fluid, as was described in equation 2.12. The third term ($c_A v_M$) is the convective flux of A relative to the moving fluid. Equation 2.14 can now be written as follows:

$$N_A = J_A + c_A v_M \tag{2.15}$$

By letting N be equal to the total convective flux of the whole stream relative to the stationary point, it follows that:

$$N = c v_M = N_A + N_B \tag{2.16}$$

And now solving for v_M:

$$v_M = \frac{N_A + N_B}{c} \tag{2.17}$$

Substituting equation 2.17 back into equation 2.15 provides:

$$N_A = J_A + \frac{c_A}{c}\left(N_A + N_B\right) \tag{2.18}$$

From equation 2.11 it can be seen that J_A is the molar flux (Fick's law) and the general equation for diffusion with convection can be written as follows:

$$N_A = -cD_{AB}\frac{dx_A}{dz} + \frac{c_A}{c}\left(N_A + N_B\right) \tag{2.19}$$

For the case of the diffusion of a species A through a stagnant, non-diffusing species B, N_B = 0. Substituting this into the general equation 2.19 gives:

$$N_A = -cD_{AB}\frac{dx_A}{dz} + \frac{c_A}{c}\left(N_A + 0\right) \tag{2.20}$$

By assuming ideal gas conditions, constant temperature and constant total pressure the following substitutions can be made into equation 2.20:

$$c = \frac{P}{RT} \tag{2.21}$$

$$p_A = x_A P \tag{2.22}$$

$$\frac{c_A}{c} = \frac{p_A}{P} \tag{2.23}$$

Equation 2.20 can therefore be written as follows:

$$N_A = -\frac{D_{AB}}{RT}\frac{dp_A}{dz} + \frac{p_A}{P}N_A \tag{2.24}$$

Equation 2.24 can now be rearranged and integrated as follows:

$$N_A\left(1 - \frac{p_A}{P}\right) = -\frac{D_{AB}}{RT}\frac{dp_A}{dz} \tag{2.25}$$

$$N_A\int_{z1}^{z2} dz = -\frac{D_{AB}}{RT}\int_{pA1}^{pA2}\frac{dp_A}{1 - p_A/P} \tag{2.26}$$

$$N_A = \frac{D_{AB}P}{RT\left(z_2 - z_1\right)}\ln\left(\frac{P - p_{A2}}{P - p_{A1}}\right) \tag{2.27}$$

Equation 2.27 is the final equation and is used to calculate the diffusion coefficient of species A through a stagnant gas B. The diffusion flux, however, can be obtained from the mass loss measurement of species A and the tube dimensions as follows:

$$N_A = \frac{\Delta m}{M_A . t_{\exp} . \left(\frac{\pi}{4}\right) . d_{tube}^2} \qquad [\text{mol/s.m}^2] \qquad (2.28)$$

where: N_A is the diffusion flux [kmol/s.m^2]

Δm is the mass loss of species A [g]

M_A is the molecular weight of species A [g/mol]

$t_{\exp}$ is the duration of the diffusion period [s]

d_{tube} is the diffusion tube diameter [m]

2.3.2 Establishment of steady state (Fick's second law)

It is important to determine the time required to reach conditions sufficiently near to steady state in order to apply equation 2.27 with negligible error. The diffusion process can be represented by Fick's second law by assuming the gas in the diffusion tube is initially saturated with vapour at a very small partial pressure p_{A1} [19]. The basic form of Fick's second law is as follows:

$$\frac{\partial p}{\partial t} = D_{AB} \frac{\partial^2 p}{\partial z^2} \qquad (2.29)$$

where: p is the partial pressure of the diffusing vapour [Pa]

t is the total diffusion time [s]

z is the diffusion path length [cm]

Integration of equation 2.29 was done by Lee *et al.* [19] and the ratio of the rate of evaporation at any time (t) to the rate at time $t = \infty$ (i.e. the steady state) is given by the following equation:

$$\frac{(N_A)_{t=t}}{(N_A)_{t=\infty}} = 1 - 2e^{-\frac{D\pi^2 t}{z^2}} + 2e^{-\frac{4D\pi^2 t}{z^2}} - 2e^{-\frac{9D\pi^2 t}{z^2}} + 2e^{-\frac{16D\pi^2 t}{z^2}} - 2e^{-\frac{25D\pi^2 t}{z^2}} \qquad (2.30)$$

2.3.3 Determination of the vapour pressure of naphthalene

From the naphthalene review document by Goldstein *et al.* [22] it is apparent that the correlations proposed by Ambrose *et al.* [39] and de Kruif *et al.* [40], for the determination of the vapour pressure of naphthalene, are the most accurate. The correlation by Ambrose *et al.* [39] has an uncertainty of 3.77 % [15] and is accurate over the temperature range -43 to 71 ^{o}C. The correlation is as follows:

$$T \log p = \frac{1}{2} a_0 + \sum a_s E_s(x) \tag{2.31}$$

where:

$$a_0 = 301.6247 \qquad x = (2T - 574)/114$$
$$a_1 = 791.4937 \qquad E_1(x) = x$$
$$a_2 = -8.2536 \qquad E_2(x) = 2x^2 - 1$$
$$a_3 = 0.4043 \qquad E_3(x) = 4x^3 - 3x$$

and: p is the vapour pressure [Pa]

T is the temperature [K]

The correlation by de Kruif *et al.* [40] has an uncertainty of 1.6 % [22] (doubt over the stated level of uncertainty is expressed in literature [22]) and is valid over the temperature range 0 to 80 ^{o}C. The correlation is as follows:

$$R \ln p = 20.0885 + 72513\left(\frac{1}{298.15} - \frac{1}{T}\right) - 57.53\left[\frac{298.15}{T} - 1 + \ln\left(\frac{T}{298.15}\right)\right] \tag{2.32}$$

where: R is the ideal gas constant [8.3143 J/mol.K]

p, T is the vapour pressure [Pa] and temperature [K] respectively

2.4 Experimental

The Stefan tube method was chosen for the measurement of the diffusion coefficient of naphthalene into the different carrier gases in this investigation. Although Marrero *et al.* [13] denounces the Stefan tube technique, several of this method's inaccuracies are not encountered when working with a solid to gas system [14]. The main error resulting from this method is the problem of the moving interface between the sublimating/evaporating substance and the carrier gas. With the sublimation of naphthalene this error becomes negligible, since the saturated vapour pressure of naphthalene is so low that the diffusion path length stays virtually constant throughout the duration of the experiment. The other sources of error mentioned by Marrero *et al.* [13] can be removed by modifying the system and are as follows:

1. End effects caused by surface tension at the solute/gas interface and turbulence at the tube outlet. The effects of surface tension is negligible when the solute is in the solid state, but the cause, effects and negation of turbulence will be discussed in detail in the following sections.
2. The sensitivity of the determination of the diffusion coefficient due to changes in the system temperature. This effect can be minimised through accurate control of the system temperature and will be discussed in the following section.
3. Contamination of either of the two substances can lead to inaccurate experimental results. The purities of the substances used in this investigation are stated by the suppliers and will be provided in the following section.

2.4.1 Apparatus

The apparatus constructed is similar to the design by Lee et al [19], where the carrier gas is passed through a diffusion unit placed in a water bath. Figure 2.6 depicts the process flow diagram and shows that the carrier gas is supplied by a gas cylinder (with a pressure regulator). The gas flow rate is controlled by a Fischer Porter rotameter (FI in Figure 2.6) and the temperature and pressure of the gas entering the water bath are indicated by the sensors TI01 and PI01 (as shown by Figure 2.6).

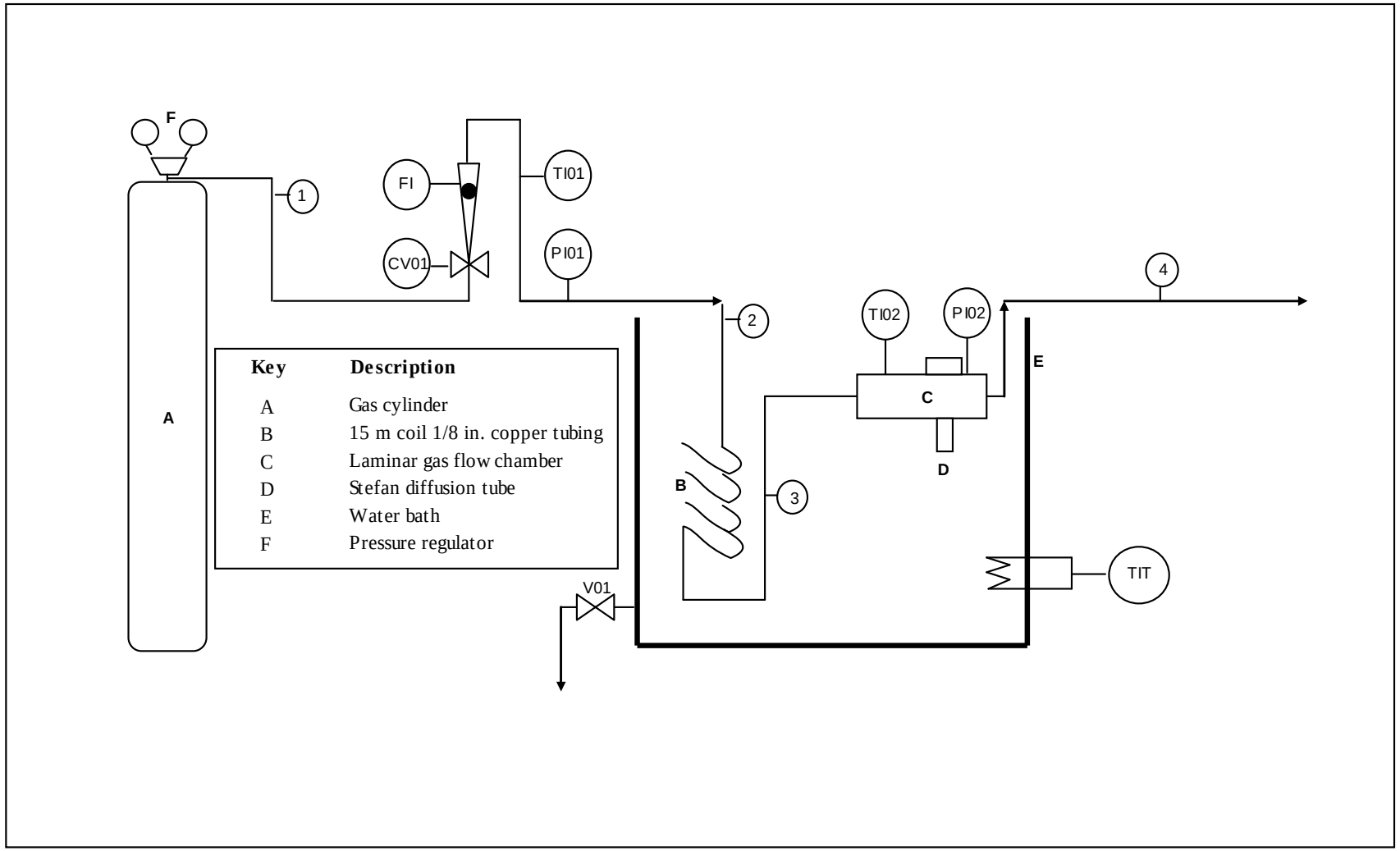

Figure 2.6: *Flow diagram of experimental apparatus*

The temperature of the gas flowing through the diffusion unit is monitored through a PT100 temperature sensor (TI02), with an accuracy of 0.1 ^{o}C. Before the gas enters the diffusion unit it is first preheated to the temperature of the water bath by passing the gas through a 15 meter coil of copper tubing immersed in the water bath. The temperature of the water bath is controlled by a Julabo series immersion circulator (accuracy stated as being within 0.1 ^{o}C), which is fastened to the bath wall by a bracket clamp. A nozzle ensures even mixing and a good temperature distribution throughout the entire bath.

The diffusion unit consists of two separate pieces of equipment, namely the laminar gas flow chamber and the diffusion tube. A schematic representation of the diffusion unit is shown in Figure 2.7.

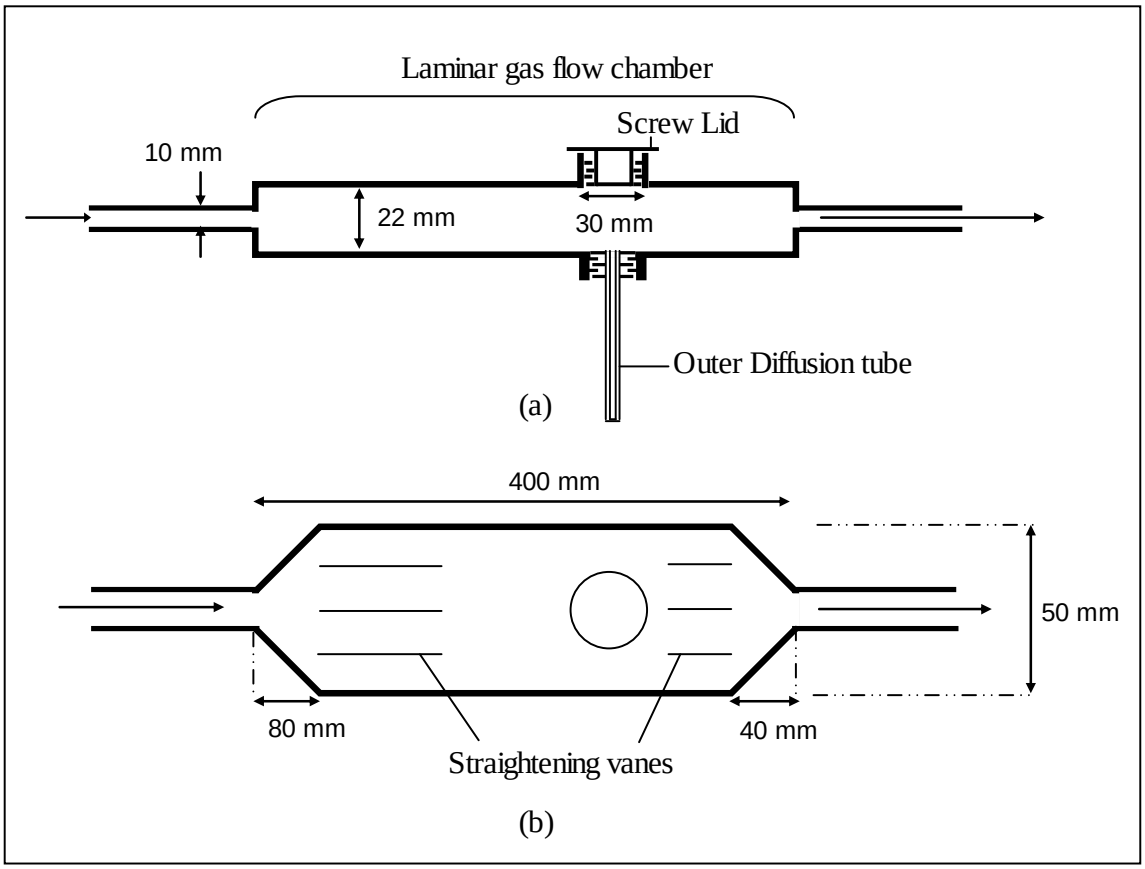

Figure 2.7: *Simplified illustration of the diffusion unit (a) Side view, (b) Top view*

The material of construction for the diffusion tube is brass, since satisfactory heat conduction to the sublimating solid is of extreme importance. The material of construction for the gas flow chamber is stainless steel (SS 304), as the gas entering

the chamber is already heated to the necessary temperature by the copper coil submerged in the water bath. The malleability of brass also contributed to the decision to manufacture the gas flow chamber from stainless steel, as machining brass can become difficult and any inconsistencies in the chamber can lead to turbulence in the gas flow.

The diffusion tube also consists of two separate components: an inner tube and outer casing. A schematic representation of the diffusion tube is seen in Figure 2.8 and Figure 2.9 is provided in order to illustrate how the inner tube fits into the outer casing.

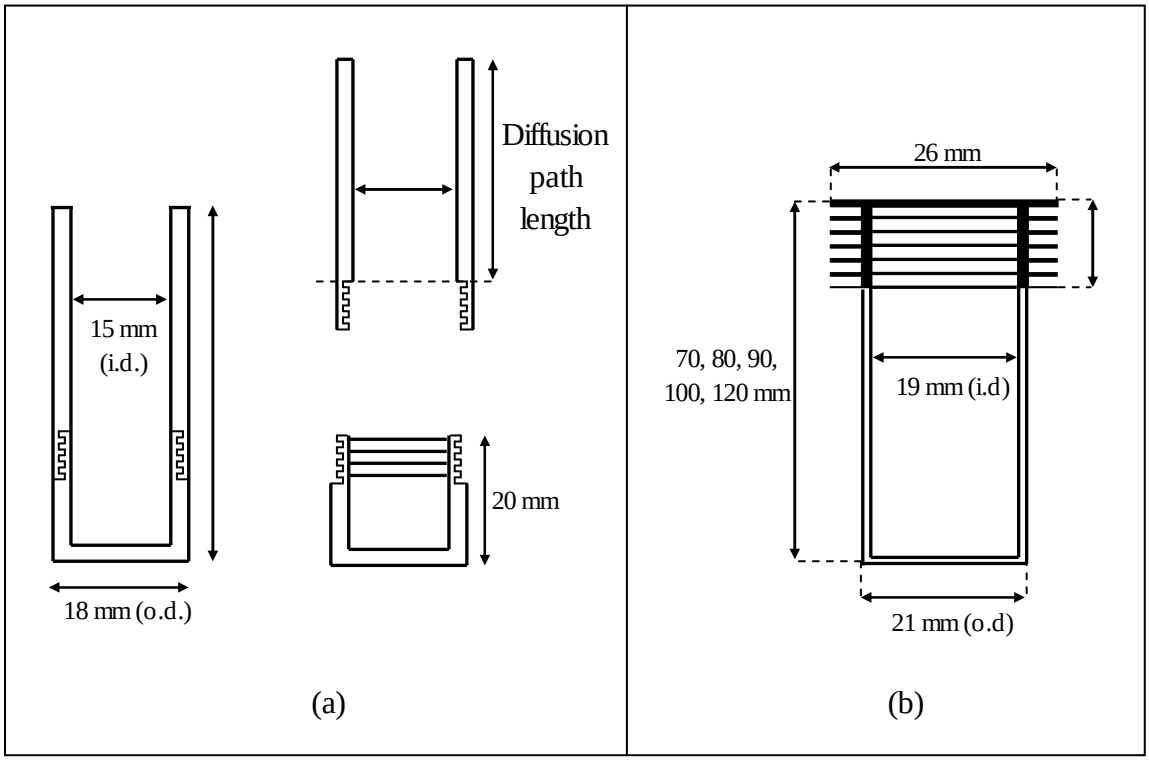

Figure 2.8: *Schematic representation of (a) the inner diffusion tube and (b) outer casing*

From Figure 2.8 it can be seen that the outer casing screws into the bottom of the gas flow chamber. The outer casing has an outer diameter of 21 mm (as indicated on the diagram) and an inner diameter of 19 mm. The inner diffusion tube has an outer diameter of 18 mm, giving a space of 0.5 mm between the two tubes. Seeing as both the inner tube and outer casing are constructed of the same material, shrinking and

expansion of the material due to heat effects should not cause any problems with the removal of the inner tube from the outer casing.

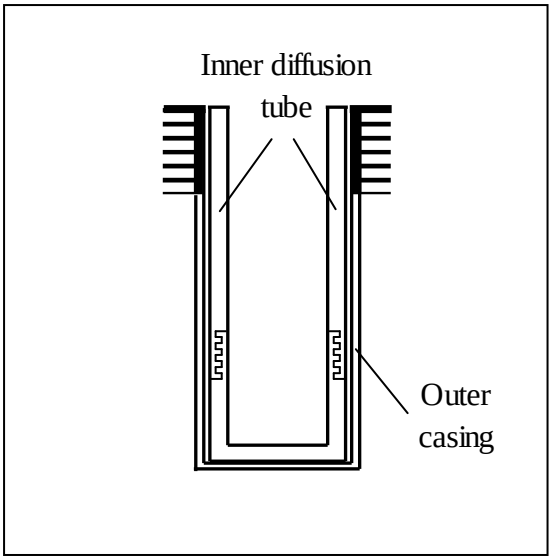

Figure 2.9: *Proper fitting of the inner tube within the outer casing*

From Figure 2.8 it can also be seen that the bottom section of the inner tube can be removed. This is done in order to aid the insertion of the sublimating solid into the tube, thereby removing the possibility of accidentally depositing some of the solid on the inner wall of the diffusion tube. It also has the added benefit of reducing the amount to be weighed, providing a more accurate weighing procedure.

The length of the inner diffusion tube was varied between 70 and 120 mm (Figure 2.8). Five separate inner diffusion tubes and outer casings were constructed, of lengths 70, 80, 90, 100 and 120 mm. Since the bottom section of the inner tube (naphthalene holder/crucible) is 20 mm in height the diffusion path length of the five tubes mentioned previously are 50, 60, 70, 80 and 100 mm respectively. This provides sufficient variation of the diffusion path length (Figure 2.3) without changing the diffusion tube inlet diameter, which might cause unforeseen changes in the gas flow at the tube entrance.

The watertight screw lid (Figure 2.7) at the top of the gas flow chamber acts as an easy access point to remove the diffusion tube for weighing, without it being necessary to remove the entire diffusion unit from the water bath. The tube is therefore extracted upwards, through the opening concealed by the screw lid.

The gas flow chamber comes equipped with stainless steel straightening vanes that are 11.6 mm apart (Figure 2.7). The vanes extend from the inlet of the gas flow chamber to a midpoint position between the gas flow chamber entrance and the diffusion tube. The straightening vanes then also extend from the diffusion tube to the end of the gas flow chamber (view Appendix A1.1 for the specifications on the gas flow chamber design). From Figure 2.7 it can also be seen that the straightening vanes are only found in the vertical position, thus imparting flow channels to the gas flow chamber that are comparable in size to that of the tube carrying the gas to the gas flow chamber. This was done in order to reduce potential turbulence associated with the sudden enlargement of the flow path.

The experiment was set up within a fume cabinet in order to vent the outlet gas to the atmosphere (an illustration of the experimental setup within the fume cabinet is shown in Appendix A1.3). The weight measurements were performed using an OHAUS semi-micro balance (model DV 215CD) that has an accuracy to within 0,01mg. The complete piping and instrumentation specifications are shown in Appendix A1.2. All the length measurements (tube diameters, diffusion path lengths, etc.) were completed with an accuracy of 0.01 mm.

2.4.2 Experimental procedure

The experiment was started by submerging the diffusion unit in the water bath and adjusting the water bath temperature to the desired setting. When the water bath temperature was reached the gas flow was opened and left for approximately 1 hour. This was done in order to obtain a stable temperature reading within the diffusion unit, as well as to stabilise the supply pressure from the gas cylinder. The first 30 minutes after opening the gas flow the pressure set on the regulator decreased marginally. This, however, caused a slight drop in the rotameter setting. The 1 hour period before commencing the experiment therefore ensured that a stable gas flow rate was maintained throughout the duration of the experiment.

When the 1 hour period had elapsed the naphthalene was inserted into the naphthalene holder (bottom section of the inner diffusion tube). Care was taken that the naphthalene surface was smooth and lay level with the top of the crucible. This was

done in order to ensure the actual diffusion path length was as designed. The holder (with the naphthalene) was then weighed with the semi-micro balance. During the naphthalene insertion into the holder, and its subsequent weighing, it was important that skin contact with the holder was avoided. Due to the sensitive nature of the mass measurement, possible skin oil deposits could affect the reading.

The naphthalene holder was then carefully reattached to the top section of the inner diffusion tube. By opening the screw lid on top of the gas flow chamber the inner diffusion tube was lowered into the diffusion unit until it came to rest within the outer casing. The screw lid was replaced and the starting time of the experiment was noted. Regular readings of the gas temperature within the gas flow chamber (sensor TI02 in Figure 2.6) and the gas flow rate were taken throughout the duration of the experiment. This was done in order to ascertain that the settings remained constant throughout the experiment.

When the experiment was stopped, the inner diffusion tube was extracted from the diffusion unit and the naphthalene holder was removed from the inner diffusion tube. The naphthalene holder was then placed on a *clean* metal surface and a glass cap placed over the holder. The holder was left for 5 to 10 minutes (depending on the temperature at which the experiment was conducted) in order to equilibrate (holder and naphthalene) at room temperature. The glass cap served the function of minimising the amount of naphthalene sublimation after the experiment had been stopped and before the weighing procedure commenced. The naphthalene holder was then weighed and the measurement logged.

In order to perform experiments at higher system pressures, a needle valve was placed at the outlet line from the diffusion unit (marked line 4 in Figure 2.6). However, before starting an experiment the screw lid on top of the diffusion unit was fastened tightly in order to ensure a constant pressure was maintained in the unit.

2.4.3 Chemicals and gases used

Information on the chemicals and gases used in the diffusion experiments are presented in Table 2.2.

Table 2.2: *Chemicals and gases used in experiments*

Chemicals / Gases	Manufacturer / Supplier	Stated purity
Air (dry)	Afrox	Technical grade
Carbon dioxide	Afrox	Technical grade
Helium	Afrox	99.95 %
Naphthalene	Sigma Aldrich	99 %

2.5 Comparison between Correlations and Measurements of previous Investigators for the Naphthalene/Air system

Before commencing with the sublimation of naphthalene into helium and carbon dioxide (diffusion coefficient data on these systems are not readily available from literature) the accuracy of the apparatus constructed was first tested through the sublimation of naphthalene into air. The diffusion coefficient for the naphthalene/air system is well documented in literature and the following table gives a brief overview of the different preceding investigators and the measuring techniques they employed:

Table 2.3: *Previous investigations on the determination of the diffusion coefficient of the naphthalene/air system (experimental technique included)*

Investigator	Method
Mack [31] – 1925	Stefan tube (closed)
Caldwell [14] – 1984	Stefan tube (open)
Chen (Goldstein *et al.* [22]) – 1990	Stefan tube (closed)
Cho *et al.* [27] – 1992	Stefan tube (closed)
Gustafson *et al.* [15] – 1994	Gas chromatography
Siddiqi *et al.* [28] – 2007	Thermo gravimetric analysis

Although the naphthalene/air system has been researched by various investigators, consensus has not been reached on the actual diffusion coefficient for this system. Figure 2.10 shows the results from the correlations by Cho *et al.* [27], Chen *et al.* [22] and Gustafson *et al.* [15] (over the temperature range investigated), as well as the results from the empirical correlations by Fuller *et al.* [36] and Arnold [35]. The actual experimental measurements from Caldwell [14], Mack [31] and Siddiqi *et al.* [28] are also

presented for each temperature investigated, as correlations were not compiled by them.

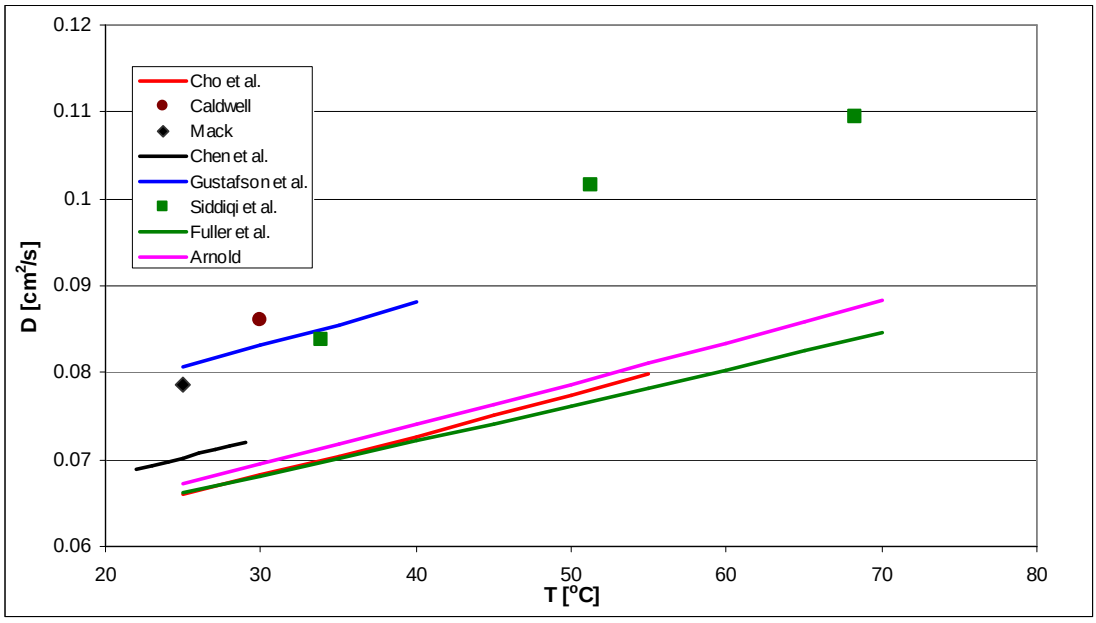

Figure 2.10: *Experimental diffusion coefficient data from previous investigators on the naphthalene/air system*

From Figure 2.10 it can be seen that the results by Cho *et al.* [27] and Chen *et al.* (cited by Goldstein *et al.* [22]) lie reasonably close to the empirical correlations by Arnold [35] and Fuller *et al.* [36]. The correlation by Fuller *et al.* [36], discussed in detail in section 2.2.2, is the recommended general equation for the prediction of molar diffusion coefficients, specifically in air. Since the correlation by Cho *et al.* [27] provides predictions that correspond well to the predictions from the correlation by Fuller *et al.* [36] it is seen as the most accurate equation for the determination of the diffusion coefficient of naphthalene in air [22].

As stated in section 2.2.1, Cho *et al.* [27] made use of the closed Stefan tube method by placing a naphthalene pellet (diameter d) at the top of a diffusion tube, with an activated charcoal surface placed a length (L) below the pellet. The space between the pellet and charcoal was then filled with atmospheric air to provide the medium through which the naphthalene vapour diffuses to the charcoal surface. The system temperature was controlled through a water jacket surrounding the structure [27].

In order to use this method the assumption is made that the concentration of naphthalene at the activated charcoal surface is zero, while the concentration at the surface of the naphthalene pellet is calculated from the saturated vapour pressure of naphthalene. A concentration gradient therefore exits causing the naphthalene to diffuse from the pellet towards the activated charcoal. According to Cho *et al.* [27] the main advantage of this experimental setup is the larger mass loss obtained in comparison to previous methods employed (this is due to a larger diameter naphthalene pellet used). Cho *et al.* [27] sublimated in the region of 250 to 400 mg per experiment, compared to the mass loss of 1 to 50 mg of previous researchers [27]. Even though a larger naphthalene pellet is employed, the larger mass loss did not cause an appreciable change in the diffusion path length. The assumption of a constant diffusion path length therefore remains valid.

Cho *et al.* [27] conducted their experiments using two different diffusion path lengths, namely 0.5 and 1 cm, and a pellet diameter of 8.36 cm. The activated charcoal employed had a surface area of 750 m^2/g and a bulk density of 0.460 g/ml. The reasoning behind the choice of the short diffusion path length and large pellet diameter was not only to obtain a larger naphthalene mass loss, but also to minimise the area ratio of the tube walls along the diffusion path length to the diffusing naphthalene surface. According to Cho *et al.* [27] a 'too large' area ratio could cause the adsorption of naphthalene along the diffusion length, thus resulting in a diffusion coefficient that is larger than the actual value. However, no indication is given of what a 'too large' area ratio would be. It should also be noted that even though Cho *et al.* [27] used two different diffusion path lengths in their study they found no conclusive evidence that the wall adsorption effect exists in their system.

The investigations by Mack [31] and Caldwell [14], whose work preceded that of Cho *et al.* [27] (both researchers determined the diffusion coefficient only at 1 temperature) show results that are in the order of 20 % higher than the results by Cho et al [27].

The comments made by Cho *et al.* [27], specifically on the work done by Mack [31] and Caldwell [14], were analysed. In the paper by Cho *et al.* [27], the authors highlight certain possible error sources as to why the results obtained by Mack [31] and Caldwell [14] differ so significantly from their own findings. Their main misgiving of Mack [31]

and Caldwell's [14] work is that the longer diffusion path length in their experiments could give rise to naphthalene adsorption on the walls of the diffusion tube, thus incorrectly increasing the value of the diffusion coefficient.

Another possible source of error in the work performed by Caldwell [14], who used an open tube evaporation method similar to the setup used in this study, was the effect that the gas stream flowing over the top of the tube had on the actual diffusion path length. The occurrence of turbulence at the top of the tube (due to high gas flow rate) would effectively shorten the effective diffusion path length, thereby giving an inaccurate diffusion coefficient reading [27].

Gustafson *et al.* [15] determined the diffusion coefficient of various polycyclic aromatic hydrocarbons (PAHs), such as naphthalene, benzene, toluene etc., in air and obtained results that were similar to the results by Mack [31] and Caldwell [14]. The technique employed was gas chromatography through the arrested flow elution method. Gustafson *et al.* [15] compared their experimental results with the results from the predictive equations of Lee *et al.* [19] and Fuller *et al.* [36] and found that the correlations tended to underestimate the diffusion coefficient of the larger aromatic compounds, such as naphthalene. The effect of adsorption in gas chromatographic methods, specifically the arrested flow elution method, is not mentioned by Gustafson *et al.* [15] or by the other researchers that utilised similar methods [16-18]. The possible effect that wall adsorption could have in this technique is therefore unknown.

Siddiqi *et al.* [28] made use of a novel thermo-gravimetric analysis technique (refer to section 2.2.1) and found results that are comparable to the results by Mack [31], Caldwell [14] and Gustafson *et al.* [15]. The validity of the previously accepted value for the diffusion coefficient of the naphthalene/air system (from the work by Cho *et al.* [27]) therefore comes into question.

2.6 Results and Discussion

The naphthalene mass loss from the experimental procedures was converted to a vapour phase diffusion coefficient using equations 2.27 and 2.28. The saturated

vapour pressure of naphthalene was determined using equations 2.31 and 2.32, depending on the temperature at which the experiment was conducted. According to Goldstein *et al.* [22] the method by Ambrose *et al.* [39] gives the most accurate naphthalene vapour pressure data. This method was also used in numerous preceding naphthalene sublimation studies, such as the studies performed by Caldwell [14], Cho *et al.* [27] and Erasmus [3].

2.6.1 Verification of the accuracy of the experimental technique with the naphthalene/air system

From the studies performed by the preceding investigators it becomes apparent that the following factors need close scrutiny in order to obtain accurate diffusion coefficient measurements:

- The effect of temperature measurements on the diffusion coefficient.
- The effect that the gas flow rate, i.e. turbulence, has on the diffusion path length.
- The effect that changes in the area ratio of the tube walls along the diffusion path length to the diffusing naphthalene surface area would have on the diffusion coefficient (due to possible wall adsorption).
- The time required to reach steady state conditions

<u>The sensitivity of diffusion coefficient measurements to temperature:</u>

From literature it is apparent that any molecular diffusion measurement technique is extremely sensitive to the temperature measurements performed [14, 19, 22, 27]. Care is therefore taken in this investigation to ensure that the temperature of the naphthalene at the bottom of the inner diffusion tube is at the same temperature as the carrier gas and that this temperature is kept at a constant value throughout the duration of the experiment. The existence of a temperature gradient within the Stefan tube, combined with the concentration gradient, will lead to inaccurate diffusion coefficient measurements.

Figure 2.11 illustrates the importance of accurate temperature measurements. From the graph it can be seen that, for the naphthalene/air system at 26 ^{o}C, an error of approximately 9 to 10 % can be made if a 1 ^{o}C error is made in the temperature measurement. The error estimate was obtained by calculating the diffusion coefficient (equation 2.27) at incorrect system temperatures. Due to the extreme sensitivity of the saturated vapour pressure of naphthalene to temperature, especially at lower temperatures, this graph represents the maximum error possible through inaccurate temperature measurements.

As stated in section 2.4 the temperature indicators used in the current investigation have accuracies to within 0.1 ^{o}C. From Figure 2.11 it is clear that the maximum error possible from inaccurate temperature control/measurement is less than 2 % in the current investigation. For a detailed error-analysis refer to Appendix 2.

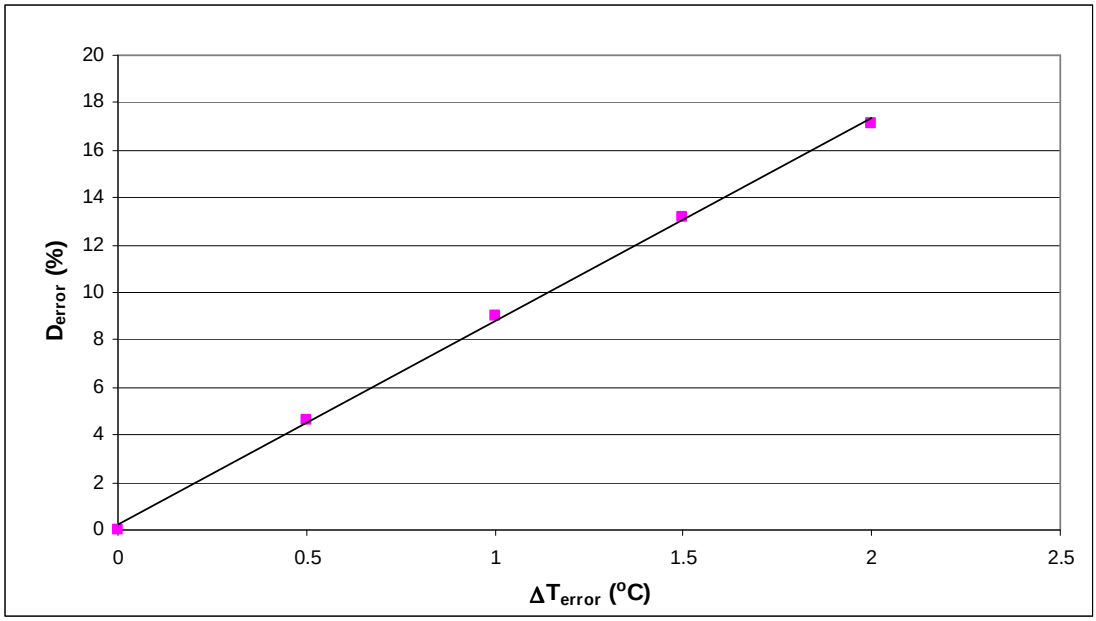

Figure 2.11: Maximum e*rror (%) in diffusion coefficient determination versus error in the temperature measurement (at the lowest system temperature of 26 ^{o}C)*

<u>The effect of turbulence:</u>

In order to validate the assumption that the concentration of naphthalene at the top of the diffusion tube is zero the carrier gas flow rate needs to be of sufficient magnitude,

since a ‘too low’ flow rate will cause a build-up of naphthalene at the top. This will effectively result in a smaller concentration gradient, which will inhibit the diffusion of the naphthalene vapour producing an inaccurate diffusion coefficient measurement.

A ‘too high’ carrier gas flow rate will, however, have the same result. A ‘too high’ gas flow rate will cause turbulence at the top of the diffusion tube, which will effectively shorten the measured diffusion path length and lead to inaccurate diffusion coefficient measurements. It is therefore important to determine the gas flow rate where the effect of turbulence becomes negligible.

Figure 2.12 shows the experimental results for the diffusion coefficient measurement at different actual gas linear velocities (calculated at atmospheric pressure and ambient temperature) for the upper and lower limit of the temperature range (299 and 346 K) investigated. From the graph it is clear that for linear sweep velocities below 0.04 m/s the carrier gas flow rate has a negligible effect on the diffusion coefficient. This is seen at both the lower and upper temperature range limit (299 and 346 K). The experimental readings and calculated results are depicted in tabular form in Appendix 2.

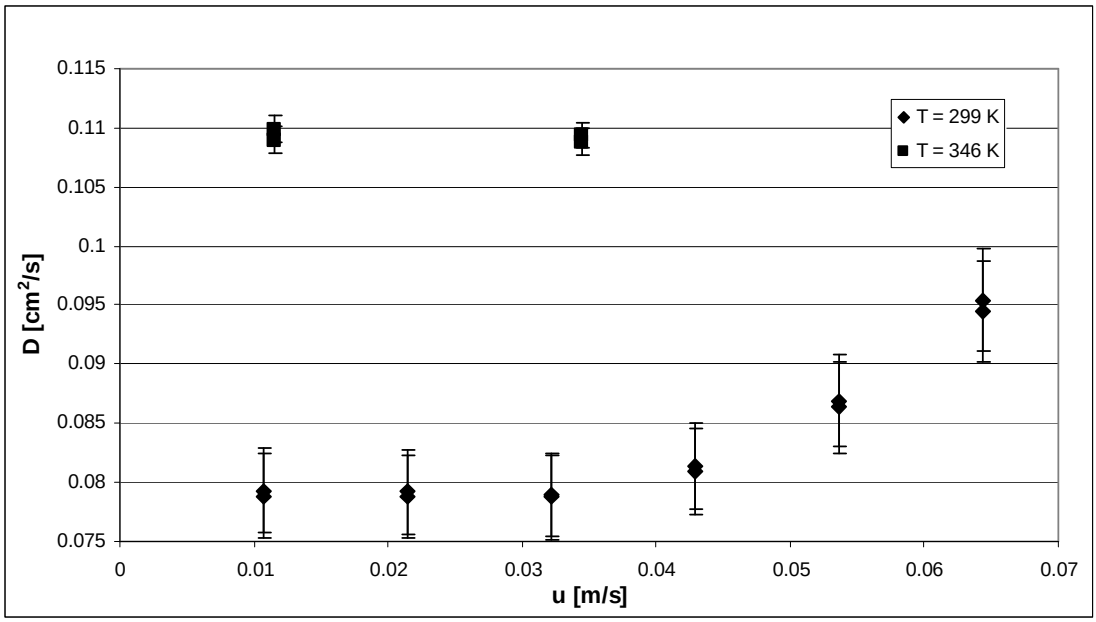

Figure 2.12: *Diffusion coefficient at various gas linear sweep velocities (Tube specifications: (a) Diffusion path length = 62 mm, (b) Tube diameter = 15.2 mm)*

A carrier gas linear sweep velocity of 0.0107 m/s (actual) is therefore chosen for experimentation in the naphthalene/air system as the assumption is made that in the current experimental setup the effect of turbulence is small enough to be ignored at the before mentioned velocity. Additionally, the experimental results in Figure 2.12 contain error bars (view Appendix A2.5 for the detailed account of the error analysis).

Possible wall effects:

In order to investigate the effect that possible wall effects could have on the determination of the diffusion coefficient it was necessary to vary the area ratio of the tube walls along the diffusion path length to the diffusing naphthalene surface. This was achieved using the following two experimental methods:

1. Varying the diffusion path length (L) and
2. Varying the diameter of the diffusion tube (d_{tube}).

Figure 2.13 shows the effect that increasing the diffusion path length has on the experimentally determined diffusion coefficient.

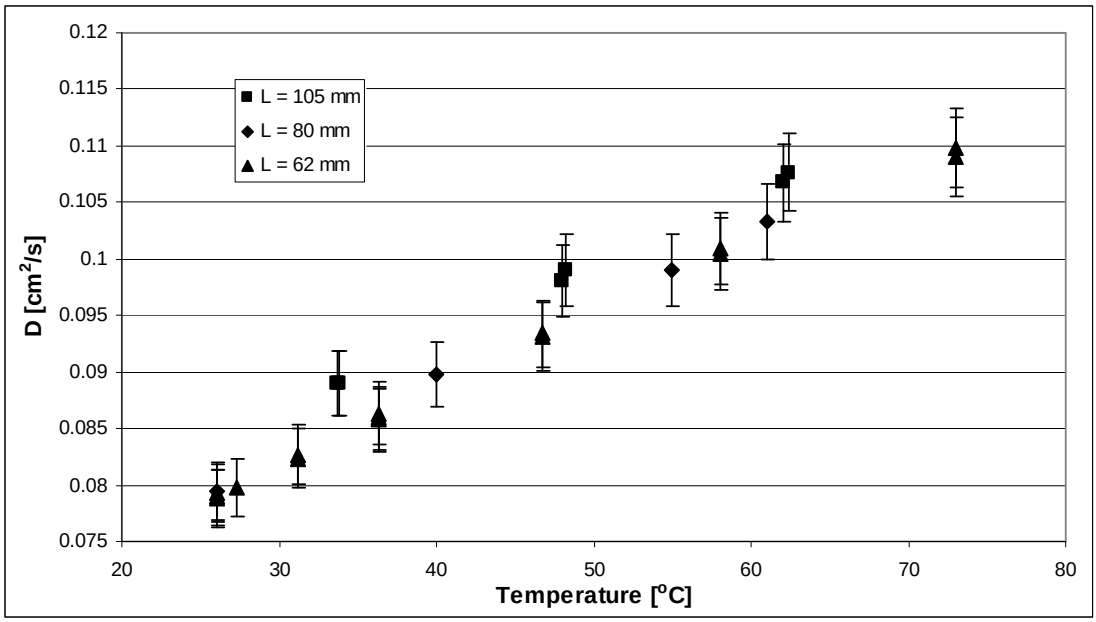

Figure 2.13: *The effect of an increase in the diffusion path length (L) on the experimentally determined diffusion coefficient (d_{tube} constant at 15.2 mm)*

From the Figure 2.13 it can be seen that the experimental diffusion coefficient results for the 62 and 80 mm path length tests are virtually identical, signifying that possible wall effects are not yet a significant factor for the diffusion path lengths in question. A marginal increase of approximately 5 % in the experimentally determined diffusion coefficients are, however, observed for the 105 mm diffusion path length experiment. It is not clear whether this slight increase in the diffusion coefficient for the longest diffusion path length is due to possible wall effects. The possibility of wall *adsorption* can be tested by weighing the inner diffusion tube (without the naphthalene holder) before and after each experiment. However, in order to measure any possible weight increase in the tube an accurate micro-balance is required, since the maximum possible mass adsorbed on the tube will be extremely low.

It was therefore decided that in order to eliminate any possible wall effects, only diffusion path lengths of 80mm or less would be used in further tests. It should, however, be noted that the results shown in Figure 2.13 were all conducted at a constant diffusion tube diameter of 15.2 mm. Refer to Appendix A2.5 for the detailed error analysis.

Figure 2.14 shows the effect of decreasing the diffusion tube diameter on the experimentally determined diffusion coefficient. This variation was achieved by manufacturing different sets of inner diffusion tubes, with differing wall thicknesses. The choice of brass as construction material ensured sufficient heat transfer to the sublimating solid. From the graph it can be seen that the experimental results for the diffusion tube diameters of 15.2 and 12.2 mm are virtually identical, indicating that possible wall effects do not significantly affect the experimental measurements at tube diameters of 12.2 mm or more. The 10.2 mm diameter experiments show a slight increase (approximately 9 %) over the experimental results observed for the 12.2 and 15.2 mm diameter tests.

The results from the 8.2 and 5 mm diameter tests, however, show a marked increase over the diffusion coefficient results obtained for the 12.2 and 15.2 mm diameter tests. This increase in the calculated diffusion coefficient at smaller tube diameters might be due to possible wall effects (possibly a wall creeping effect that is found in capillary type tubes).

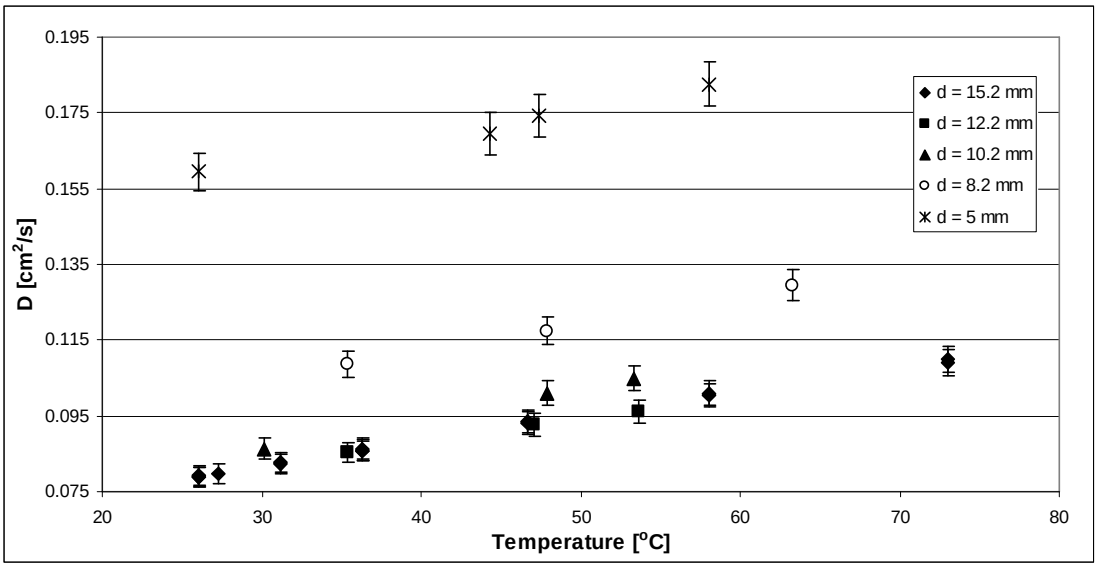

Figure 2.14: *The effect of decreasing the diffusion tube diameter on the experimentally determined diffusion coefficient (L constant at 62 mm)*

Figure 2.15 shows the effect that changes in the ratio of the inner wall area along the diffusion path length to the naphthalene surface area have on the calculated diffusion coefficient.

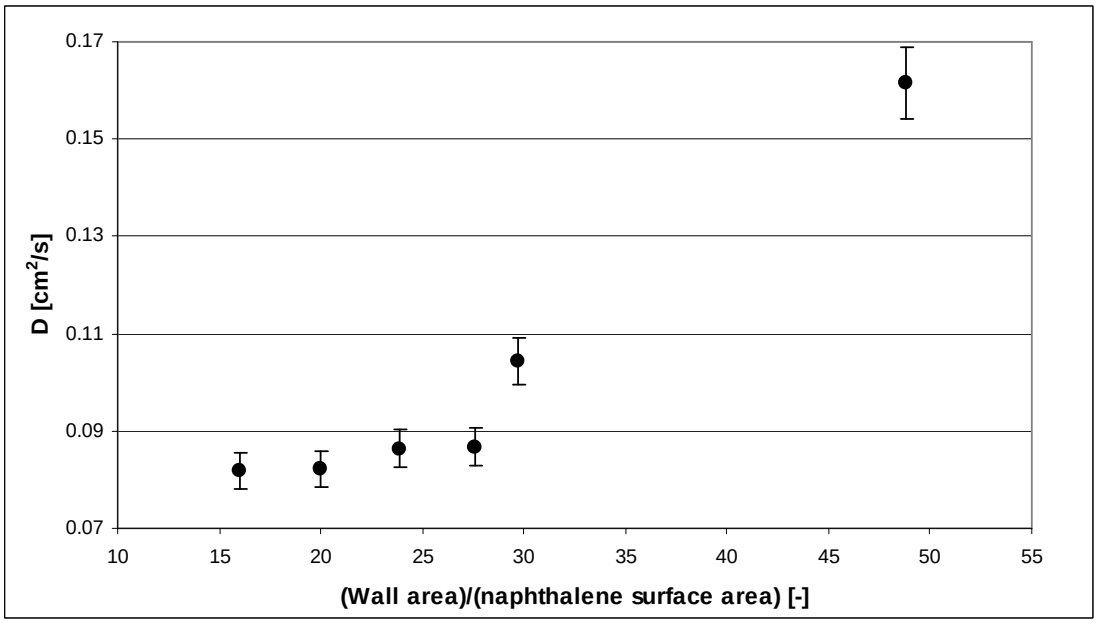

Figure 2.15: *The effect of increasing the ratio of the inner wall area along the diffusion path length to the naphthalene surface area on the experimentally determined diffusion coefficient*

From Figure 2.15 it is clear that the calculated diffusion coefficient stays relatively constant when the ratio of the wall area to naphthalene surface area is in the range of 15 to 28. When the value of the area ratio becomes greater than 28 the calculated diffusion coefficients increase markedly. The system parameters chosen for experimentation on the naphthalene/air system are therefore as follows: diffusion path length = 62 mm and tube diameter = 15.2 mm. The combined influence of these parameters corresponds to the lowest area ratio of 16 (refer to Figure 2.15).

Figure 2.16 shows the effect of varying the tube diameter on the diffusion mass flux (the data points represented on the graph are for a constant diffusion path length and system temperature, as indicated). As expected, the mass flux does indeed decrease with a decrease in the tube diameter. This merely illustrates that the mass flux of the naphthalene vapour moving upwards within the Stefan tube decreases as the cross-sectional area available for movement decreases.

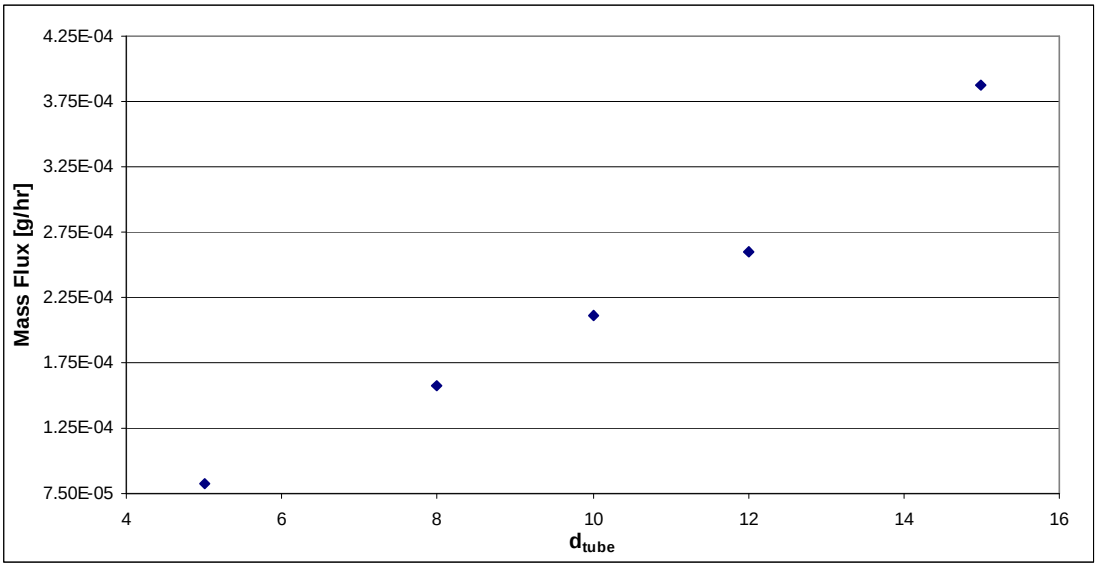

Figure 2.16: *Diffusion mass flux at various tube diameters (Experimental conditions: (a) Diffusion path length = 62 mm, (b) Temperature = 47 ^{o}C)*

Figure 2.14, however, shows that the diffusion coefficient increases with decreasing tube diameter (at a constant diffusion path length). The decrease in the mass flux with decreasing tube diameter (Figure 2.16) is therefore insufficient. This, in effect, means that although the mass flux decreases with decreasing tube diameter the mass flux is

still higher than expected/predicted. This results in a larger than expected diffusion coefficient.

It therefore appears that wall effects possibly interfere with the natural diffusion process when the ratio of the wall area along the diffusion path length to the naphthalene surface area becomes too large. The accurate measurement of the diffusion coefficient of naphthalene through the Stefan tube method is therefore highly dependant on the tube diameter and diffusion path length and care needs to be taken in obtaining the optimum conditions for these parameters.

Time to reach steady state:

Figure 2.17 shows the results for when equation 2.30 is applied to the system where naphthalene vapour diffuses through air in a tube with a diffusion path length of 82 mm and a diffusion coefficient corresponding to the diffusion at 26 ^{o}C. This system relates to the situation in the present experiments requiring the longest period of time to approach steady state. The sublimation rate reaches 99.92 % of the steady state rate in approximately 11 minutes and the assumption of steady state diffusion is therefore acceptable, since the duration of the experiments performed on the naphthalene/air system are usually in the region of 20 hours.

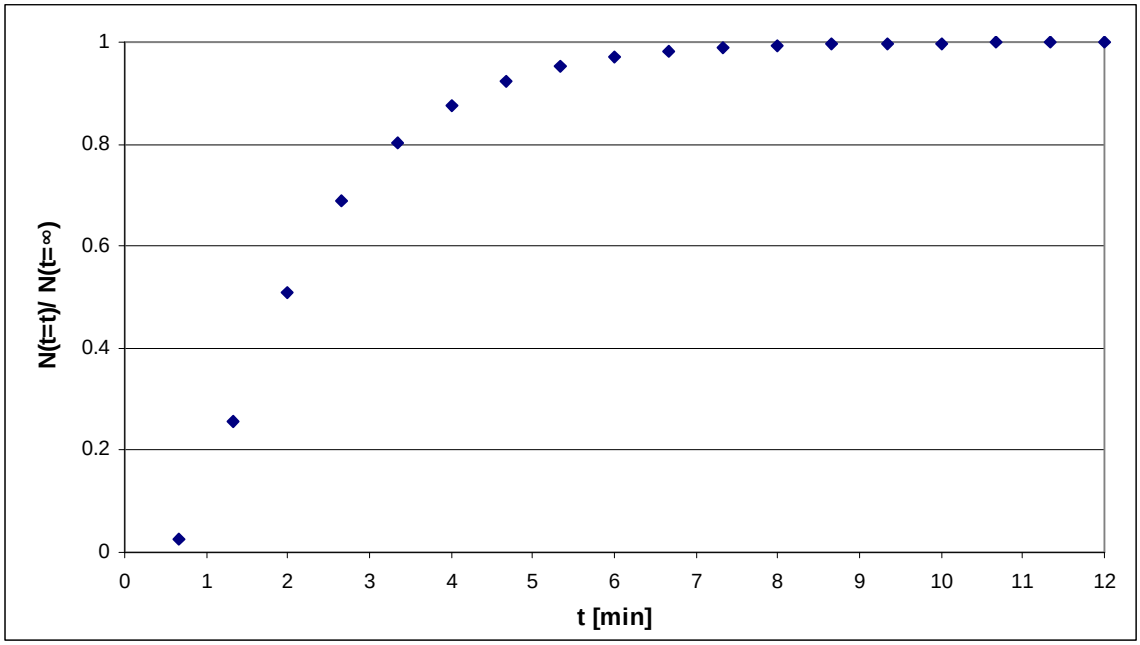

Figure 2.17: *Time to reach steady state for the naphthalene/air system*

The issue of the time required for the solid naphthalene to approach thermal stability is, however, in question. Due to the long experimental duration of the experiments the assumption is made that the time to reach thermal stability is negligible. This assumption is confirmed through the investigation performed by Cho *et al.* [27]. As stated in section 2.2.1 Cho *et al.* [27] employed a much larger volume of solid naphthalene in their experimental procedure and performed their experiments over a shorter time span than the experiments in the present investigation. The temperature range over which their experimental procedures were conducted were also similar to the range of temperatures investigated in the present study. Their choice of experimental setup made it possible to monitor the temperature of the solid naphthalene throughout the duration of their experiments. Even though Cho *et al.* [27] made use of a significantly larger volume of solid naphthalene and shorter experimental duration than in the current study they still found that the time to reach thermal stability is negligible. The assumption that the time to reach thermal stability in the present investigation is negligible is therefore valid.

The final results for the naphthalene/air system are shown in Figure 2.18, where the results are compared with the findings from the previous investigators as well as the empirical correlations by Arnold [35] and Fuller *et al.* [36].

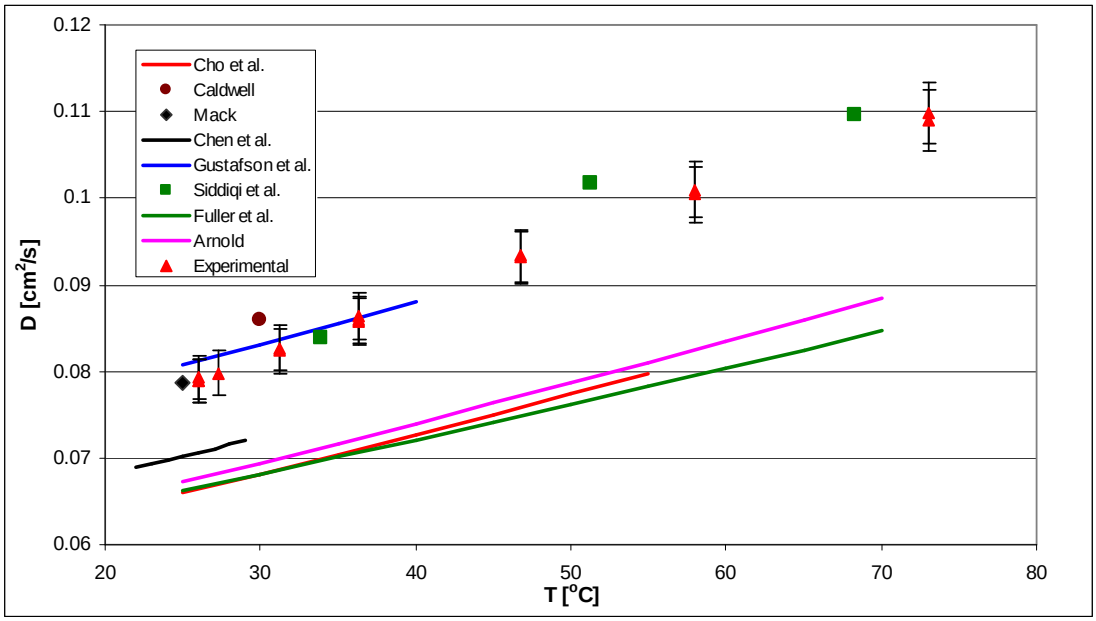

Figure 2.18: *Diffusion coefficient results for the naphthalene/air system compared with previous investigators and empirical correlations*

The diffusion coefficient results for the present study (marked Experimental on the graph) includes an error analysis, which is based on the readings of the mass, temperature and experimental duration, as well as the determination of the diffusion path length and naphthalene surface area. A maximum absolute error of 4.5 % was found for the system at 26°C. This error was mainly the result of the large effect that temperature has on the determination of the saturated vapour pressure of naphthalene at low temperatures. At higher system temperatures this error is lower, since a similar error in the temperature measurement at these elevated levels does not result in such a large error in the vapour pressure determination (this refers to the percentage error in the vapour pressure calculation). An error in the mass loss reading can also be significant at the lower temperatures, as a smaller total mass loss is logged and errors in the mass loss reading would therefore have a greater effect on the final determination of the diffusion coefficient. A detailed account of the error analysis performed is set forth in Appendix A2.5.

From Figure 2.18 it can be seen that the results obtained in the present study agree well with the results from Mack [31], Caldwell [14], Gustafson *et al.* [15] and Siddiqi *et al.* [28]. The results from Siddiqi *et al.* [28], however, show diffusion coefficient values that are slightly larger than the results obtained in this study, particularly at the higher temperatures. This discrepancy might be due to inaccuracies in the weighing procedure, since continuous calibration of the balance is required in the technique employed by Siddiqi et al [28]. The comment by Gustafson *et al.* [15] that the correlation by Fuller *et al.* [36] tends to underestimate the diffusion coefficient of the larger aromatic compounds, such as naphthalene, seems to be accurate. It therefore appears that the commonly accepted values for the diffusion coefficient of naphthalene in air, namely those of Cho *et al.* [27], may be in error.

One possible source of error for the investigation performed by Cho *et al.* [27] is that even though the activated charcoal in their experiment has the capacity to absorb the naphthalene diffusing towards it, the assumption that the concentration of naphthalene at the charcoal surface is zero may not valid. If the concentration of naphthalene at the charcoal is not zero, this would cause a smaller concentration gradient, which in turn would explain why the experimentally obtained diffusion coefficients are smaller than found in this study. The choice of the short diffusion path length (5 and 10 mm)

by Cho *et al.* [27] can also be a possible source of error. As in the present investigation, Cho *et al.* [27] assumed that the effective diffusion path length is the actual measured length of the diffusion tube. If the effective diffusion path length differs by only 1 mm from the measured tube length an error of up to 20 % can be obtained for the investigation by Cho *et al.* [27]. The same error of 1 mm for the effective diffusion path length in the current investigation, however, results in a maximum error of less than 2 %.

2.6.2 The diffusion of naphthalene in carbon dioxide (CO_2)

The optimal experimental parameters, i.e. diffusion tube diameter (15.2 mm) and diffusion path length (62 mm), used for the naphthalene/air system were found to be identical for the naphthalene/CO_2 system. The following section provides a detailed analysis into the identification of the optimum parameters. Figure 2.19 shows the experimental diffusion coefficient results obtained for the naphthalene/CO_2 system over the temperature range 25.4 to 73.1 ^oC.

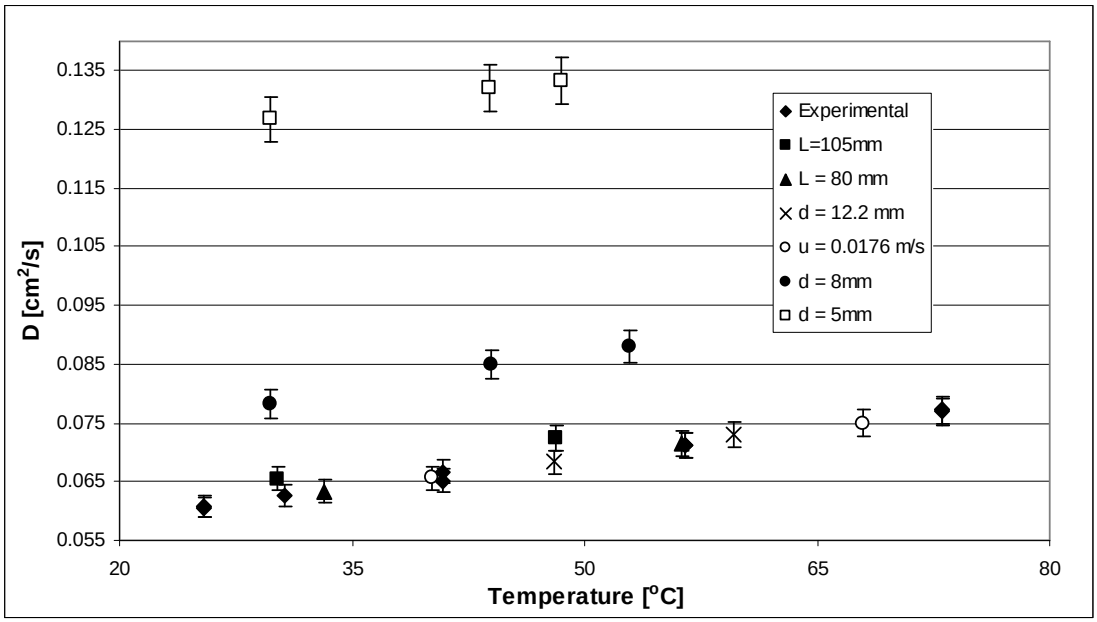

Figure 2.19: *Experimental diffusion coefficient results for the naphthalene/CO_2 system*

Figure 2.19 shows that the diffusion path length, diffusion tube diameter and gas linear sweep velocity were also varied. This was done in order to ensure that the

influence of possible wall interference and turbulence were negligible. The data points shown as 'Experimental' in Figure 2.19 were obtained through experimentation at the optimal tube diameter (15.2 mm), diffusion path length (62 mm) and gas sweep velocity (0.0088 m/s). From the graph it can be seen that for the 105 mm diffusion path length system (at a constant tube diameter of 15.2 mm) there was an approximate increase of 5 % in the experimentally determined diffusion coefficient. Virtually no difference was, however, observed between the measured diffusion coefficient values for the 62 and 80 mm diffusion path length systems.

The experiments were also conducted for four different tube diameters, namely 15.2, 12.2, 8 and 5 mm, while the diffusion path length was kept constant at 62 mm. Figure 2.19 shows that the diffusion coefficient measurements for the two tube diameter experiments of 15.2 and 12.2 mm were virtually identical. The experimental results for the 5 and 8 mm diameter test once again showed a marked increase. The assumption that the influence of possible wall interference was negligible at the chosen optimal parameters was therefore valid, as it was only at the smaller diameter tests that an increase in the diffusion coefficient was observed.

Two experiments at gas sweep velocities of 0.0088 and 0.0176 m/s were also performed at the chosen parameters set forth previously. No effect on the measured diffusion coefficient was observed by the variation in the gas flow rate. The assumption that turbulence at the top of the diffusion tube is negligible was therefore valid. The same approach for the error analysis performed on the naphthalene/air system was followed for the naphthalene/CO_2 system.

Figure 2.20 indicates the time to reach steady state when naphthalene vapour diffuses through CO_2 in a tube with a diffusion path length of 80 mm and a diffusion coefficient corresponding to the diffusion at 25.4 ^{o}C (these parameters represent the situation where the longest time is needed in the present investigation to obtain steady state conditions). The sublimation rate reached 99.93 % of the steady state rate in approximately 15 minutes (900 s) and the assumption of steady state diffusion was therefore acceptable, since the duration of the experiments performed on the naphthalene/CO_2 system were usually in the region of 50 hours for the experiments at the lower temperatures.

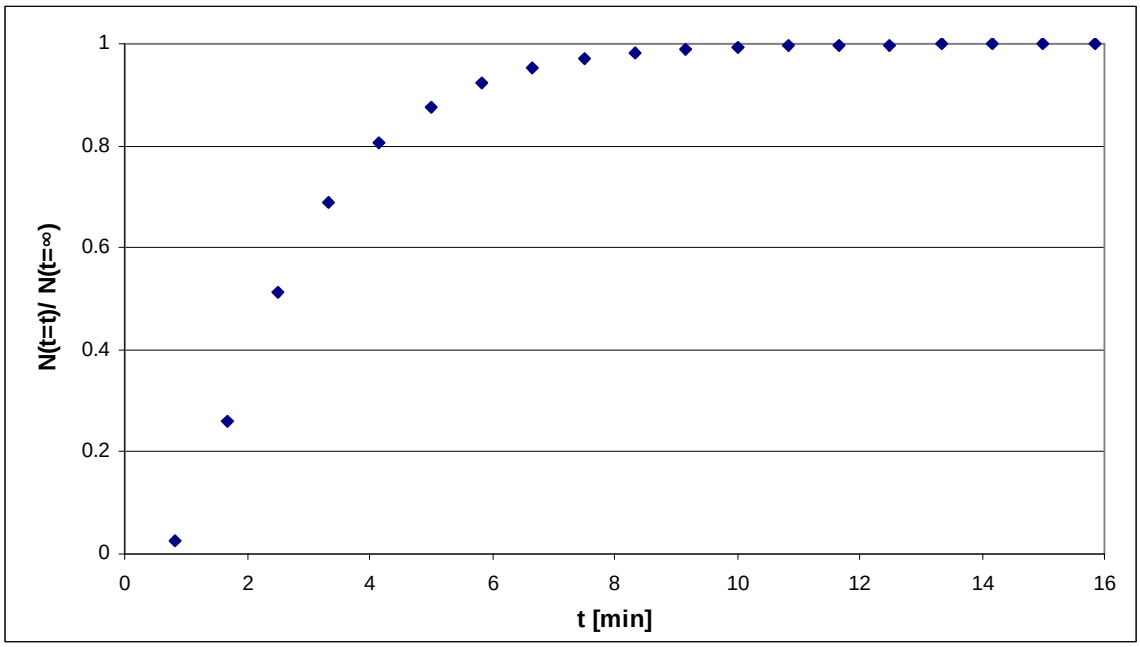

Figure 2.20: *Time to reach steady state for the naphthalene/CO_2 system*

The optimal parameters for the naphthalene/CO_2 system were therefore as follows:

- Diffusion tube diameter = 15.2 mm
- Diffusion path length = 62 mm
- Gas sweep velocity = 0.0088 m/s (actual)

From the Chapman-Enskog kinetic theory of gases (equation 2.1 in section 2.2.2) it can be seen that the diffusion coefficient is indirectly proportional to the total absolute pressure at which the experiments are performed. This fact is also mentioned by numerous investigators in literature [22, 28, 38]. This, in effect, means that if the system pressure is doubled, the diffusion coefficient is halved and vice versa.

Figure 2.21 shows the results for the diffusion coefficient measurement of the naphthalene/CO_2 system at an absolute system pressure of 2 bar (200 kPa). The graph also shows the experimental results for the atmospheric pressure system, which is adjusted to 100 kPa, as well as the theoretical results for the 200 kPa system (these values were simply calculated by halving the 100 kPa experimental results).

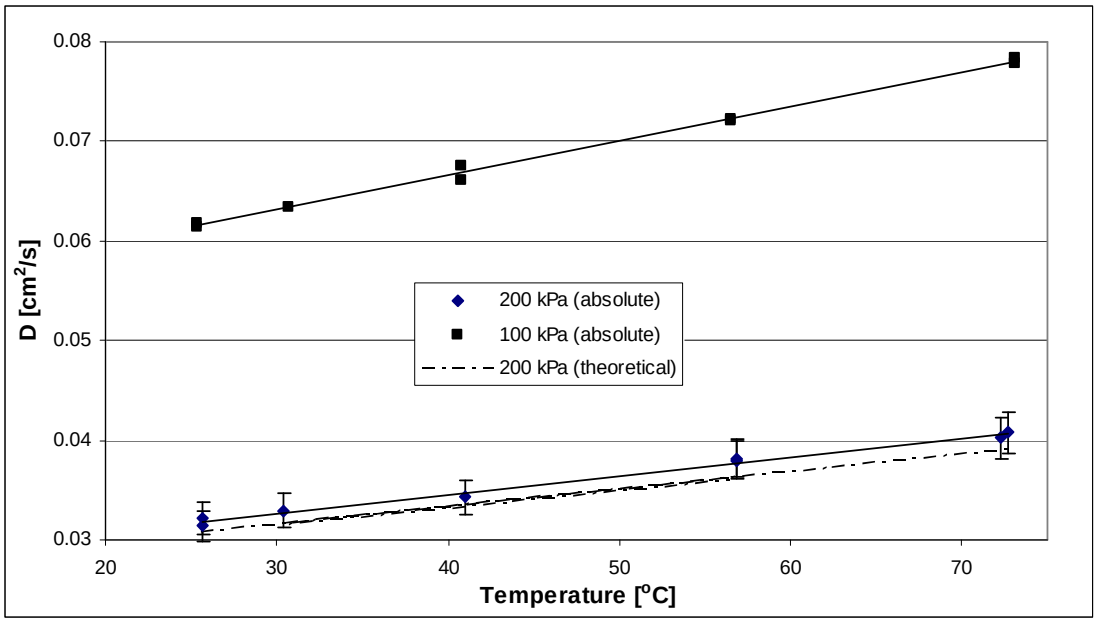

Figure 2.21: *Results obtained for the naphthalene/CO_2 system at 200 kPa absolute pressure*

From the graph it can be seen that the results obtained closely match the theoretical results (within a 3 % margin). The results therefore indicate that the diffusion coefficient/total absolute pressure relationship is indeed accurate. The error bars on the graph are, however, set to 5 % as the accuracy of the pressure reading from the mechanical pressure gauge (glycerine filled) adds an additional uncertainty to the measurements.

2.6.3 The diffusion of naphthalene in helium

The optimal experimental parameters, i.e. diffusion tube diameter (15.2 mm) and diffusion path length (62 mm), used for the experiments performed in air and CO_2 were once again identical for the naphthalene/helium system. The following section provides a detailed account of the identification of the optimal parameters. Figure 2.22 shows the experimental diffusion coefficient results obtained for the naphthalene/helium system over the temperature range 25.2 to 71.4 ^{o}C. The tube diameter, diffusion path length and gas sweep velocity were once again varied in order to ensure that the possible influence of wall interference and turbulence on the measured diffusion coefficients remained negligible. The data points shown as 'Experimental' in Figure 2.22 were obtained through experimentation at the optimal

tube diameter (15.2 mm), diffusion path length (62 mm) and gas sweep velocity (0.024 m/s).

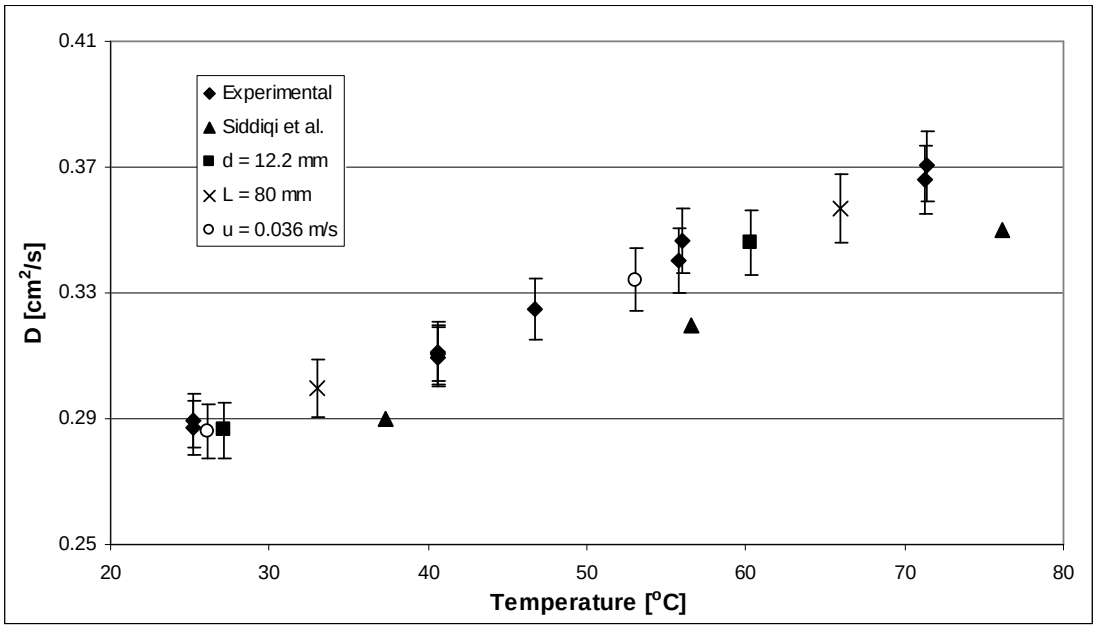

Figure 2.22: *Experimental diffusion coefficient results for the naphthalene/helium system*

From Figure 2.22 it can be seen that the results obtained for the 62 and 80 mm diffusion path length systems (at a constant tube diameter of 15.2 mm) were virtually identical. No variation in the measured diffusion coefficients could be detected by decreasing the tube diameter from 15.2 to 12.2 mm (at a constant diffusion path length of 62 mm). From these findings it is clear that the influence of possible wall interference does not significantly influence the experimentally obtained diffusion coefficient at the chosen optimal parameters. The assumption of a negligible amount of wall interference was therefore assumed to be valid. Experiments were also performed for a higher gas sweep velocity of 0.036 m/s. The results obtained for the two different carrier gas sweep velocities are almost identical and the assumption that the effect of turbulence is negligible is therefore valid.

Figure 2.22 also shows the only diffusion coefficient measurements for the naphthalene/helium system found in literature. These results were compiled by Siddiqi *et al.* [28] and the measurement technique employed was the thermo-gravimetric analysis method. From the graph it can be seen that the results from this

study and the results obtained by Siddiqi *et al.* [28] compare well, with a deviation of 5 to 7 %. As mentioned in the discussion for the naphthalene/air system, the thermo-gravimetric analysis method needs continuous calibration of the balance (buoyancy effects etc.). The discrepancy between the results might therefore be due to calibration errors with the balance.

Figure 2.23 shows the time needed to obtain steady state conditions for the naphthalene/helium system. The results for Figure 2.23 were calculated for a diffusion path length of 80 mm and a diffusion coefficient at 25.2 ^{o}C (these are the conditions for which the present system needs the longest amount of time to reach steady state). From the graph it can be seen that the sublimation rate reached 99.95 % of steady state in approximately 3 minutes. The assumption of steady state diffusion is therefore accurate, seeing as the sublimation of naphthalene in helium (at low temperatures) is usually performed over a time span of approximately 15 hours. It can also be seen that the time to reach steady state for the diffusion in helium is much shorter than for the previous two systems investigated (3 minutes compared to 11 and 15 minutes). This is due to the higher diffusion rate observed for this system.

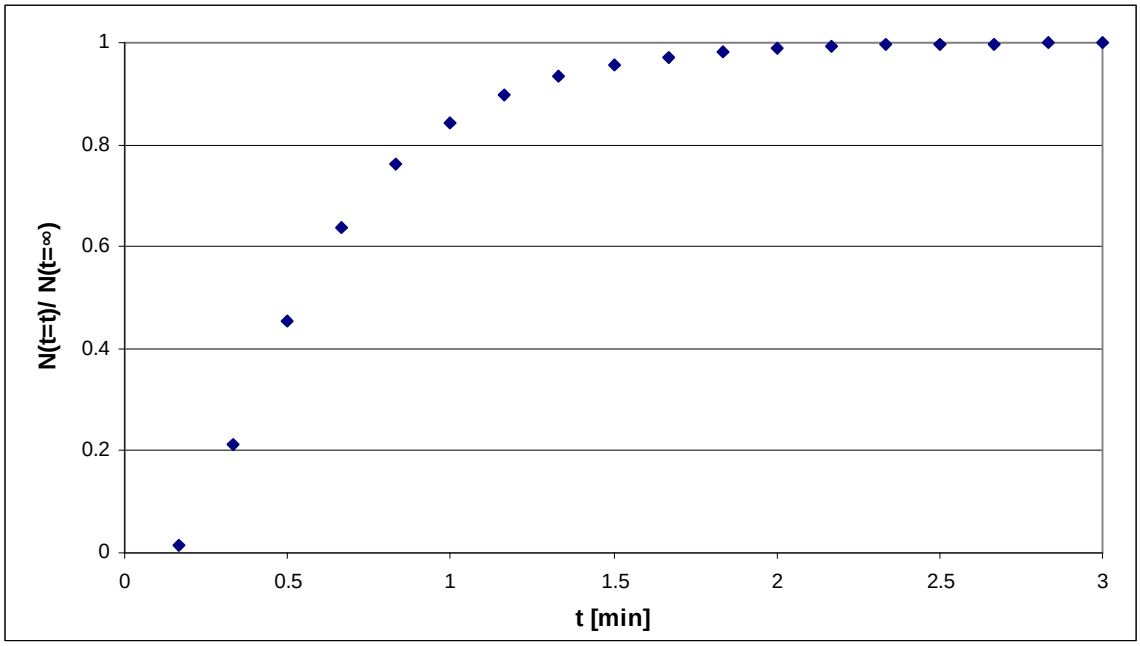

Figure 2.23: *Time to reach steady state for the naphthalene/helium system*

Figure 2.24 shows the experimental results obtained for the naphthalene/helium system at 200 kPa (absolute), as well as the theoretical results (calculated in the same

fashion as was done for the naphthalene/CO_2 system). From the graph it is clear that the repeatability of the measurements at each temperature was not as good as was observed for the naphthalene/CO_2 system, with differences of up to 5% found at certain temperatures. This was due to the difficulty in maintaining a stable total pressure within the diffusion unit. Throughout the duration of the experiments constant manipulation of the needle valve was necessary to obtain a reasonably stable pressure reading. Even with this manipulation a perfectly stable pressure reading could not be achieved. This difficulty in maintaining a constant pressure was attributed to the very low density, i.e. molar mass, of helium gas. Obtaining a sufficiently tightly sealed diffusion unit was therefore a problem that might warrant further investigation.

Even though the results tend to vary over quite a large range, Figure 2.24 still represents results that are reasonably close to the theoretical results for the system at 200 kPa (absolute). The results therefore indicate that the diffusion coefficient/total pressure relationship can indeed be assumed to be accurate.

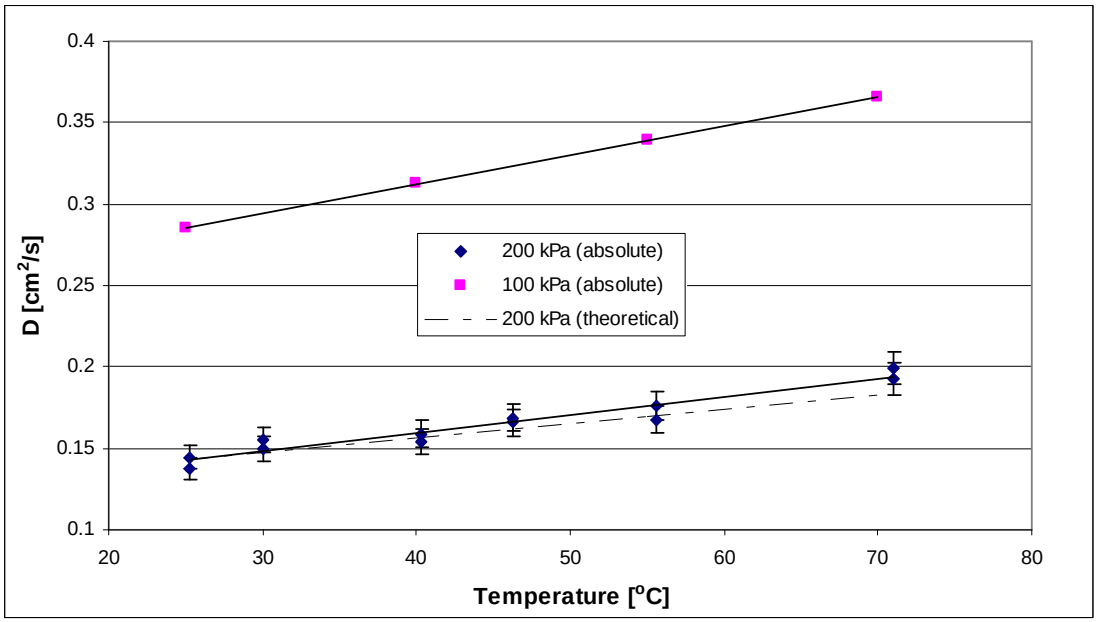

Figure 2.24: *Results obtained for the naphthalene/helium system at 200 kPa absolute pressure*

2.6.4 Investigating the effect of changes in the tube diameter

As was seen in the previous sections the diffusion coefficient seems to be affected (increased) when the diffusion tube diameter is decreased below a certain value. Although the diffusion mass flux decreases with decreasing tube diameter (this is due to a smaller area available for the diffusing specie, i.e. naphthalene), the diffusion coefficient increases. As stated in section 2.6.1 this indicates that the diffusion mass flux does not decrease enough, or at a fast enough rate, to cause the diffusion coefficient to remain constant. The question therefore becomes the following: *What causes the higher than expected diffusion mass flux at the lower tube diameters*?

As stated previously, in the investigation by Cho *et al.* [27] the possibility of wall interference is mentioned. This would explain the higher than expected values of the diffusion mass flux and the diffusion coefficient. However, this phenomenon is only speculation and no evidence of the actual occurrence of wall interference could be found by Cho *et al.* [27] in their study.

A more recent investigation by Salcedo-Diaz *et al.* [41] presented a different theory. This study specifically targeted the effect that decreasing the tube diameter has on the accuracy of tests performed with a Stefan tube. In the study in question the Stefan tube method was investigated for the Nitrogen/water system at different tube diameters. The study showed that the classic Stefan-diffusion equation (Fick's law), as used in the present study, was accurate for wide tubes but became increasingly inaccurate when dealing with narrower tubes. Salcedo-Diaz *et al.* [41] stated that the reason for this inaccuracy was that for narrow tubes the viscous shear effects of the individual species starts to dominate, causing velocity gradients between the species. Circulation of the carrier gas within the tube therefore occurs and the assumption that the carrier gas remains stagnant within the tube is no longer valid.

These 'shear effects' were discussed in detail in the multicomponent diffusion review article by Kerkhof *et al.* [42]. Kerkhof *et al.* [42] stated that for diffusion occurring in large diameter tubes the classic approach (Fick's law) is accurate. In the classic approach the flow approaches that of a single species, the mixture. In other words, for diffusion in large diameter tubes a single equation of motion is sufficient for the

whole mixture, with a single mixture viscosity (classic approach). The theory is that for diffusion in large diameter tubes the friction force between the different species is more important than the viscous shear force between the species. The classic approach therefore assumes that the gradients between the species velocities are small enough to be ignored. However, when dealing with narrow tubes the shear forces between the species starts to dominate causing the classic approach, which does not account for shear forces, to become less accurate. The assumption of negligible velocity gradients is therefore no longer valid for narrow tube diameters.

Figure 2.25 illustrates the deviation (%) in the diffusion coefficient for the various tube diameters investigated for each system studied. From the graph it is clear that for the naphthalene/helium system the diffusion coefficient only deviates from the expected constant values at tube diameters below 8 mm. At the smallest tube diameter investigated (5 mm) the deviation was close to 30%. For both the naphthalene/CO_2 and the naphthalene/air system the deviation is more pronounced and starts occurring at tube diameters below 12.2 mm. For the naphthalene/air system the deviation is approximately 96% for the smallest tube diameter investigated, while the naphthalene/CO_2 system shows an even larger deviation of approximately 105% at the smallest tube diameter investigated.

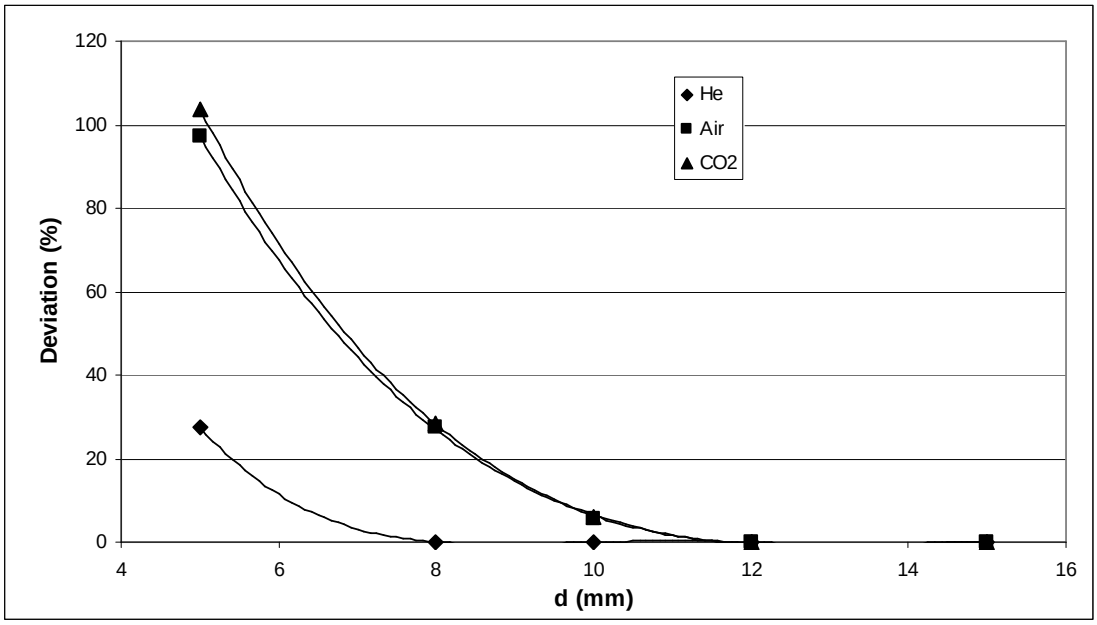

Figure 2.25: *Deviation of the diffusion coefficient versus tube diameter for the three systems investigated*

From Figure 2.25 it is therefore clear that the density (molecular mass) of the carrier gas greatly influences the diffusion coefficient at the smaller tube diameters. Figure 2.25 shows that, at the smaller tube diameters, a less severe deviation from the expected diffusion coefficient is observed when a less dense carrier gas is employed. This is evident by the fact that the denser carrier gas (CO_2) exhibits the largest deviation, while the least dense gas (helium) exhibits the smallest deviation.

This lends more credibility to the findings by Salcedo-Diaz *et al.* [41] and Kerkhof *et al.* [42], since viscous shear forces between the individual species in the denser carrier gas (more viscous gas) will be more pronounced than for the less dense carrier gases. The lack of evidence for the occurrence of wall interference in the Stefan tube system further extends the credibility of the shear effects explanation for the increase in the diffusion coefficients at the lower tube diameters.

2.6.5 Correlating the results

From the previous sections it is clear that the carrier gas density has a significant impact on the diffusion rate of the naphthalene vapour. This sensitivity of diffusion rate to gas density was also observed by Siddiqi *et al.* [28] in his naphthalene sublimation experiments.

From the naphthalene sublimation tests performed in air, helium and CO_2 (sections 2.6.1, 2.6.2 and 2.6.3) it is evident that the rate of diffusion increases as the density of the carrier gas decreases. This is logical, since the upward movement of the naphthalene molecules in the diffusion tube will occur more rapidly if less obstructions are encountered in the medium through which the transport occurs, which is the case for less dense carrier gases. Figure 2.26 illustrates the relationship between the experimentally obtained diffusion coefficient for each system investigated. From the graph it is clear that the diffusion coefficient is greater for the less dense carrier gas, i.e. helium, while the densest carrier gas, i.e. carbon dioxide, exhibits the lowest diffusion coefficient.

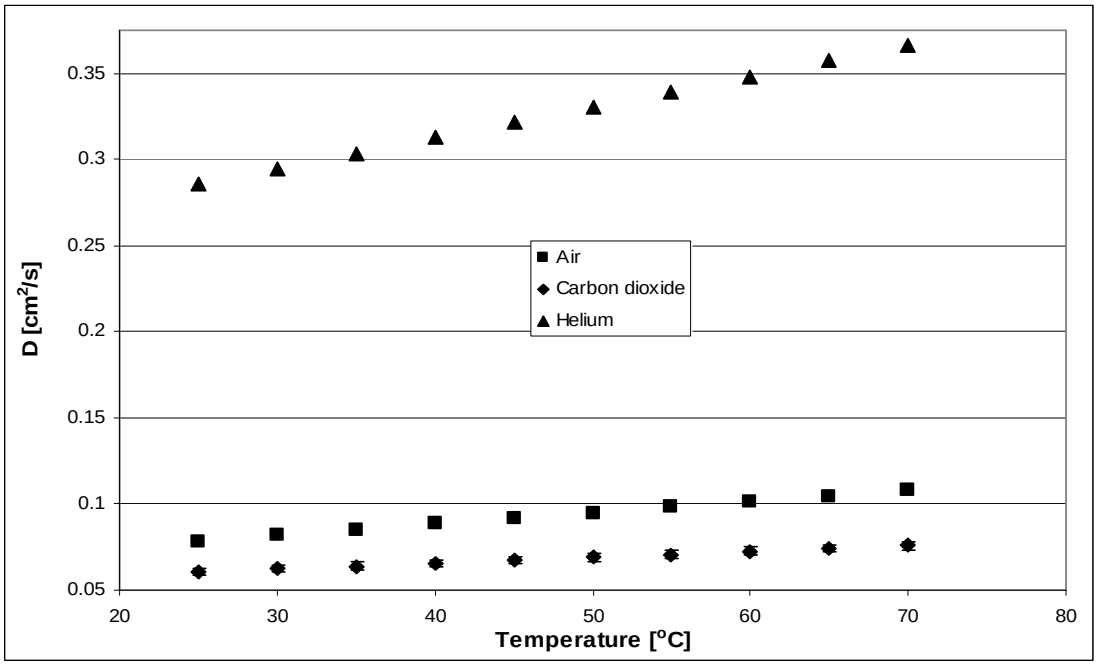

Figure 2.26: *Comparison between the experimentally obtained diffusion coefficient data for each system investigated*

The next step is therefore to set up a correlation that predicts the diffusion coefficient of naphthalene in different carrier gases. A least squares approach is followed in order to obtain an accurate correlation that incorporates the minimum number of variables. Initially a correlation containing a temperature and carrier gas density term was evaluated, but the resulting correlation failed to predict the diffusion coefficient to within the 95 % certainty limit over the whole experimental temperature range. However, by adding terms for the molecular weight and viscosity of the carrier gas, as well as a term for the saturated vapour pressure of naphthalene the predictions from the correlation proved to be sufficiently accurate. The final correlation for the prediction of the diffusion coefficient of naphthalene in air, helium and CO_2 is as follows:

$$D = 1.034\times10^{-3}.\frac{T^{0.0986}\cdot M_G^{2.24}\cdot \mu_G^{0.261}}{\rho_G^{2.86}\cdot p_{Naph}^{0.0731}} \qquad (R^2 = 0.9997) \qquad (2.33)$$

where: D is the diffusion coefficient [cm^2/s]

ρ_G is the density of the carrier gas [kg/m^3]

T is the system temperature [^{o}C]

M_G is the molecular weight of the carrier gas [g/mol]

μ_G is the dynamic viscosity of the carrier gas [Pa · s]

p_{Naph} is the vapour pressure of naphthalene at the system pressure [Pa]

Figures 2.27 and 2.28 shows how the predicted values for the diffusion coefficient (using equation 2.33) compare with the experimental measurements. Figure 2.27 illustrates the comparison between the experimental and correlated results in the form of a parity plot. From this graph it can be seen that the correlated and experimental results match very well.

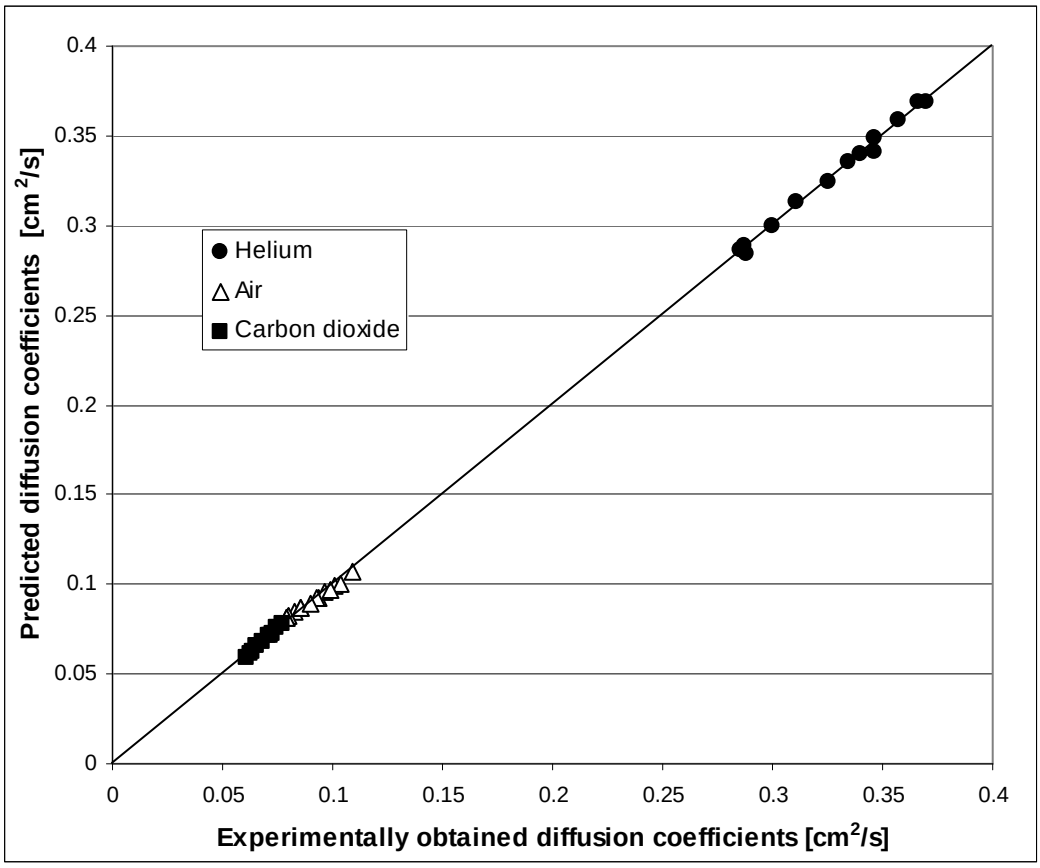

Figure 2.27: *Parity plot between the correlated and experimental results for the diffusion coefficient of naphthalene in air, helium and CO_2.*

Figure 2.28 shows the deviation (in %) between the predicted and experimentally obtained values. From the graph it can be seen that the predicted values for all three systems lie within the 95 % certainty limit, with the predictions for the naphthalene/helium system being the most accurate (virtually all the predictions are

within the 1 to -1 % deviation limits). The predictions for the naphthalene/CO_2 system are also accurate, with virtually all the predictions being in the 2 to -2 % deviation limits. Of the three systems investigated the predictions for the naphthalene/ air system are the least accurate. Virtually all the predictions for the naphthalene/air system, however, are within the 3 to -3 % deviation limits. In order to obtain accurate predictions using the correlation presented by equation 2.33 it is recommended that the correlation only be used over the temperature range of 25 to 73 ^{o}C.

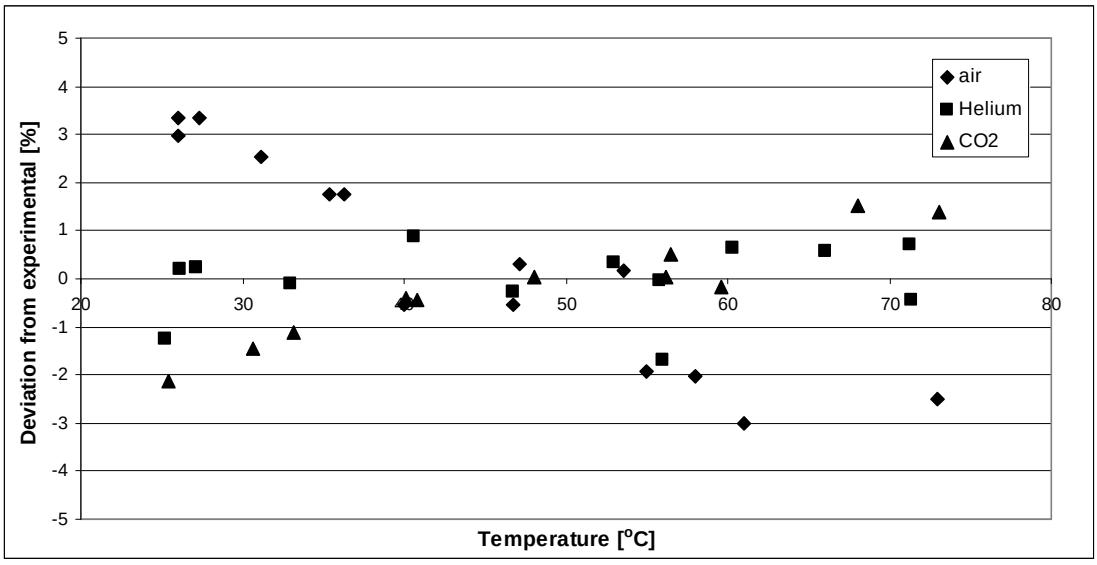

Figure 2.28: *Deviation (%) between the correlated and experimental results*

2.7 Concluding Remarks

The following conclusions are drawn from the measurement of the diffusion coefficient of naphthalene in different carrier gases:

- The diffusion coefficient of naphthalene in air is well documented in literature, but the diffusion coefficient of naphthalene in carrier gases other than air is virtually non-existent. The only additional system researched was the investigation performed by Siddiqi *et al.* [28] where naphthalene was sublimated in helium.

- Although the naphthalene/air system is widely researched, consensus has not been reached on what the actual diffusion coefficient should be. The results obtained by Cho *et al.* [27] are widely accepted as the most accurate values for the diffusion coefficient of naphthalene in air [22]. Numerous investigators, whose research precede and follow the work by Cho *et al.* [27], have found results that are approximately 20 % larger in magnitude. The results from this study compare well with the results obtained by the researchers whose findings contradict those of Cho *et al.* [27]. It therefore seems that the previously accepted values for the diffusion coefficient of naphthalene in air, by Cho *et al.* [27], may be inaccurate.

- The main misgiving that Cho *et al.* [27] had with the two researchers whose work preceded his own was that possible wall interference could influence the natural diffusion process, thus increasing the measured diffusion coefficient above the actual value. No proof, only speculation was offered as to the possible adverse effects of wall interference on diffusion coefficient measurements in the Stefan tube method. The possibility of turbulence (from too high gas sweep velocities) was an additional error source mentioned by Cho *et al.* [27]. In the present study the possible influence of wall interference was investigated by varying the area ratio of the wall area along the diffusion path length to the naphthalene surface area. This was done by varying the tube diameter and the diffusion path length. All three systems investigated exhibited an unexpected increase in the experimentally determined diffusion coefficient when the diffusion tube diameter was decreased below a certain value. This increase was found to be more pronounced the denser the carrier gas used. Although possible wall interference effects was set forth as a likely explanation for this phenomenon, by Cho *et al.* [27], no evidence was found to confirm this. Recent work on the Stefan tube system [41, 42], however, showed that viscous shear effects of the individual species start to dominate when the diffusion tube diameter becomes too small. These viscous shear effects are not taken into account in the determination of the diffusion coefficient by the classic equations, as was used in the present study. These shear effects lead to velocity gradients and causes circulation of the carrier gas within the diffusion

tube. One of the main assumptions of the Stefan diffusion method, namely that the carrier gas remains stagnant within the diffusion tube, is therefore no longer valid. The use of the classic Stefan diffusion equation (Fick's law) therefore becomes inaccurate at small diffusion tube diameters.

- The optimum operating conditions were as follows for the three systems investigated (these parameters relate to the conditions where the possible error sources mentioned by previous researchers were minimised):
    - Diffusion path length = 62 mm
    - Diffusion tube diameter = 15.2 mm
    - Carrier gas sweep velocity = 0.0107 m/s (naphthalene/air system)
    - Carrier gas sweep velocity = 0.0088 m/s (naphthalene/CO_2 system)
    - Carrier gas sweep velocity = 0.024 m/s (naphthalene/helium system)

- A comparison between the results obtained in the three systems investigated showed that the rate of diffusion of the naphthalene vapour was strongly influenced by the density of the carrier gas. It was found that the diffusion rate increased as the carrier gas density decreased. This is logical as the less dense carrier gases will provide a medium for diffusion that contains fewer obstructions to the diffusion of the naphthalene molecules.

- A correlation predicting the diffusion coefficient of naphthalene in different carrier gases was subsequently created through a least squares analysis. The correlation requires, as input parameters, the molecular weight, density and viscosity of the carrier gas as well as the vapour pressure of naphthalene and the system temperature. A comparison between the results from the correlation and the experimentally obtained measurements proved satisfactory; with the predicted values over the entire temperature range investigated falling within the 95 % certainty limit. The resulting correlation was as follows:

$$D = 1.034 \times 10^{-3} . \frac{T^{0.0986} \cdot M_G^{2.24} \cdot \mu_G^{0.261}}{\rho_G^{2.86} \cdot p_{Naph}^{0.0731}} \qquad (R^2 = 0.9997) \qquad (2.33)$$

It is recommended that the Stefan diffusion apparatus be rebuilt/adapted in order to test the influence that increasing the tube diameter has on the diffusion coefficient. The maximum tube diameter possible in the current study is 15mm. However, by increasing the diameter of the protuberance at the bottom of the laminar gas flow chamber (refer to Appendix A1 for detail design) it is possible to increase the maximum tube diameter to approximately 50mm. Care, however, needs to be taken when increasing the tube diameter, especially when dealing with the *open* Stefan tube method. With the *closed* tube method the effects of turbulence is a non-issue, but increasing the tube diameter in the *open* tube method could give rise to turbulence. The effect of turbulence therefore needs to be carefully monitored if the tube diameter is increased. In addition, a larger tube diameter will result in a longer time for thermal stability to be reached. Methods for monitoring the temperature of the solid naphthalene should therefore be compiled.

CHAPTER **3**

Mass Transfer in Structured Packing

3.1 Introduction

The use of structured and randomly packed columns is an important method in mass and heat transfer equipment [2, 4, 43-46]. It is widely used in the chemical process industries, typically in processes such as distillation, extraction, absorption, etc. [4, 47, 48]. Structured packing in particular has become irreplaceable in the process industries, mainly due to the improved capacity and efficiency and lower pressure drop that it offers in contrast to the previous contacting methods [44, 45, 49].

The packed bed height equivalent to a theoretical plate (HETP) method is often used in order to express the mass transfer performance of a packed column in distillation operations [3, 4, 48, 50]. According to the mass transfer in packed columns review paper by Wang *et al.* [4], the two film theory can be applied to establish the relationship between HETP and the height mass transfer unit for gas phase (HTU_G) and liquid phase (HTU_L). This relationship is given by:

$$HETP = \frac{\ln \lambda}{\lambda - 1}\left(HTU_G + \lambda HTU_L\right) \tag{3.1}$$

By including the definitions of HTU_G and HTU_L, equation 3.1 can be expressed as follows:

$$HETP = \frac{\ln \lambda}{\lambda - 1}\left(\frac{u_{G,s}}{k_G a_e} + \lambda \frac{u_{L,s}}{k_L a_e}\right) \tag{3.2}$$

where: λ is the stripping factor

$u_{G,s}$ is the gas phase superficial velocity [m/s]

$u_{L,s}$ is the liquid phase superficial velocity [m/s]

k_G is the gas phase mass transfer coefficient [m/s]

k_L is the liquid phase mass transfer coefficient [m/s]

a_e is the effective interfacial area of the packing [m^2/m^3]

In order to use the model represented in equation 3.2, it is therefore important to have accurate correlations for the prediction of the mass transfer coefficient [3, 4, 51]. It is, however, widely agreed that the resistance in the vapour phase determines the overall mass transfer rate [3, 5]. The focus of this chapter is therefore on the vapour phase mass transfer coefficient in structured packing. In order to create the necessary correlations for the prediction of the vapour phase mass transfer coefficient accurate diffusion coefficient data is needed. As stated in Chapter 1 (equation 1.1) the vapour phase mass transfer coefficient can be correlated through a simple power law series. The flow properties (velocity, etc.) are taken into account through the Reynolds number term, while the transport properties (diffusion coefficient, etc.) are taken into account by the Schmidt number term. The diffusion coefficient data gathered through the investigation in Chapter 2 is therefore essential. By applying the diffusion coefficient data from Chapter 2 to the experimental results from this Chapter it will be possible to create a correlation for the prediction of the vapour phase mass transfer coefficient in the various carrier gases employed in this investigation.

3.2 Literature Review

The prediction of mass transfer coefficients (liquid and gas phase) for random packing is well documented in literature. The main published results include the work of Shulman *et al.*[52], Bravo *et al.* [53], Shi *et al.* [54], Wagner *et al.* [55] and Piche *et al.* [56]. Since the introduction of structured packing, however, research studies have been greatly promoted in this field, with the commercial appeal stemming from the advantages discussed in the previous section [4].

Due to the well-defined geometry of the channels formed by the structured packing elements and the accurate knowledge of the packing surface area, it has been assumed that the mass transfer process in structured packing can be modelled along the lines of the wetted-wall theory. This point of view has been implemented by numerous investigators in their studies of structured packed columns [6-10, 57-62]. The shortcomings of using wetted-wall experiments to predict the mass transfer rate in structured and random packings are therefore well known. The major shortcoming with the use of wetted-wall experiments to describe the mass transfer is that the wetted-wall analogy is based on the assumption of laminar flow [4]. Unfortunately, the presence of liquid flow instabilities, due to waves, film detachment etc., often negate this assumption [4]. The basic form of this theory was discussed in Chapter 1 and is once again provided:

$$Sh_G = a\,\mathrm{Re}_G^b\,Sc_G^c \tag{1.1}$$

where: $$Sh_G = \frac{k_G d_h}{D_G} \tag{1.2}$$

$$Sc_G = \frac{\mu_G}{D_G \rho_G} \tag{1.3}$$

$$\mathrm{Re}_G = \frac{\rho_G u_G d_h}{\mu_G} \tag{1.4}$$

The wetted-wall theory (equation 1.1) is robust and easy to use. A disadvantage of this method is that accurate diffusion coefficient data is needed when using the model to predict the mass transfer coefficient. Unfortunately, diffusion coefficient data for certain systems are not easily available in literature.

The mass transfer rate in structured packing can also be modelled through the penetration theory (also known as the surface renewal theory) [3, 50, 63]. The penetration theory states that a fluid element moves from the bulk fluid phase to an interface and resides at the interface for a certain exposure time (t_e). During the exposure time mass transfer occurs between the fluid element and the adjoining phase and this mass transfer process occurs through unsteady-state molecular diffusion.

During the exposure time the fluid element is inactive or moves along the interface in plug flow. After the exposure time, during which mass transfer occurs, the fluid elements return to the bulk fluid phase and are replaced by other fluid elements. The classic approach by this theory is the assumption that each fluid element has the same exposure time at the interface. A simplified schematic representation of this model is presented in Figure 3.1.

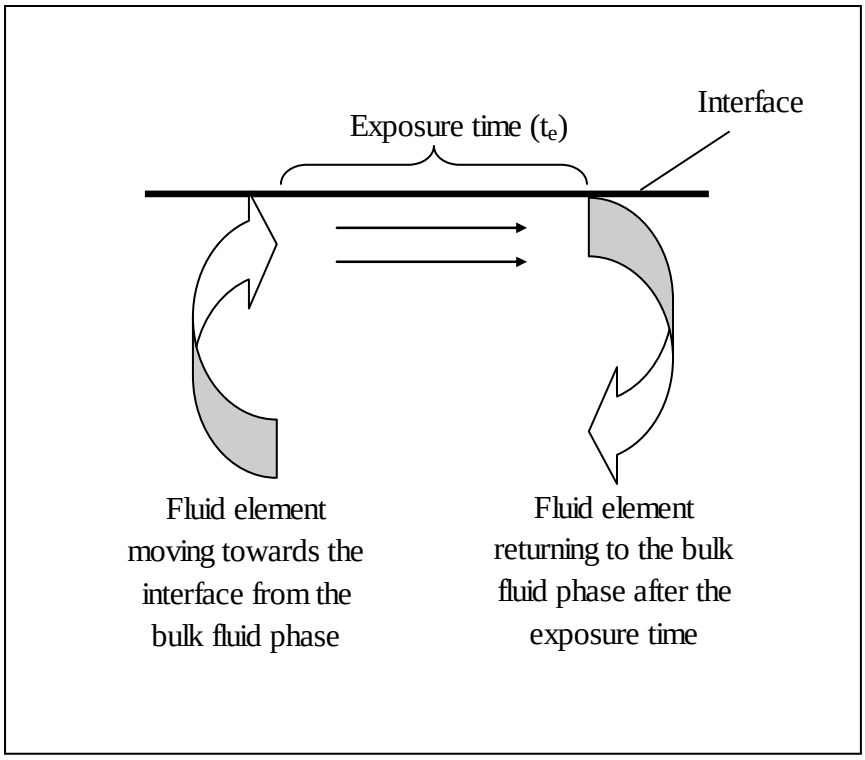

Figure 3.1: *Simplified schematic representation of the penetration theory*

The basic form of the equation for the calculation of the mass transfer coefficient, according to the penetration theory, is as follows:

$$k_G = 2\sqrt{\frac{D_G}{\pi \cdot t_e}} \qquad \text{[m/s]} \qquad (3.3)$$

The first investigation in the development of a model to predict the vapour phase mass transfer coefficient in structured packing was conducted by Bravo *et al.* [7]. The model (known as the SRP (I) model) was developed for a gauze-type structured packing and the vapour phase mass transfer coefficient is based on previous

investigations of wetted-wall columns. The correlation of Johnstone and Pigford [50] is used for the prediction of the vapour phase mass transfer coefficient (with minor adjustments to the original constants). It is also assumed that the effective surface area is equal to the specific surface area, i.e. complete wetting of the packing surface. The final correlation proposed by Bravo *et al.* [7] is as follows:

$$Sh_G = 0.0338\left(\frac{u_{G,e}\rho_G d_{eq}}{\mu_G}\right)^{0.8} Sc_G^{0.333} \tag{3.4}$$

where: $u_{G,e} = \dfrac{u_{G,s}}{\varepsilon \sin\theta}$ [m/s]

$d_{eq} = Bh\left(\dfrac{1}{B+2S} + \dfrac{1}{2S}\right)$ [m]

$u_{G,s}$ is the superficial gas velocity [m/s]

$u_{G,e}$ is the effective gas velocity [m/s]

ε is the void fraction [-]

θ is the corrugation angle [^{o}]

B, S and h is packing specific flow channel geometries [m]

The channel base (B), channel side (S) and crimp height (h) refers to the flow channel geometry of the structured packing. The parameters (B, S and h) can be obtained from the triangular cross section of the structured packing in question. Figure 3.2 depicts a schematic representation of the flow channel geometry of a structured packing element.

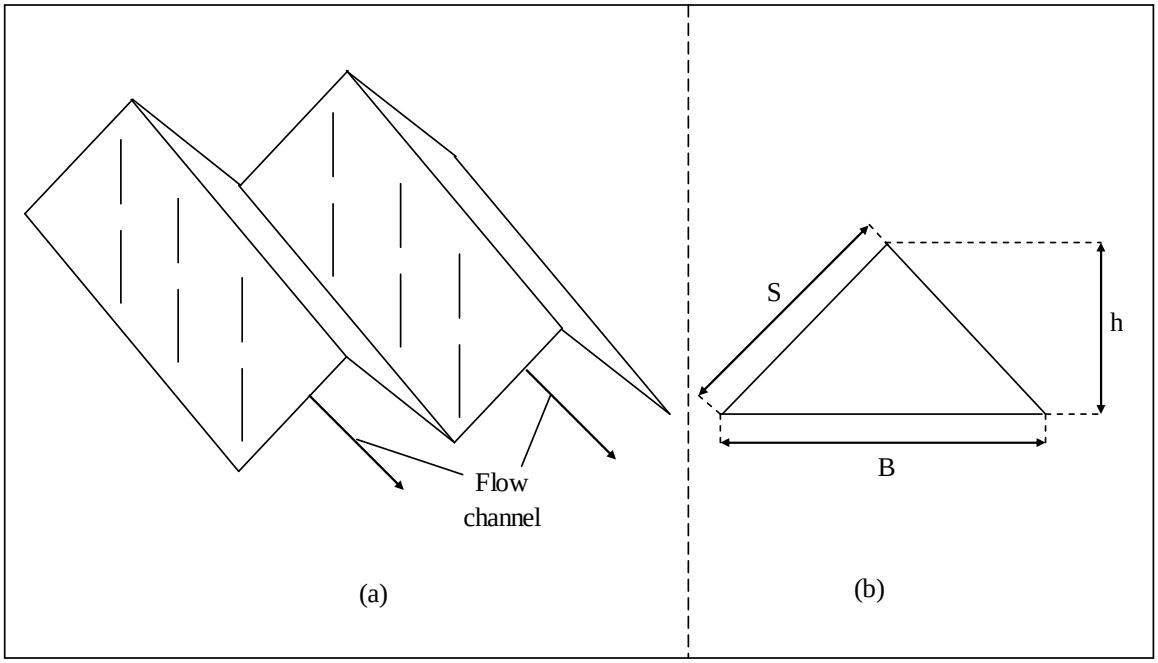

Figure 3.2: *Geometry of a structured packing sheet with (a) the arrangement and (b) the geometry of the triangular cross section of the flow channel.*

Nawrocki *et al.* [57] implemented similar relationships to those used by Bravo *et al.* [7] in their investigations on corrugated structured packing. In addition, Nawrocki *et al.* [57] included liquid distribution in their model to obtain more reliable liquid phase mass transfer coefficients [4]. The vapour phase mass transfer coefficient was modelled as proposed by Bravo *et al.* [7] (equation 3.4).

Rocha *et al.* [9, 64] improved and extended the model by Bravo *et al.* [7] and proposed the SRP (II) model. An important feature of the SRP (II) model is that the hydrodynamic performance and mass transfer of columns containing structured packing are related by a key factor, namely liquid holdup [4]. This term is used for the height of liquid 'held up' in the packing element. An increase in the liquid holdup will cause a decrease in the effective void fraction, which in turn will increase the pressure drop. In the SRP (II) model the wetted wall relationship has been retained, with minor adjustments to the constants. Additionally, the effective interfacial area is not assumed to be equal to the specific surface area, as is the case in the model proposed by Bravo *et al.* [7]. The empirical equation proposed by Shi *et al.* [54] is used to determine the effective surface area. The correlation proposed by Rocha *et al.* [9] for the prediction of the vapour phase mass transfer coefficient is as follows:

$$Sh_G = 0.054\left(\frac{\left(u_{G,e}+u_{L,e}\right)\rho_G S}{\mu_G}\right)^{0.8} Sc_G^{0.33} \qquad (3.5)$$

where: $u_{G,e} = \dfrac{u_{G,s}}{\varepsilon\left(1-h_L\right)\sin\theta}$ [m/s]

$u_{L,e} = \dfrac{u_{L,s}}{\varepsilon h_L \sin\theta}$ [m/s]

h_L is the fractional holdup of liquid

S, ε, θ, $u_{G,s}$ and $u_{G,e}$ has the same descriptions and units as for equation 3.4

Billet *et al.* [63] and Hanley *et al.* [8] also related the hydrodynamic performance and mass transfer of structured packing columns through the liquid holdup. Billet *et al.* [63] set up a model for the prediction of mass transfer in columns containing both random and structured packing. The approach of the model is the assumption that the effective empty space of random and structured packings can theoretically be substituted by vertical flow channels, through which the liquid trickles downward while the gas flows upwards counter currently. Both the vapour and liquid phase mass transfer correlations are developed through the application of the penetration theory, as opposed to the wetted wall theory [4]. These equations, however, contain numerous packing-specific constants which are only obtainable for a limited amount of commercially available structured packing. The correlation for the prediction of the vapour phase mass transfer coefficient proposed by Billet at al. [63] is as follows:

$$k_G a_e = C_G \frac{1}{\left(\varepsilon - h_L\right)^{1/2}} \frac{a^{3/2}}{d_h^{1/2}} D_G \left(\frac{u_{G,s}}{a\nu_G}\right)^{3/4} \left(\frac{\nu_G}{D_G}\right)^{1/3} \left(\frac{a_e}{a}\right) \quad [\mathrm{m^3/s}] \qquad (3.6)$$

where: $d_h = 4\dfrac{\varepsilon}{a}$ (hydraulic diameter [m])

C_G is the packing specific constant [-]

a is the specific surface area of the packing [m^2/m^3]

a_e is the effective surface area of the packing [m^2/m^3]

ν_G is the kinematic viscosity of the gas [m^2/s]

D_G is the vapour phase diffusion coefficient [m^2/s]

$u_{G,s}$ is the gas velocity with reference to the empty column cross-section [m/s]

d_h, h_L and ε has the same descriptions and units as for equation 3.4 and 3.5

Hanley *et al.* [8] based their correlation for the prediction of the vapour phase mass transfer coefficient on the wetted-wall analogy. The correlation looks remarkably similar to the correlation by Bravo *et al.* [7] and Rocha *et al.* [9], but changes have been made in the calculation of the effective vapour velocity ($u_{G,e}$). A common assumption in the calculation of the effective vapour velocity is that it can be determined by simply dividing the superficial vapour volumetric flux by the void fraction. According to Hanley *et al.* [8] this assumption is strictly true only when dealing with a dry packing. The reasoning behind this statement is that as more and more of the packing channels are obstructed, the effective vapour velocity increases in order to keep the total mass flow at a constant value. The correlation proposed by Hanley *et al.* [8] is as follows:

$$Sh_G = \left(\frac{d_{eq} K_V \left(\rho_L / \rho_G \right)^{0.5} \rho_G}{\varepsilon \mu_G \left(1 - f / f_c\right)^p} \right)^{0.8} Sc_G^{0.333} \qquad (3.7)$$

where: $u_{G,e} = \dfrac{K_V \left(\rho_L / \rho_G \right)^{0.5}}{\varepsilon \left(1 - f / f_c\right)^p}$ [m/s]

$K_V \left(\rho_L / \rho_G \right)^{0.5}$ is the superficial vapour volumetric flux

f is the fraction of liquid filled channels [-]

f_c is the incipient percolation threshold [-]

The incipient percolation threshold (f_c) is the fraction of liquid filled channels at which liquid flooding of the structured packing occurs. A continuous liquid surface

across the top of the structured packing signifies the column is flooded and the pressure-drop increases infinitely with increasing gas velocity.

Brunazzi *et al.* [59] incorporated the influence of packing height on the liquid phase mass transfer coefficient after a thorough examination of the liquid film [4]. The vapour phase mass transfer coefficient was estimated through the correlation proposed by Rocha *et al.* [9] (equation 3.5), with changes in the calculation of the effective gas- and liquid velocities. The correlation for the vapour phase mass transfer coefficient proposed by Brunazzi *et al.* [59] is as follows:

$$Sh_G = 0.054\left(\frac{\left(u_{G,e}+u_{L,e}\right)\rho_G d_h}{\mu_G}\right)^{0.8} Sc_G^{0.33} \tag{3.8}$$

where: $u_{G,e} = \dfrac{u_{G,s}}{\left(\varepsilon - h_L\right)\sin\theta}$

$u_{L,e} = \dfrac{u_{L,s}}{h_L \sin\alpha}$

α is the slope of the steepest decent line with respect to the horizontal axis [^{o}]

{The other symbols in equation 3.8 has the same descriptions and units as in equation 3.5}

Xu *et al.* [65] used the model set up by Billet *et al.* [63] (from the penetration theory), together with an alternative correlation for the determination of the effective surface area, to predict the mass transfer in columns containing structured packing [4]. The correlation proposed by Xu *et al.* [65] for the vapour phase mass transfer coefficient is as follows:

$$k_G = \sqrt{\frac{4D_G \cdot u_{G,s}}{\pi \cdot S\left[\varepsilon - \left(\frac{4F_t}{S}\right)^{2/3}\left(\frac{3\mu_L \cdot u_{L,s}}{\rho_L \cdot \varepsilon \cdot g_e \cdot \sin\theta}\right)^{1/3}\right]}} \tag{3.9}$$

where: F_t is a correction factor for total liquid holdup

S is the side dimension of the corrugation [m]

g_e is the effective gravity [m/s^2]

{The other symbols in equation 3.9 have the same descriptions and units as in equation 3.6}

The correction factor for the calculation of the total liquid holdup (F_t) in structured packing was developed by Rocha *et al.* [9]. This factor is a function of the Weber and Froude number for liquid. Since this investigation is performed on dry structured packing a detailed account of the liquid holdup term falls outside the scope of this study.

Shetty *et al.* [60] investigated the flow patterns over the inclined corrugations of a structured packing element. From the gathered data, together with a penetration theory model, it was possible to obtain a more fundamental approach to estimate the liquid phase mass transfer coefficient in structured packing. The correlation for the vapour phase mass transfer coefficient is identical to the correlation proposed by Rocha *et al.* [9] (equation 3.5).

Olujic [66] developed a model (known as the Delft model) to predict the mass transfer efficiency for corrugated structured packing by following a geometry-based approach (referring to the relationship between the micro and macro geometry of the structured packing and the mass transfer process). The model has also undergone further revisions for refinement [58, 67-69]. In the Delft model, transitional flow (the flow discontinuity at the transition among packing elements) is taken into account. By invoking the heat/mass transfer analogy the vapour phase mass transfer coefficient is calculated by including the contributions from both the laminar and turbulent regimes. The correlation proposed by Olujic *et al.* [58, 66-68] for the vapour phase mass transfer coefficient is as follows:

$$k_G = \sqrt{\left(\frac{Sh_{G,lam} D_G}{d_{hG}}\right)^2 + \left(\frac{Sh_{G,turb} D_G}{d_{hG}}\right)^2} \qquad (3.10)$$

where: $Sh_{G,lam} = 0.664 Sc_G^{1/3} \sqrt{\mathrm{Re}_{Grv} \frac{d_{hG}}{l_{G,pe}}}$

$$Sh_{G,turb} = \frac{\mathrm{Re}_{Grv}\, Sc_G \xi_{GL} \frac{\varphi}{8}}{1+12.7\left(\xi_{GL}\frac{\varphi}{8}\right)^{1/2}\left(Sc_G^{2/3}-1\right)}\left[1+\left(\frac{d_{hG}}{l_{G,pe}}\right)^{2/3}\right]$$

d_{hG} is the hydraulic diameter for the gas phase [m]

Re_{Grv} is the relative velocity Reynolds number [-]

$l_{G,pe}$ is the length of the gas flow channel in a packing element [m]

ξ_{GL} is the gas/liquid friction factor [-]

φ is the fraction of the triangular flow channel occupied by liquid [-]

Fair *et al.* [70] evaluated the SRP (II) model and the Delft model based on a comprehensive total reflux study of sheet metal structured packing. It was found that the SRP (II) model has a tendency to underestimate the mass transfer efficiency, while the Delft model tended to predict slightly larger HETP values. According to Fair *et al.* [70], the accuracy and reliability of both models could be increased by improving the modelling of the effective interfacial area.

Crause [6] and Erasmus [10] investigated the vapour phase mass transfer coefficient, through the evaporation of pure liquids, in a novel short wetted-wall column. The reasoning behind the choice of the short column was that for the short column a fully developed concentration boundary layer would not be present. The assumption was that the conditions created by the short column were more representative of the actual flow conditions in structured packing, as the multitude of abrupt changes in the flow channel (in structured packing) prevents the attainment of a fully developed velocity profile. The correlation proposed by Crause [6] is as follows:

$$Sh_G = 0.00283\, \mathrm{Re}_{G,e}\, \mathrm{Re}_{L,e}^{0.08}\, Sc_G^{0.5} \qquad (3.11)$$

Erasmus [10] used the same experimental setup as Crause [6], but included an investigation into the effect that a liquid film flowing down a complex surface has on

the measured mass transfer rate. The correlation proposed by Erasmus [10] is as follows:

$$Sh_G = 0.0081 \mathrm{Re}_{G,e}^{0.94} Sc_G^{0.5} \tag{3.12}$$

Erasmus [3] continued to physically measure the vapour phase mass transfer coefficient under conditions where the mass transfer process is accomplished through contributions from the total geometric surface area of the structured packing. This novel approach was accomplished by coating a packing element with naphthalene and inserting the coated element in a column between two normal/uncoated packing elements. Air was blown through the column at various flow rates and the vapour phase mass transfer coefficient was determined through the measurement of the naphthalene mass loss from the coated element.

However, Erasmus [3] only performed his experiments for the naphthalene/air system. Due to the large scale of the experimental setup employed by Erasmus [3], it was considered to not be economically feasible to conduct his naphthalene sublimation experiments in different carrier gases. By making use of the wetted wall analogy and assuming that $k_G \propto D_G^{0.67}$ and $k_G \propto D_G^{0.5}$, it was possible to set up two correlations for the prediction of the vapour phase mass transfer coefficient for other systems as well. This, however, resulted in an untested correlation, in which the assumed dependency of the vapour phase mass transfer coefficient on the diffusion coefficient was not corroborated. As stated in Chapter 1 the two assumed dependencies of the vapour phase mass transfer coefficient (as used by Erasmus [3]) were selected since most of the dependencies found in literature are in that range. The correlations proposed by Erasmus [3] are as follows:

$$Sh_G = 0.3053 \mathrm{Re}_{G,e}^{0.62} Sc_G^{0.33} \tag{3.13}$$

$$Sh_G = 0.2641 \mathrm{Re}_{G,e}^{0.62} Sc_G^{0.5} \tag{3.14}$$

Erasmus [3] found that equation 3.14 ($k_G \propto D_G^{0.5}$) resulted in a marginally better fit of the correlation on the experimental results. The correlations proposed by Bravo *et al.*

[7], Rocha *et al.* [9] and Billet *et al.* [63], however, all make use of the $k_G \propto D_G^{0.67}$ dependency. By varying the Schmidt number in the experiments performed by Erasmus [3], this assumed dependency can be verified.

Lastly, Erasmus [3] compared the experimental results obtained from his naphthalene-sublimation experiments to the correlations proposed by Bravo *et al.* [7], Rocha *et al.* [9], Crause [6] and Erasmus [10]. He found that all four of the correlations from literature underestimated the actual vapour phase mass transfer coefficient, with the correlation of Rocha *et al.* [9] giving the most accurate results.

However, the results from Chapter 2, where the diffusion coefficient of naphthalene in various carrier gases was determined, showed that the commonly accepted values of the diffusion coefficient for the naphthalene/air system were possibly in error. These possible incorrect diffusion coefficient values were used by Erasmus [3] in setting up his mass transfer correlation. The statement by Erasmus [3], that the correlations in open literature tend to underestimate the actual vapour phase mass transfer coefficient in structured packing could therefore be in error.

The present study investigated naphthalene sublimation from the surface of structured packing, with a geometry similar to the Flexipac 350Y (as used by Erasmus [3]). Due to the high gas flow rates needed to obtain turbulent conditions, the experiment was conducted at small scale in order to keep operational costs reasonable.

3.3 Theory

3.3.1 Diffusion through a stagnant gas

The diffusion of a species (A) from a solid/gas interface into the gas phase (B) can be described by the diffusion of species A through a stagnant gas (Fick's law). This derivation was fully covered in section 2.4.2 and the final equation obtained was as follows:

$$N_A = \frac{D_{AB}P}{RT(z_2 - z_1)} \ln\left(\frac{P - p_{A2}}{P - p_{A1}}\right) \tag{2.27}$$

Equation 2.27 was written in the most convenient format for use in the diffusion coefficient experiments (Chapter 2), with the driving force indicated in terms of the partial pressures. In literature the driving force of the diffusion flux can also be indicated in terms of concentration or mol fractions [72]. From literature, equation 2.27 can now be written as follows [3, 72]:

$$N_A = -\frac{D_{AB} \cdot c_T}{\ell \cdot y_{B,m}} \left(y_{A,b} - y_{A,i}\right) \tag{3.15}$$

where: N_A is the diffusion flux [mol/m^{2}s]

ℓ is the distance in the direction of mass transfer [m]

c_T is the total concentration in the gas phase [mol/m^3]

$y_{B,m}$ is the logarithmic mean mol fraction of component B [-]

$y_{A,b}$ is the mol fraction of component A in the bulk phase [-]

$y_{A,i}$ is the mol fraction of component A at the interface [-]

For the sublimation of naphthalene, where the concentration of the diffusing component (naphthalene) is small, the assumption that $y_{B,m} \approx 1$ is valid. Furthermore, the vapour phase mass transfer coefficient $\left(k_G\right)$ can be substituted into equation 3.15, as was done by Erasmus [3], and the explanation thereof is found in literature [72]. Equation 3.15 can now be written as follows:

$$N_A = k_G c_T \left(y_{A,i} - y_{A,b}\right) \qquad [\text{mol/m}^2\text{s}] \tag{3.16}$$

where: $k_G = \dfrac{D_{AB}}{\ell \cdot y_{B,m}}$ [m/s]

3.3.2 Naphthalene sublimation in structured packing

In order to determine the total mass transfer rate in structured packing the following integration, over the height, width and depth of the packing, needs to be performed:

$$n_A = \int_0^h \int_0^W \int_0^D a_p \cdot k_G \cdot c_T \left(y_{A,i} - y_{A,b} \right) dD \cdot dW \cdot dh \tag{3.17}$$

where: n_A is the mass transfer rate of the sublimating/evaporating specie [mol/s]

a_p is the specific surface area of the coated packing [m^2/m^3]

W, D, h are the width, depth and height of the coated packing respectively [m]

If it is assumed that the variables are independent of W and D, that c_T is constant (negligible pressure drop) and that k_G is constant over the height of the packing, then equation 3.17 can be simplified as follows:

$$\begin{aligned} n_A &= a_p \cdot k_G \cdot c_T \cdot W \cdot D \int_0^h \left(y_{A,i} - y_{A,b} \right) dz \\ &= a_p \cdot k_G \cdot c_T \cdot W \cdot D \cdot h \cdot \Delta y_{A,Lm} \\ &= a_p \cdot k_G \cdot c_T \cdot V_C \cdot \Delta y_{A,Lm} \\ &= k_G \cdot c_T \cdot A_C \cdot \Delta y_{A,Lm} \end{aligned} \tag{3.18}$$

and:

$$\Delta y_{A,Lm} = \frac{\left(y_{A,i} - y_{A,b} \right)_h - \left(y_{A,i} - y_{A,b} \right)_0}{\ln \left(\dfrac{\left(y_{A,i} - y_{A,b} \right)_h}{\left(y_{A,i} - y_{A,b} \right)_0} \right)} \tag{3.19}$$

where: $\Delta y_{A,Lm}$ is the logarithmic mean driving force [-]

V_C is the volume of the test section of the packing [m^3]

A_C is the specific area of the test section of the packing [m^2]

The final equation for the calculation of the vapour phase mass transfer coefficient in structured packing is as follows:

$$k_G = \frac{n_A}{c_T A_C \Delta y_{A,Lm}} \tag{3.20}$$

It is important to note that $y_{A,i}$ is calculated from the saturated vapour pressure data (as discussed in section 2.4.2) and that $y_{A,b}$ at $h = 0$ is assumed to be equal to zero. The mass loss measurement is related to a mass transfer rate (n_A) and the total concentration of the gas phase (c_T) is calculated from the experimental readings. Refer to Appendix A4.5 for detailed sample calculations.

3.4 Experimental

3.4.1 Apparatus

The naphthalene sublimation experiments conducted by Erasmus [3] were performed on large scale (column diameter of 200 mm). Repeating the experiments in different carrier gases was therefore, from an economical viewpoint, not feasible. This design therefore focused on the construction of a small-scale column, wherein it was possible to obtain the high gas flow rates necessary to obtain sufficiently high gas phase Reynolds numbers, while keeping the operational costs to a minimum. Figure 3.3 depicts the flow diagram of the experimental setup.

From the flow diagram it can be seen that the gas entering the test column was preheated through a 1500 W inline gas heater. The gas heater is a double wall pipe with a length of 1 meter. The centre segment is the heating element, which fits snugly inside the outer tube. The gas enters and exits at right angles to the pipe direction and the gas flows between the heating element and outer tube, providing efficient heat transfer. The gas temperature was controlled using feedback control via a calibrated PT100 temperature sensor (marked TI02 in Figure 3.3), situated at the inlet to the test column.

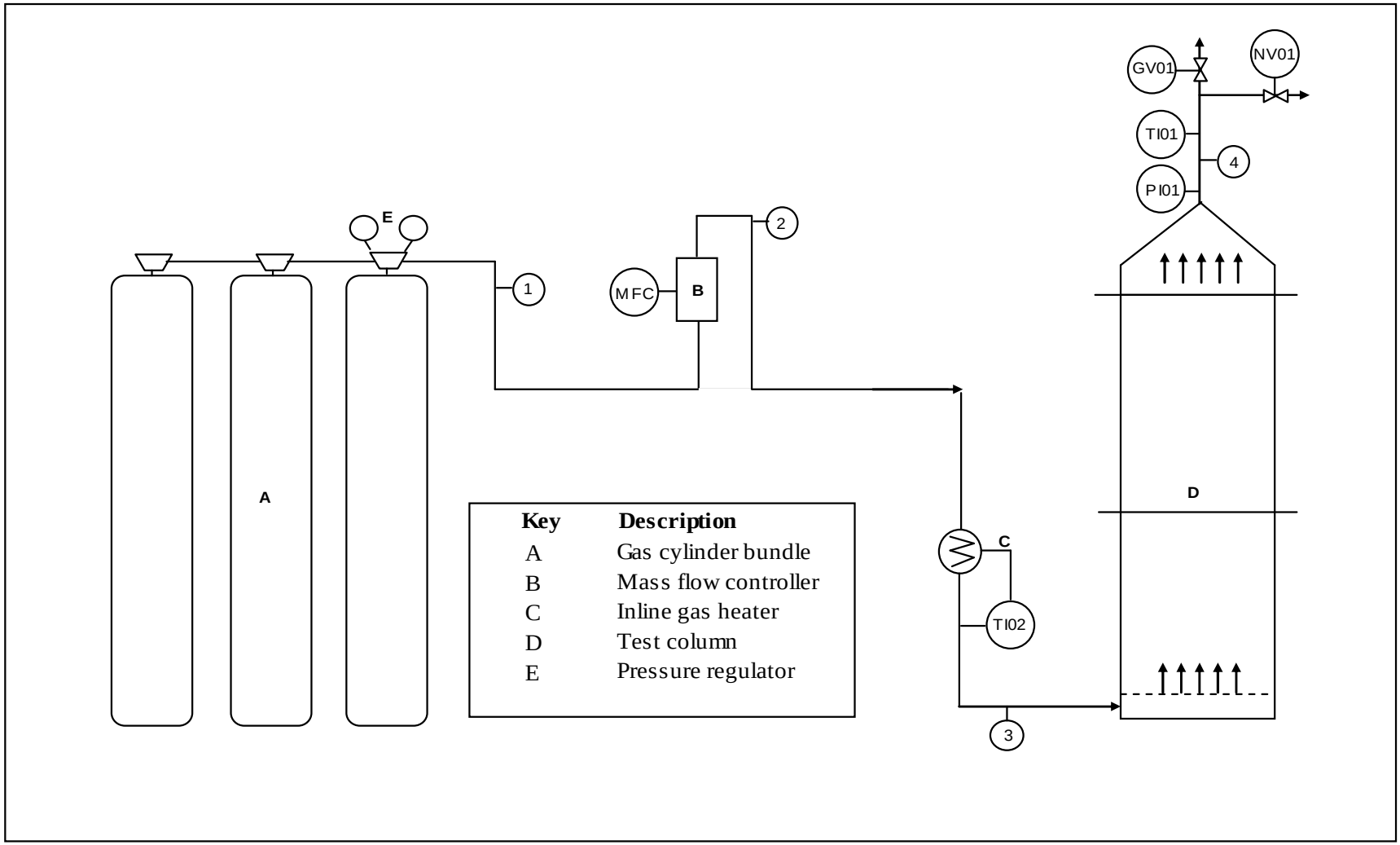

Figure 3.3: *Flow diagram of small-scale test column*

Although performing the experiments at different temperatures has a negligible effect on the Schmidt number (the main aim being to vary the Schmidt number) the benefit of running the experiments at higher temperatures is that each experimental run requires a shorter time span to obtain sufficiently weighable mass losses. This, in effect, results in lower operational costs, since less gas is needed to obtain the same results that would be obtained for the longer experimental runs at lower temperatures.

From Figure 3.3 it can also be seen that the gas flow rate is controlled though a mass flow controller, which is situated in the line preceding the inline gas heater. The mass flow controller provides more accurate control of the gas flow rate than other flow control options, such as rotameters. Due to the extreme importance of knowing the exact flow rate, for the calculation of the effective Reynolds number, the mass flow controller was chosen as the flow control method in this design.

The test column, schematically represented in Figure 3.4, consists of three separate components. The gas enters the test column through the bottom section (marked as Section A), where the gas is distributed through a sparger-type setup (perforated plate). In order to obtain good gas distribution throughout the column, a layer of inert glass beads was added directly above the sparger.

The middle section (marked as section B) is connected to both the upper and lower sections (sections A and C) by means of 3mm thick flanges. The top section (marked as section C) is cone-shaped and from the flow diagram (Figure 3.3) it can be seen that the line exiting this section (line 4) contains a globe valve (GV01), with a needle valve (NV01) situated on a bleed stream. The globe valve serves the important function of throttling the gas stream in order to obtain a higher system pressure within the column. The needle valve is added for further fine-tuning of the system pressure. The gas temperature at the outlet of the column and system pressure is monitored by the temperature and pressure indicators (marked TI01 and PI01 on the flow diagram) situated at the line exiting the column (line 4). See Appendix A3 for detail design.

Lastly, a fume hood is placed directly above the outlet section of the column, whereby the exiting gas is vented to the atmosphere.

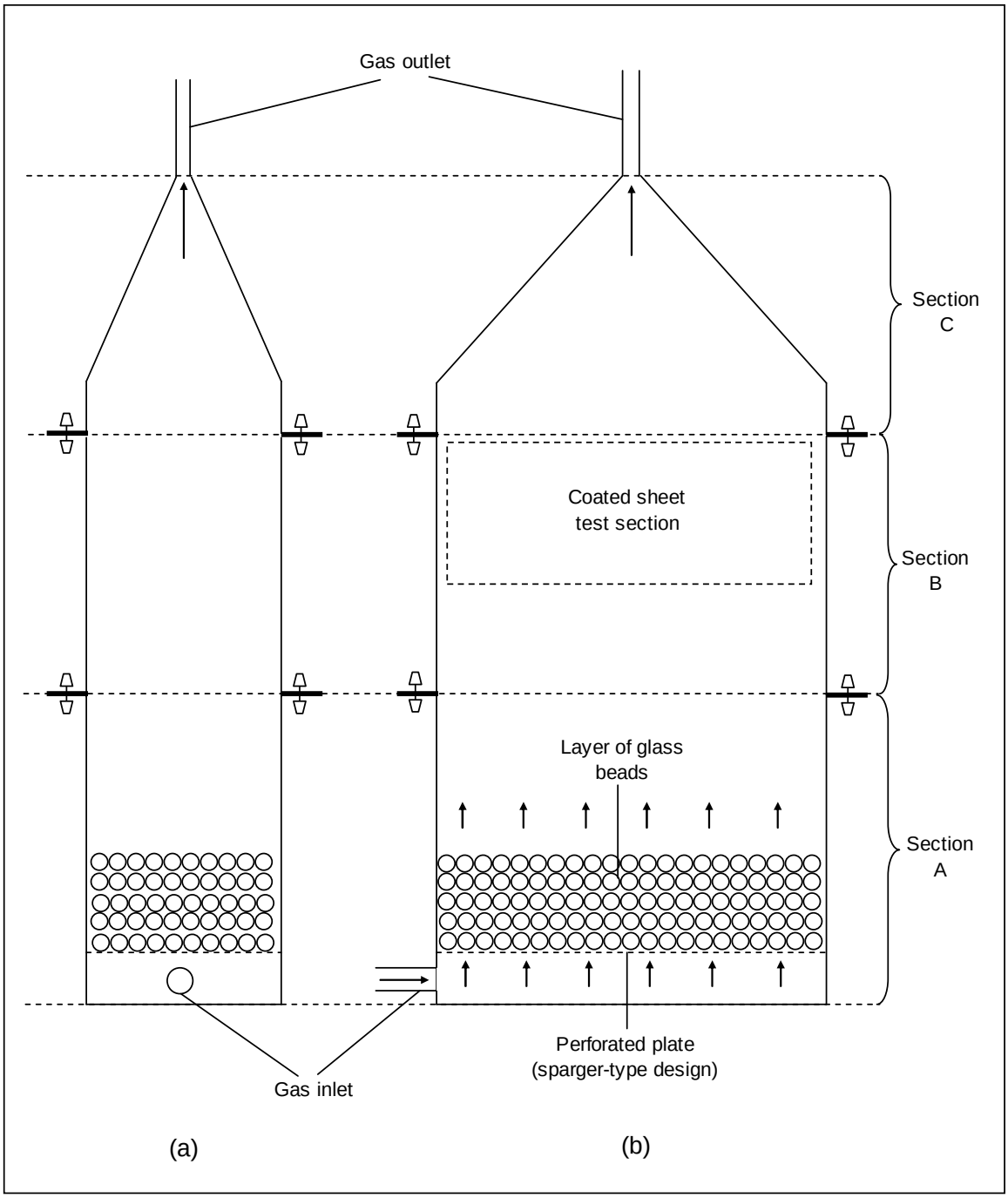

Figure 3.4: *Simplified schematic representation of the test column (a) Side view and (b) Front view*

3.4.2 Naphthalene coating procedure

The naphthalene coating procedure followed in this study was similar to the procedure employed by Erasmus [3] in his experiments. Wire gauze packing was used for the naphthalene coating procedure, as a smooth and consistent coating could be achieved

with this type of packing material [3]. Coatings applied to wire gauze packing are known to be particularly resistant to a certain amount of deformation (bending etc.) of the packing [3]. The wire gauze packing used in this study had the same channel dimensions/geometry as the Flexipac 350Y structured packing manufactured by Koch-Glitsch.

Before commencing with the naphthalene coating procedure, the sheet was first washed in acetone and then dried. The coating was then applied by repeatedly submerging half the sheet into molten naphthalene, which was kept at a constant temperature of 85 ^{o}C. The steel container, containing the molten naphthalene, was kept in a thermostat controlled water bath. The reasoning behind the coating of only half the sheet was merely that this simplified the dipping procedure. After submerging the sheet in the molten naphthalene the sheet was removed and the coated naphthalene was given time to solidify. The dipping procedure was then repeated in order to apply another layer of coating. This procedure was repeated until a sufficiently thick layer of coating was achieved. The total weight of the naphthalene coating was determined by weighing the sheet before the coating procedure commenced and after each subsequent coating procedure. Care, however, was taken during the dipping procedure to submerge the sheet at a steady rate. A clear (colourless) coating was an indication of a correct coating procedure.

After the coating procedure was completed any loose naphthalene pieces were removed from the sheet using a brush. When the naphthalene coating was deemed insufficient for further experimentation (after performing a certain amount of experimental runs) the sheet was recoated. In order to obtain a smooth, consistent coating the remaining naphthalene was removed from the sheet. This was achieved by heating the molten naphthalene to a higher setting of 90 ^{o}C and submerging the coated sheet in the molten naphthalene. The higher temperature therefore melted the residual naphthalene coating at a faster rate. The coating procedure was then repeated, starting with the acetone wash.

3.4.3 Experimental procedure

At the onset of the experimental run the naphthalene coated sheet was accurately weighed and the height of the coating measured. The sheet was then carefully sandwiched between two uncoated sheets. The packing section was then inserted into section B of the test column (refer to Figure 3.4). Figure 3.5 is a schematic representation of the top-view of the middle section, which shows the placement of the naphthalene-coated structured packing inside the column. From Figure 3.5 it can be seen that the flow channels of the two uncoated sheets that face towards the walls of the column are sealed. This was done in order to restrict the gas flow to only the middle flow channel, which contained the naphthalene coated sheet.

In order to effectively seal the outer gas flow channels the whole structured packing segment was fitted snugly into the column. A certain amount of deformation of the naphthalene-coated sheet was therefore observed. To determine the mass loss of naphthalene due solely to the insertion and removal process, the packing segment was weighed, inserted into the column and removed. This procedure was completed without switching on the gas flow. By weighing the packing segment after removal the mass loss due to the insertion and removal procedure was determined.

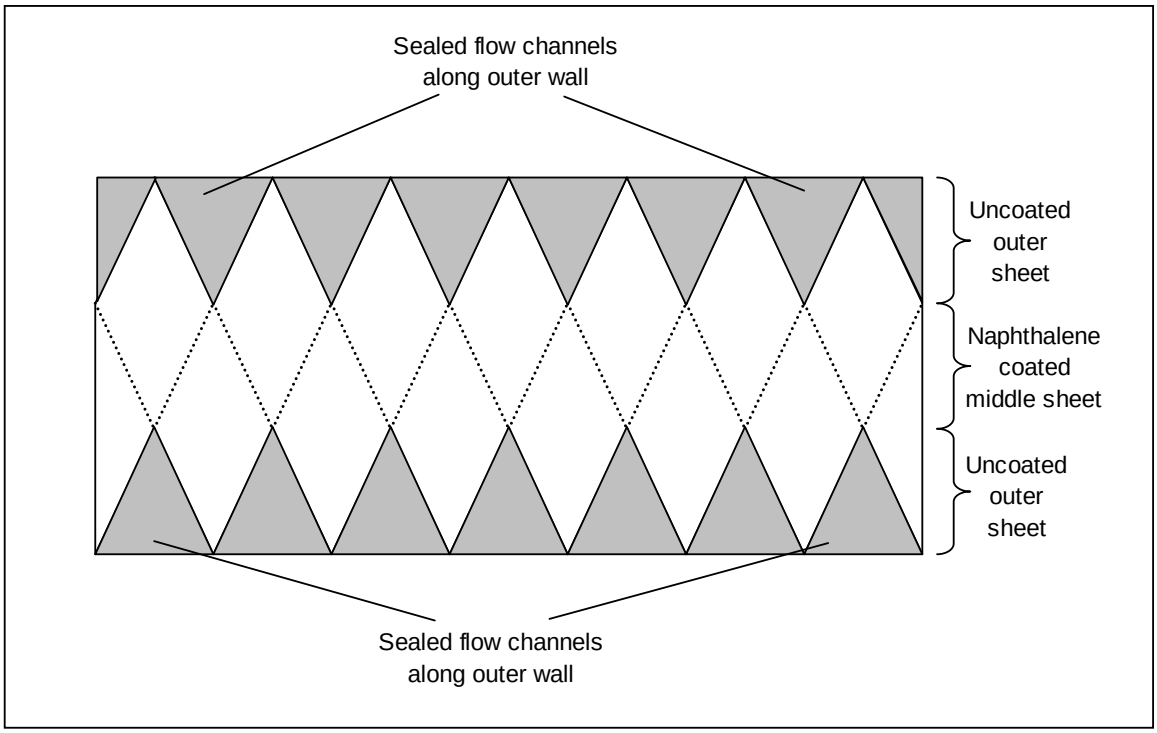

Figure 3.5: *Top view of the placement of the packing sheets within the test column*

After inserting the packing segment into the column, the top section (section C) was secured and fastened to the column. The coated sheet was inserted with the coated section facing upwards in order to provide the proper flow geometry for the gas before passing over the coated section. The gas flow was initiated and the gas temperature entering and exiting the column logged. The atmospheric and system pressure was also logged and temperature control was attained by switching on the inline gas heater and adjusting it to the desired setting.

After a certain amount of time the gas flow was stopped, the top section of the column detached and the naphthalene coated packing segment removed and weighed. After the naphthalene weight loss was logged the naphthalene coated sheet was inspected and recoated if the layer of coating was deemed to be insufficient for another run.

3.5 Results and Discussion

3.5.1 Experimental calculations

As in Chapter 2 (determination of the vapour diffusion coefficient) the saturated vapour pressure of naphthalene is determined using equations 2.31 and 2.32, depending on the system temperature. The equation by Ambrose *et al.* [39] is generally accepted as the most accurate method [22]. The gas flow in the following discussion is represented as an effective Reynolds number ($\mathrm{Re}_{G,e}$) and is defined as follows:

$$\mathrm{Re}_{G,e} = \frac{\rho_G u_{G,e} d_h}{\mu_G} \tag{3.21}$$

where: ρ_G is the density of the gas [kg/m^3]

μ_G is the viscosity of the gas [N.s/m^2]

d_h is the hydraulic diameter [m]

$u_{G,e}$ is the effective gas velocity [m/s]

The effective gas velocity was calculated as in the model by Bravo *et al.* [7] and was also used in the study performed by Erasmus [3]. The method of calculation is as follows:

$$u_{G,e} = \frac{u_{G,s}}{\varepsilon \sin\theta} \qquad \text{[m/s]} \qquad (3.22)$$

where: ε is the void fraction [-]

θ is the corrugation angle [^{o}]

$u_{G,s}$ is the gas velocity with reference to the empty column cross-section [m/s]

The hydraulic diameter (d_h) is calculated for a unitary 'criss-cross' cell. The calculation thereof is the same as was used in the study performed by Erasmus [3] and is as follows:

$$d_h = \frac{Bh}{S} \qquad \text{[m]} \qquad (3.23)$$

where: B is the corrugation base [m]

S is the corrugation side [m]

h is the crimp height [m]

Table 3.1 gives the pertinent dimensions for the structured packing used in the current investigation.

Table 3.1: *Dimensions of structured packing for current investigation*

Dimension	**Value and unit**
Corrugation base (B)	17.4 mm
Corrugation side (S)	11.2 mm
Crimp height (h)	7.05 mm
Corrugation angle (θ)	45 ^{o}

Refer to Appendix A4.5 for the detailed sample calculations.

3.5.2 Verification of the accuracy of the experimental setup: *Sublimation of naphthalene in air at atmospheric pressure*

Figure 3.6 shows the experimental results for the sublimation of naphthalene in air at atmospheric pressure. The experimental results obtained by Erasmus [3] are also shown in Figure 3.6. From the graph it can be seen that the results obtained in the present study compare well with the results obtained by Erasmus [3]. From this it can be inferred that the present experimental setup is indeed accurate.

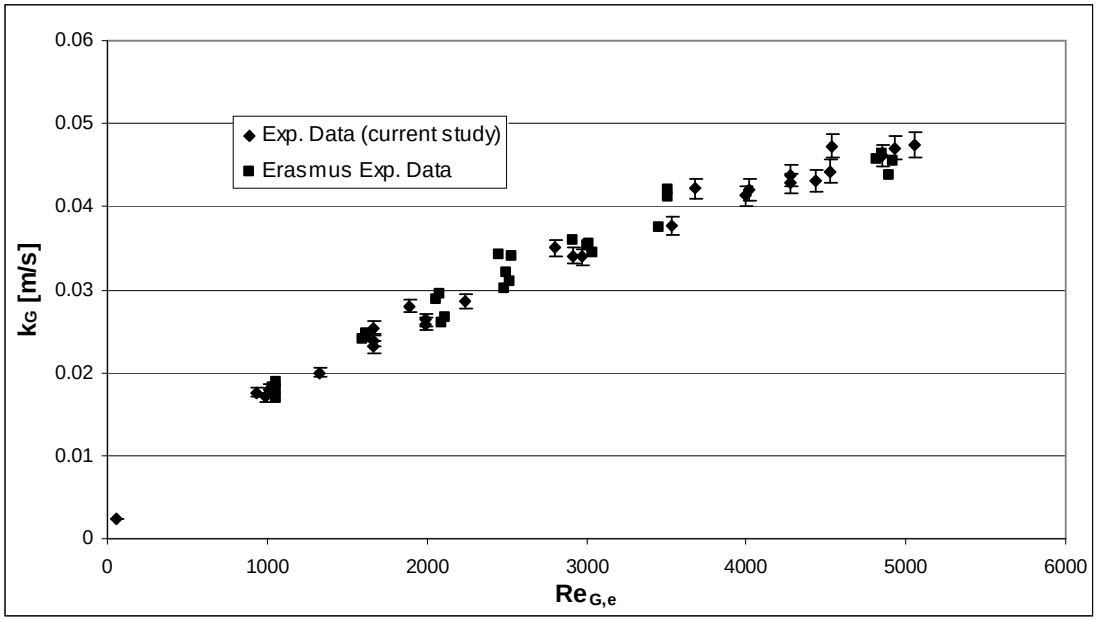

Figure 3.6: *Experimental results for the naphthalene sublimation in air (atmospheric pressure) compared to the experimental results from the study performed by Erasmus [3]* $Sc_G \approx 1.95$

The main variables that can influence the results and thus cause an error in the calculation of the final result are as follows:

1. <u>Accuracy of the temperature measurement:</u>

   The inlet and outlet gas temperatures are measured with calibrated PT100 temperature sensors. The calibration certificate (Appendix A3) states that an error of 0.1 ^{o}C is possible in its measurement. Taking this potential

measurement error into account when calculating the mass transfer coefficient results in a maximum absolute error of approximately 1 %.

2. Mass losses due to transporting the coated packing sheet:

   As stated in the experimental section it is clear that a certain amount of the coated naphthalene is 'lost' due to the transportation of the coated sheet to and from the test column. Additionally the insertion and extraction of the coated sheet into and from the test column also results in a certain amount of naphthalene losses. To determine this mass loss the coated sheet is weighed, inserted into the column (without gas flow), removed from the column and weighed. This mass loss is typically in the region of 0.03 g and when comparing this to the mass of naphthalene sublimated during the experiments it represents approximately 0.8 to 3 % of the total mass loss. When taking this mass loss into account in calculating the mass transfer coefficient it results in a maximum absolute error of approximately 0.7 to 1.4 %.

By taking both these influences into account the maximum absolute error in the calculation of the mass transfer coefficient amounts to approximately 3%. The error bars on the experimental data points in Figure 3.6 are therefore set to 3%.

Figure 3.7 shows the comparison between the experimental results from the present study and the main correlations found in literature. The correlations by Billet *et al.* [63] and Xu *et al.* [65] are omitted, as they contain numerous packing-specific constants which are not available for the Flexipac 350Y packing used in the present study. The correlation by Olujic [66], known as the Delft model, is also omitted due to the presence of vapour/liquid interaction terms. The correlations by Crause [6] and Erasmus [10] are also omitted as the study performed by Erasmus [3] indicated that these correlations, set up from short wetted wall experiments, severely underestimates the mass transfer coefficients under turbulent flow conditions.

From Figure 3.7 it is clear that the correlations by Rocha *et al.* [9] and Bravo *et al.* [7] underestimate the experimentally obtained mass transfer coefficients. This was also observed by Erasmus [3] in his study. The findings by Fair *et al.* [70], where the SRP

(II) model (by Rocha *et al.* [9]) is evaluated, is thus confirmed. As stated previously Fair *et al.* [70] found that the SRP (II) model has a tendency to underestimate the mass transfer efficiency, which is the case for the results obtained in the present study.

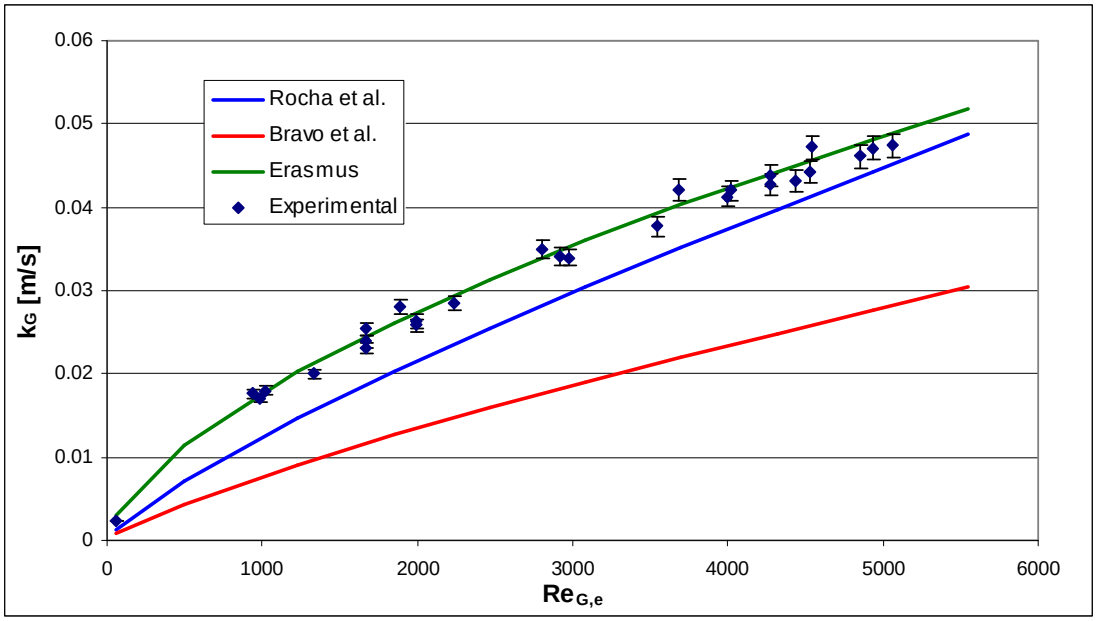

Figure 3.7: *Experimental results for the naphthalene sublimation in air (atmospheric pressure) compared to k_G correlations from literature. $Sc_G \approx 1.95$*

The correlation by Erasmus [3] was, however, constructed using the diffusion coefficient data from Cho *et al.* [27]. Some doubts on the accuracy of the data by Cho *et al.* [27] have been brought to light in the previous chapter. It therefore becomes necessary to set up a new correlation, applying the diffusion coefficient data gathered from the present study (refer to Chapter 2). The correlation was set up in the same fashion as was done by Erasmus [3], with a basic power law series:

$$Sh_G = a\,\mathrm{Re}_{G,e}^{b}\,Sc_G^{c} \qquad (1.1)$$

Two correlations were compiled; one with a mass transfer dependency of $k_G \propto D_G^{0.5}$ and the other with a dependency of $k_G \propto D_G^{0.67}$. This was done in order to verify which dependency provides the more accurate predictions. By fitting the experimental results to equation 1.1 and regressing the data through a least squares

analysis the optimum parameters were obtained. The correlations obtained from the least squares analysis are as follows:

$$Sh_G = 0.1864\,\mathrm{Re}_{G,e}^{0.64}\,Sc_G^{0.5} \qquad \text{(RMS = 3.874 and } R^2 = 0.964) \qquad (3.24)$$

$$Sh_G = 0.2259\,\mathrm{Re}_{G,e}^{0.65}\,Sc_G^{0.33} \qquad \text{(RMS = 4.147 and } R^2 = 0.945) \qquad (3.25)$$

Where: $RMS = \sqrt{\dfrac{\sum_n \left(Sh_{predicted} - Sh_{experimental}\right)^2}{n}}$

$=$ the root mean square error

From the RMS and R^2 values in equations 3.24 and 3.25 it can be seen that the correlation with the dependency of $k_G \propto D_G^{0.5}$ provides the better fit (equation 3.24). Figure 3.8 depicts a parity plot between the predicted values from equation 3.24 and the experimental results.

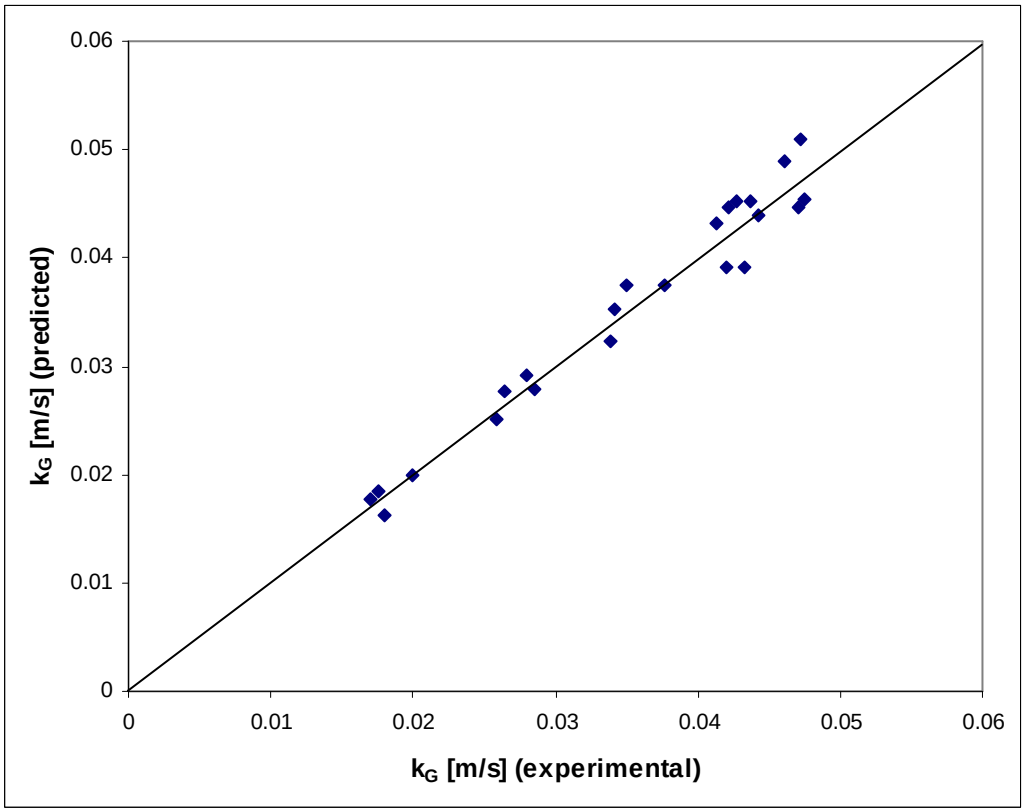

Figure 3.8: *Parity plot of the values predicted by equation 3.24 versus the experimental results*

The $k_G \propto D_G^{0.67}$ dependency assumed by Bravo *et al.* [7] and Rocha *et al.* [9] and the favourable performance of the $k_G \propto D_G^{0.5}$ dependency in the present study (as well as in the study by Erasmus [3]) now needs further investigation.

3.5.3 Sublimation of naphthalene in air for a system pressure above atmospheric conditions

In the following section mass transfer experiments were conducted at system pressures above atmospheric conditions for the naphthalene/air system. As stated in Chapter 1, one of the main aims of this study is to test the assumed dependency of the mass transfer coefficient on the diffusion coefficient. This was achieved by varying the Schmidt number in sublimation experiments. In this section, however, only a marginal difference was observed between the Schmidt numbers of the experimental runs for this section and those of the runs conducted at atmospheric pressure (refer to section 3.5.2).

The static behaviour of the Schmidt number was due to the fact that the Schmidt number is inversely proportional to both the diffusion coefficient and the density of the carrier gas. Furthermore, it is widely known that the diffusion coefficient is inversely proportional to the system pressure (refer to Chapter2). This, in effect, signifies that as the pressure is doubled, the diffusion coefficient is halved. Increasing or decreasing the system pressure therefore has a marginal effect on the Schmidt number.

Figure 3.9 illustrates the experimental results obtained versus various k_G correlations from literature. From Figure 3.9 it is clear that the correlations by Rocha *et al.* [9] and Bravo *et al.* [7] underestimate the experimental results. The findings of Fair *et al.* [70], who found that the SRP (II) model have a tendency to underestimate the mass transfer efficiency, are once again confirmed.

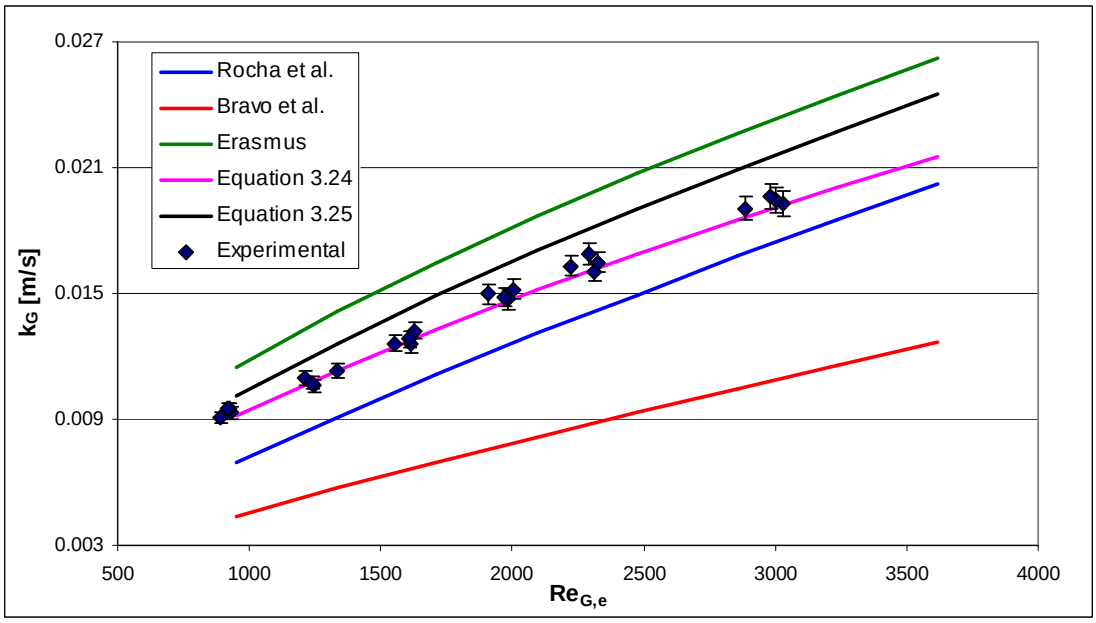

Figure 3.9: *Experimental results for the naphthalene sublimation in air (system pressure above atmospheric conditions) compared to k_G correlations. $Sc_G \approx 2.01$*

Figure 3.9 also shows that the correlation by Erasmus [3] over-estimates the experimentally obtained mass transfer coefficients. As stated in section 3.5.2 the correlation by Erasmus [3] was set up using the diffusion coefficient data from Cho *et al.* [27]. The accuracy of the results of Cho *et al.* [27] has, however, been brought into question. The most likely cause for the inaccuracy of the correlation by Erasmus [3] was therefore that the data available from literature, which was necessary in creating the correlation, was possibly in error.

Figure 3.9 also depicts the predictions from the two correlations set up in section 3.5.2. From Figure 3.7 it is clear that equation 3.24 provides a better fit of the experimental results than equation 3.25. The $k_G \propto D_G^{0.5}$ dependency, presented by equation 3.24, therefore continues to provide better results than the $k_G \propto D_G^{0.67}$ dependency of equation 3.25.

It should also be noted that the error bars on the experimental data points were set to 3%, since the sensitivity analysis was performed in the same fashion as for the previous section.

3.5.4 Sublimation of naphthalene in CO_2 at atmospheric pressure

In the following section mass transfer experiments were conducted at atmospheric conditions for the naphthalene/CO_2 system. Figure 3.10 represents the experimental results obtained versus the various k_G correlations from literature. From Figure 3.10 it can be seen that the correlations by Rocha *et al.* [9] and Bravo *et al.* [7] once again underestimate the experimental results. The findings of Fair *et al.* [70] are therefore once again confirmed. The correlation by Rocha *et al.* [9], however, provides a better fit to the experimental data than in the previous experimental sections. The most likely reason for the improved predictions using the correlation of Rocha *et al.* [9] is that the Schmidt number for the naphthalene/CO_2 system now approaches unity. Erasmus [3] states that for turbulent systems with Schmidt numbers close to unity the different mass transfer models show little difference. It is only when dealing with systems that have Schmidt numbers considerably larger or smaller than unity that the different models start diverging from one another.

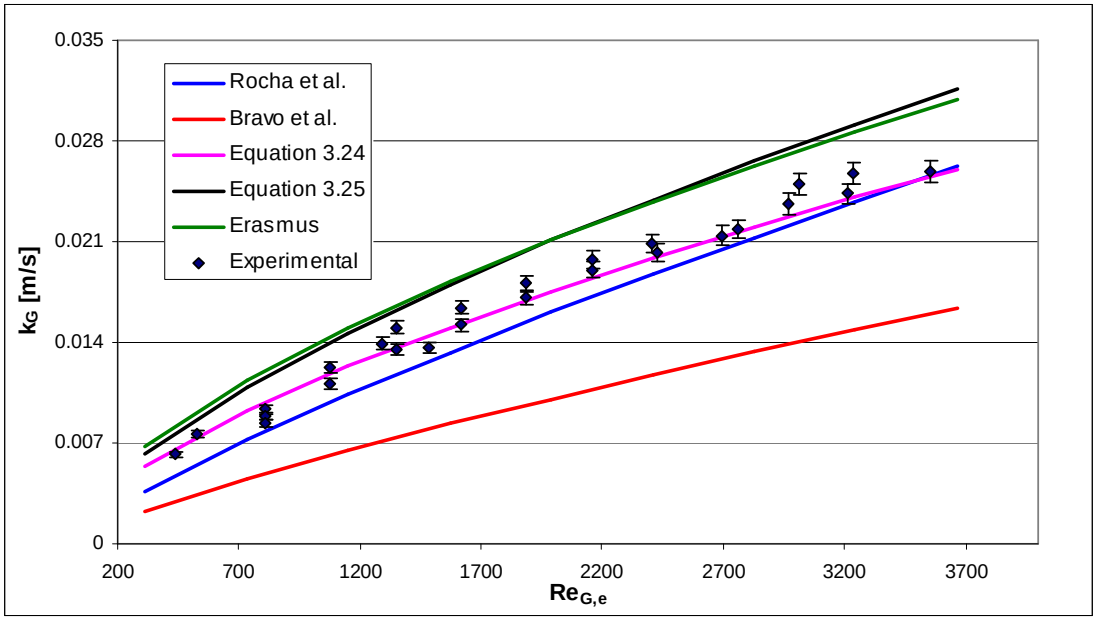

Figure 3.10: *Experimental results for the naphthalene sublimation in CO_2 (atmospheric pressure) compared to k_G correlations. $Sc_G \approx 1.39$*

Figure 3.10 also shows that the predictions by the correlation of Erasmus [3] once again overestimate the experimental results. As in the previous section, this discrepancy is most likely due to the use of the diffusion coefficient data of Cho *et*

al.[27] in setting up the correlation. The predictions from the two correlations set up in section 3.5.2 are also presented in Figure 3.10. Equation 3.24 once again provides the better fit for the experimental results, with the predictions by equation 3.25 giving results similar to the correlation of Erasmus [3]. The $k_G \propto D_G^{0.5}$ dependency, presented by equation 3.24, once again provides better results than the $k_G \propto D_G^{0.67}$ dependency of equation 3.25.

It should, however, be noted that the experimental results at higher flow rates, represented in Figure 3.10, could only be obtained by decreasing the cross-sectional area of the flow channel. This could give rise to wall effects which in turn could lead to inaccurate results. It was therefore deemed necessary to repeat the tests at the lower gas flow rates, using the smaller cross-sectional area. Figure 3.11 show the experimental results at the lower flow rates (low Reynolds numbers) for the tests performed at both the larger and smaller column cross sectional areas. The difference between the results obtained from the smaller and larger cross-sectional area tests falls mostly within the 3 % uncertainty level. The potential error, due to the use of the smaller cross-sectional area, is therefore viewed as being negligible.

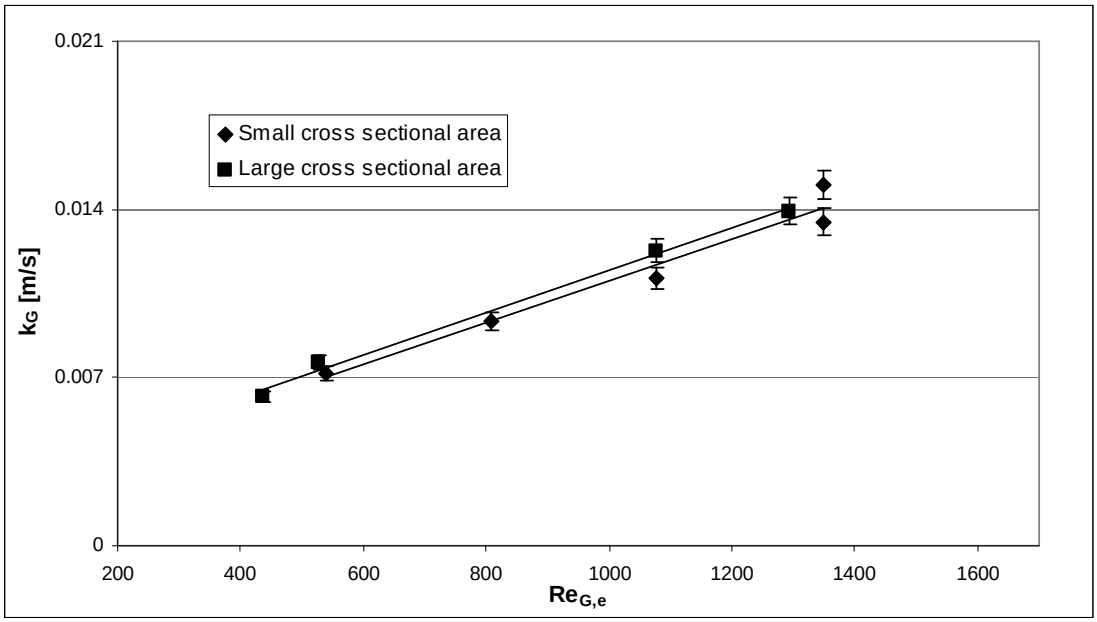

Figure 3.11: *Comparison between the experimental results for the smaller and larger cross sectional area tests.* $Sc_G \approx 1.39$

3.5.5 Sublimation of naphthalene in helium at atmospheric pressure

In the following section mass transfer experiments were conducted at atmospheric conditions for the naphthalene/helium system. Figure 3.12 represents the experimental results obtained versus the various k_G correlations.

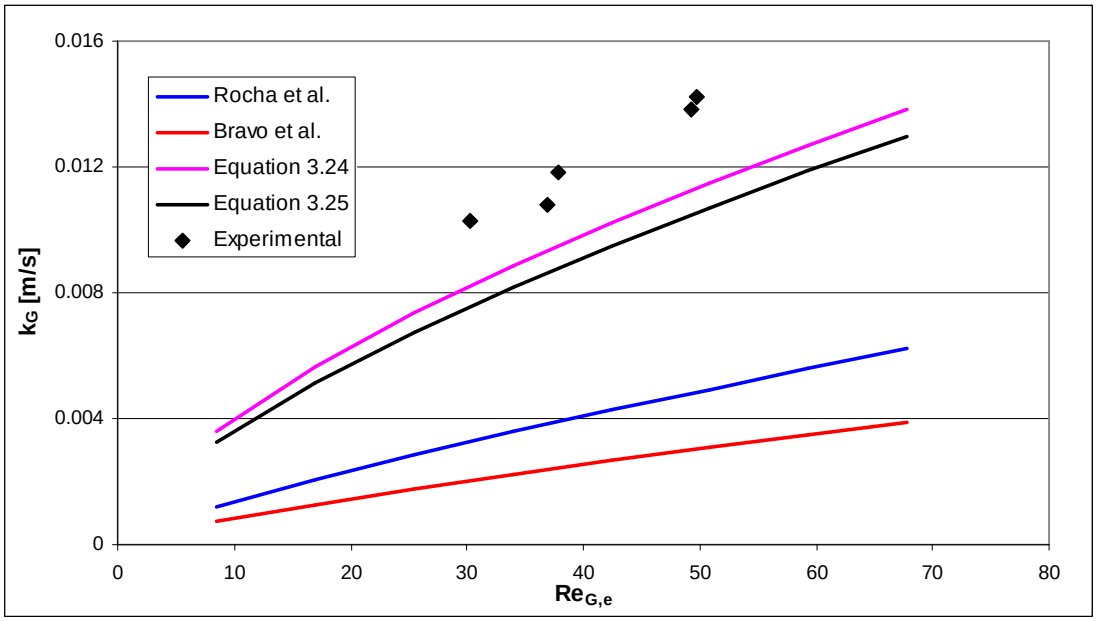

Figure 3.12: *Experimental results for the naphthalene sublimation in helium (atmospheric pressure) compared to k_G correlations. $Sc_G \approx 4.30$*

From Figure 3.12 it can be seen that the correlations by Rocha *et al.* [9] and Bravo *et al.* [7] severely underestimate the experimental results. The predictions from the two correlations created in section 3.5.2 are also shown in Figure 3.12. From Figure 3.12 it can be seen that equation 3.24 provides a marginally better fit to the experimental results than equation 3.25. Both equation 3.24 and 3.25, however, underestimate the experimental results significantly.

The most likely cause for the poor fit of the correlations on the experimental results was that the naphthalene/helium experiments were conducted in the laminar flow regime (Reynolds numbers in the region of 30 to 60). Unfortunately, due to the exceedingly low density of helium, sufficiently high flow rates could not be obtained to attain turbulent conditions. In order to reach a sufficient flow rate for turbulent conditions a cylinder of helium (containing 1.51 kilograms of helium) would have to

be emptied in approximately 1 to 2 minutes. This was not practically possible, from both an economic and experimental point of view.

The basic form of the mass transfer correlation (equation 1.1) has been discussed in detail over the previous sections.

$$Sh_G = a\,\mathrm{Re}_{G,e}^{b}\,Sc_G^{c} \tag{1.1}$$

Most of the correlations from literature, however, exhibit a potential flaw: *Mass transfer from the laminar regime is not taken into account*. This lack is clearly demonstrated by the fact that all the correlations in literature that utilise the basic form of equation 1.1 predict zero mass transfer at conditions where no gas flow is present. Mass transfer in a stagnant gas is well documented in literature [12, 14, 22] and it is therefore clear that these correlations [3, 7, 9] will be inaccurate at very low gas flow rates. The only exception found is the Delft model, developed by Olujic [66], where the contributions from both the laminar and turbulent regimes are included in the calculation of the mass transfer coefficient.

In order to improve the accuracy of the correlations set up in section 3.5.2 (equations 3.24 and 3.25) it therefore becomes necessary to include a term for the laminar flow regime into the basic from represented by equation 1.1.

3.5.6 Correlating the experimental results

As discussed in the previous section, the sum of the experimental results was used to create an accurate correlation for the prediction of the vapour phase mass transfer coefficient. In order to do this the basic from of the mass transfer correlation (equation 1.1) was altered. This was achieved by adding an additional dimensionless term, $\left(\rho_G / \rho_{G,Naph}\right)^c$, which represents the laminar regime of the gas flow. The altered basic form is as follows:

$$Sh_G = \left(a\,\mathrm{Re}_{G,e}^{b} + \left(\rho_G \big/ \rho_{G,Naph} \right)^{c} \right) Sc_G^{d} \tag{3.26}$$

With the basic form of the correlation (equation 1.1) the predicted vapour phase mass transfer coefficient is zero when the gas flow rate is zero. As stated previously this is not true, since mass transfer occurs even when the bulk gas phase is stagnant. For lower gas flow rates (laminar regime) the contribution from the added dimensionless term in the altered basic form of the correlation (equation 3.26) now takes precedence over the contribution from the Reynolds number term. The added dimensionless term contains parameters for both the carrier gas density (ρ_G) and the density of pure naphthalene gas ($\rho_{G,Naph}$), depending on the system temperature and pressure. The decision to use the carrier gas density in the additional term was based on the close relationship of the vapour phase mass transfer coefficient on the carrier gas density.

The sum of the experimental results was therefore fitted to equation 3.26 and the optimum parameters (a, b, c and d) were obtained by regressing data through a least squares analysis. It should be noted that the dependency of the vapour phase mass transfer coefficient on the Schmidt number and diffusion coefficient was not fixed in the regression analysis performed. This was done in order to obtain the optimum dependency. The correlation obtained from the least squares analysis is as follows:

$$Sh_G = \left(0.167\,\mathrm{Re}_{G,e}^{0.650} + \left(\rho_G \big/ \rho_{G,Naph} \right)^{0.349} \right) Sc_G^{0.545} \tag{3.27}$$

with: RMS = 2.37

R^2 = 0.987

From the regression results (equation 3.27) it appears that using a k_G dependency of $k_G \propto D_G^{0.5}$ provides a better fit for the prediction of the vapour phase mass transfer coefficient. This was confirmed by the fact that the regression analysis was performed without fixing a specific k_G dependency and resulted in a k_G dependency

of close to $k_G \propto D_G^{0.5}$. Referring to the RMS and R^2 values, it is clear that the correlations compiled from the sum of the experimental data (equations 3.27) provides a better fit than the correlations set up from only the naphthalene/air data (equations 3.24 and 3.25).

Figure 3.13 depicts a parity plot between the predicted values from equation 3.27 and the experimental results. From Figure 3.13 it can be seen that the predicted values match the experimentally obtained values reasonably well, with most of the predictions falling within the 5 % accuracy limits.

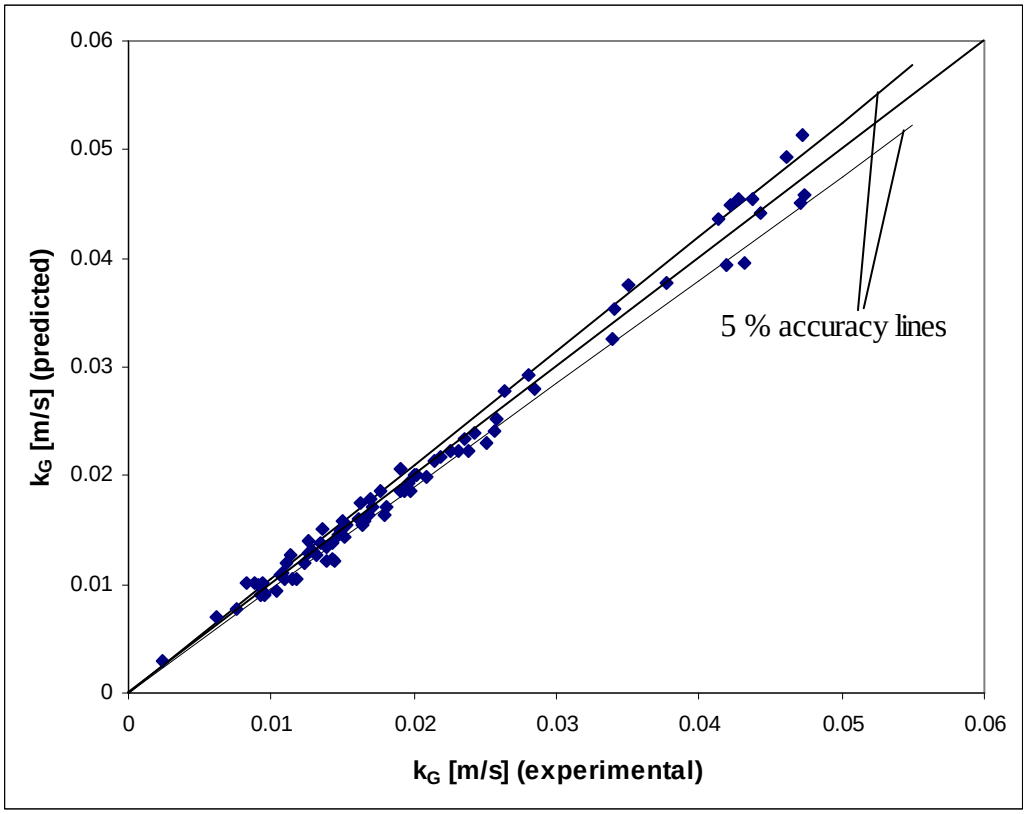

Figure 3.13: *Parity plot of the values predicted by equation 3.27 versus the experimental results*

3.6 Concluding Remarks

The following conclusions were drawn from the measurement of the vapour phase mass transfer coefficient:

- Repeating the experiments performed by Erasmus [3] (sublimation of naphthalene in air at atmospheric conditions) provided results that closely match those obtained by Erasmus [3]. From this it is concluded that the current experimental setup provides results that are accurate and repeatable.

- The predictions from the correlations of Bravo *et al.* [7] and Rocha *et al.* [9] tended to underestimate the experimentally obtained vapour phase mass transfer coefficients for all the systems investigated. The findings by Fair *et al.* [70], stating that the model by Rocha *et al.* [9] has a tendency to underestimate the mass transfer efficiency, is therefore confirmed.

- The correlation set up by Erasmus [3] tended to overestimate the vapour phase mass transfer coefficient when not dealing with the naphthalene/air system (at atmospheric conditions). The most likely cause for this inaccuracy was that the correlation by Erasmus [3] was developed using the diffusion coefficient data of Cho *et al.* [27]. In Chapter 2 the accuracy of the data by Cho *et al.* [27] was questioned and the use of inaccurate data in setting up a correlation will cause inaccurate predictions.

- For the naphthalene/CO_2 system the predictions from the correlation of Rocha *et al.* [9] showed a definite improvement. The most likely cause for this is that the Schmidt number for the naphthalene/CO_2 system approaches unity ($Sc \approx 1.39$). According to literature [3], when dealing with turbulent systems with Schmidt numbers close to unity the different mass transfer theories exhibit little difference. It is only with systems that have Schmidt numbers considerably larger or smaller than unity that the different models start diverging from one another. This is clearly seen with the naphthalene/helium system, where the Schmidt number is large ($Sc \approx 4.30$). For this system the

experimental results and the predictions from the correlations of Rocha *et al.* [9] and Bravo *et al.* [7] differ to a far greater extent.

- The inaccuracies in the predictions for the naphthalene/helium system are, however, not only the result of a larger Schmidt number. The necessity of conducting the naphthalene/helium experiments in the laminar regime brought a potential flaw to light in most of the correlations from literature: *Mass transfer from the laminar regime is not taken into account*. This lack is confirmed by the fact that all the correlations in literature that utilise the basic wetted-wall analogy (equation 1.1) predict a zero mass transfer at conditions where no gas flow is present. Mass transfer, however, occurs even when no gas flow is present. The error in predictions is small enough to be ignored when working with turbulent conditions, but at lower gas flow rates, i.e. laminar flow, this error becomes pronounced. In order to improve the accuracy of the correlations that utilise the basic wetted-wall analogy a term for the laminar flow regime needs to be added.

- Using the sum of the experimentally obtained data and conducting a least squares analysis a correlation was compiled. The correlation was created without fixing the k_G dependency to a known value. This was done in order to obtain the optimum k_G dependency for the prediction of the vapour phase mass transfer coefficient. The correlation obtained from the least squares analysis provided a k_G dependency of close to $k_G \propto D_G^{0.5}$. A parity plot indicated a good fit (within the 5 % accuracy limits) between the predicted values and the experimental values. The final correlation obtained was as follows:

$$Sh_G = \left(0.167\,\mathrm{Re}_{G,e}^{0.650} + \left(\rho_G \big/ \rho_{G,Naph} \right)^{0.349} \right) Sc_G^{0.545} \qquad (\mathrm{R}^2 = 0.987) \qquad (3.27)$$

It is recommended that equation 3.27 be tested in a system where the gas density is midway between that of air and helium. This can be accomplished by the blending of certain gases. The difference between the Schmidt number of the naphthalene/air and naphthalene/helium tests was considerable. Tests on the mass transfer coefficient for this 'midway' system can verify the accuracy of equation 3.27. The diffusion coefficient for the naphthalene/'blended gas' system will have to be determined in advance. Testing equation 3.27 for a gas denser than CO_2 might also be beneficial.

CHAPTER **4**

Conclusions and Recommendations

Numerous correlations (based on the wetted-wall theory) for the prediction of the vapour phase mass transfer coefficient (k_G) in structured packing are found in literature. These correlations relate the vapour phase mass transfer coefficient to the flow and transport properties through the dimensionless Reynolds and Schmidt numbers. Virtually all of the correlations in literature use one of two assumed dependencies for the vapour phase mass transfer coefficient on the Schmidt number. Since the Schmidt number is a function of the vapour phase diffusion coefficient this assumed dependency also extends towards the diffusion coefficient. The dependencies in question are $k_G \propto D_G^{0.5}$ and $k_G \propto D_G^{0.67}$.

The aim of this investigation was to test this assumed dependency by sublimating naphthalene in various carrier gases (air, helium and CO_2) and to propose a new correlation for the prediction of the vapour phase mass transfer coefficient. In order to create the proposed correlation accurate diffusion coefficient data were, however, required. Diffusion coefficient data for the naphthalene/air system were found to be well documented in literature, but diffusion coefficient data for systems other than naphthalene and air were found to be scarce. It was therefore necessary to include an additional experimental procedure, where the diffusion coefficient of naphthalene in CO_2 and helium was measured. The first section of this study therefore dealt with the experimental measurement of the diffusion coefficient of naphthalene in air, CO_2 and helium.

The technique employed for the measurement of the diffusion coefficient was the open Stefan tube method. The main reasons for choosing this technique were its adaptability, accuracy and its well documented sources of possible error. The

accuracy of the apparatus was first established by determining the diffusion coefficient of naphthalene in air. From literature [14, 15, 22, 27, 28, 31] it was apparent that consensus had not been reached as to what the actual diffusion coefficient for the naphthalene/air system should be. The correlation proposed by Cho *et al.* [27] was widely accepted as being the most accurate equation for the prediction of the diffusion coefficient for the naphthalene/air system. However, numerous other researchers, who performed studies before and after the study by Cho *et al.* [27], had obtained diffusion coefficient results for the naphthalene/air system that was in the order of 20% larger. The results from the current investigation (for the naphthalene/air system) agree well with the investigators whose results contradicted the results from Cho *et al.* [27]. The accuracy of the results by Cho *et al.* [27] was therefore questioned.

Cho *et al.* [27] proposed that possible wall interference effects could influence the natural diffusion process in the open Stefan tube method. No proof was, however, supplied by Cho *et al.* [27] that wall interference effects actually exist in the open Stefan tube method. By varying the area ratio of the wall area along the diffusion path length to the naphthalene surface area the possibility of the occurrence of wall interference was minimised and the optimum diffusion tube diameter and diffusion path length was subsequently determined for this investigation. An unexpected increase in the experimentally determined diffusion coefficient was observed when the tube diameter was decreased below a certain value. The theory of wall interference was thought a likely cause, but without evidence that this effect exists in this method this could not be confirmed. A recent study by Sacedo-Diaz *et al.* [41] on the effect that a decrease in the tube diameter has on the measured diffusion coefficient in the Stefan tube method provided a more plausible explanation for the unexpected increase in the diffusion coefficient observed in this investigation. Salcedo-Diaz *et al.* [41] showed that the viscous shear forces between the individual species became more pronounced as the diffusion tube diameter was decreased. The classic method for the calculation of the diffusion coefficient (Fick's law), which was used in this investigation, does not take the viscous shear forces between species into account. The gas flow rate was also identified as a possible error source, as a too high gas flow rate could cause turbulence at the top of the diffusion tube and lead to inaccurate measurements. By varying the gas flow rate the optimum flow rate was obtained.

The optimum conditions were subsequently determined for each system investigated. A comparison between the diffusion coefficient results for each system showed that the diffusion coefficient was strongly influenced by the carrier gas density. The diffusion coefficient was found to decrease as the carrier gas density increased. The less dense gas therefore provided a medium for diffusion that contained fewer obstructions for the diffusion of the naphthalene molecules. A correlation for the prediction of the diffusion coefficient of naphthalene in air, CO_2 and helium was subsequently proposed. The proposed correlation gave accurate predictions of the experimental results (within the 95 % certainty limit) and is as follows:

$$D = 1.034 \times 10^{-3} . \frac{T^{0.0986} \cdot M_G^{2.24} \cdot \mu_G^{0.261}}{\rho_G^{2.86} \cdot p_{Naph}^{0.0731}} \qquad (R^2 = 0.9997) \qquad (2.33)$$

It is recommended that the apparatus be adapted for larger diffusion tube diameters. This is to ascertain the influence that very large tube diameters has on the measured diffusion coefficient. Care, however, needs to be taken when increasing the tube diameter, since a larger tube diameter will result in a larger naphthalene volume. A larger naphthalene volume will, however, need a longer duration to obtain thermal stability, i.e. to reach the system temperature. A larger tube diameter could therefore cause inaccurate diffusion coefficient measurements. The sublimation of naphthalene in different carrier gases is also recommended, since the diffusion coefficient results could be tested against the correlation proposed in the current investigation.

The second experimental section dealt with the measurement of the vapour phase mass transfer coefficient of naphthalene in structured packing. A small diameter rectangular test column (60 x 200 mm) was constructed in order to measure the vapour phase mass transfer coefficient of naphthalene in air, CO_2 and helium. Only one other investigator measured the vapour phase mass transfer coefficient for naphthalene in structured packing [3]. Erasmus [3] measured the vapour phase mass transfer coefficient for the naphthalene/air system in a large diameter column (200 mm) and subsequently proposed a correlation. This correlation was extrapolated to other systems through an assumed dependency of k_G on the diffusion coefficient. The accuracy of the apparatus used in the current investigation was therefore first

tested by comparing the vapour phase mass transfer coefficient results for the naphthalene/air system from this investigation with the results obtained by Erasmus [3]. The vapour phase mass transfer coefficient results from this investigation closely matched the results of Erasmus [3] and the accuracy of the apparatus was therefore assumed to be satisfactory.

The k_G results for each system investigated were compared with the predictions from the correlations in literature [7, 9] and the correlation by Erasmus [3]. It was found that the correlations in literature (by Bravo *et al.* [7] and Rocha *et al.* [9]) tended to underestimate the vapour phase mass transfer coefficient. The correlation by Erasmus [3], however, tended to overestimate the vapour phase mass transfer coefficient when not dealing with the naphthalene/air system. The inaccurate predictions from the correlation by Erasmus [3] was not necessarily due to faulty assumptions in the creation of the correlation, but might also be due to the use of inaccurate diffusion coefficient data. In Chapter 2 the previously accepted diffusion coefficient data for the naphthalene/air system, by Cho *et al.* [27], was questioned. Since accurate diffusion coefficient data is required in the creation of correlations (for the prediction of k_G values) the use of inaccurate diffusion coefficient data would be detrimental to the accuracy of the correlation.

A potential error was found in the correlations from literature, namely that mass transfer in laminar flow across packing material is not taken into account. This is illustrated by the fact that most of the correlations in literature predict zero mass transfer when the gas flow rate is zero. This is not true, since mass transfer in a stagnant gas is a well documented fact. This potential error will be negligible when applying the correlations to turbulent systems, but the potential error will become more pronounced when applying the correlations to laminar gas flow systems. A correlation was therefore proposed, incorporating the sum of the experimental results gathered from this investigation (including the diffusion coefficient results from Chapter 2). This correlation contains an additional term that takes mass transfer in the laminar flow regime into account. The proposed correlation is as follows:

$$Sh_G = \left(0.167\,\mathrm{Re}_{G,e}^{0.650} + \left(\rho_G \big/ \rho_{G,Naph} \right)^{0.349} \right) Sc_G^{0.545} \qquad (R^2 = 0.987) \qquad (3.27)$$

The proposed correlation (equation 3.27) was obtained through a least squares analysis. The optimum dependency of the vapour phase mass transfer coefficient on the diffusion coefficient was obtained by not fixing a specific value to the Schmidt number exponent during the regression analysis. The least squares analysis provided a k_G dependency close to $k_G \propto D_G^{0.5}$. From the results gathered in this study it would appear that a k_G dependency of $k_G \propto D_G^{0.5}$ in correlations for the prediction of the vapour phase mass transfer coefficient in structured packing provides more accurate predictions.

Furthermore, it is recommended that equation 3.27 be tested for a carrier gas density above that of CO_2 and at a carrier gas density that lies between that of helium and air. The diffusion coefficients of the proposed carrier gases will, however, have to be measured in advance. It might also prove beneficial to look into the sublimation of another solid substance. Benzoic acid might be a suitable choice, but the extremely low vapour pressure of benzoic acid will increase the operational costs, especially referring to the consumption rate of the carrier gas.

References

1. Seader, J.D. and Henley, E.J., **Separation process principles**, John Wiley & Sons, Inc., 1998, Chapter 6.

2. Kister, H.Z., **Distillation design**, McGraw-Hill, New York, 1992, Chapter 2.

3. Erasmus, A.B., **Mass transfer in structured packing**, PhD Dissertation, Stellenbosch, University of Stellenbosch, 2004.

4. Wang, G.Q., Yuan, X.G. and Yu, K.T., *Review of mass-transfer correlations for packed columns.* **Ind. Eng. Chem. Res.** 44, 2005, 8715-8729.

5. Ovejero, G., van Grieken, R., Rodriguez, L. and Valverde, J.L., *The use of gas absorption correlations for mass transfer coefficients in distillation processes.* **Int. J. Heat Mass Transfer** 35(11), 1992, 2963-2968.

6. Crause, J.C., **A fundamental mass transfer model for an extractive distillation application**, MSc. Eng. thesis, Stellenbosch, University of Stellenbosch, 1998.

7. Bravo, J.L., Rocha, J.A. and Fair, J.R., *Mass transfer in gauze packings.* **Hydrocarbon Processing** 64, 1985, 91-95.

8. Hanley, B., Dunbobbin, B. and Bennett, D., *A unified model for countercurrent vapour/liquid packed columns. 2. Equations for the mass-transfer coefficients, mass-transfer area, the HETP, and the dynamic holdup.* **Ind. Eng. Chem. Res.** 33, 1994, 1222.

9. Rocha, J.A., Bravo, J.L. and Fair, J.R., *Distillation columns containing structured packings: A comprehensive model for their performance. 2. Mass-transfer model.* **Ind. Eng. Chem. Res.** 35, 1996, 1660-1667.

10. Erasmus, A.B. and Nieuwoudt, I., *Mass transfer in structured packing: A wetted-wall study*. **Ind. Eng. Chem. Res.** 40, 2001, 2310.

11. Nirdosh, I., Garred, L.J. and Baird, M.H.I., *Low-cost mass transfer experiments*. **Chem. Eng. Education**, 2000, 158-161.

12. Cussler, E.L., **Diffusion: Mass transfer in fluid systems**, Cambridge University Press, 1984, Chapter 4.

13. Marrero, T.R. and Mason, E.A., *Gaseous diffusion coefficients*. **J. Phys. Chem. Ref. Data** 1, No.1, 1972, 1-118.

14. Caldwell, L., *Diffusion coefficient of naphthalene in air and hydrogen.* **J. Chem. Eng. Data** 29, 1984, 60-62.

15. Gustafson, K.E. and Dickhut, R.M., *Molecular diffusivity of polycyclic aromatic hydrocarbons in air*. **J. Chem. Eng. Data** 39, 1994, 286-289.

16. Ashraf, S.M., Srivastava, R. and Hussain, A., *Determination of binary gas-phase diffusion coefficients using chromatography*. **J. Chem. Eng. Data** 31, 1986, 100-102.

17. Monfort, J. and Pellegatta, J., *Diffusion coefficients of the halocarbons* CCl_2F_2 *and* $C_2Cl_2F_4$ *with simple gases*. **J. Chem. Eng. Data** 36, 1991, 135-137.

18. Katsanos, N. A., *Studies of diffusion and other rate processes by gas chromatography*. **Pure & Appl. Chem.** 65, No. 10, 1993, 2245-2252.

19. Lee, C.Y. and Wilke, C.R., *Measurements of vapour diffusion coefficient*. **Ind. Eng. Chem.** 46, 1954, 2381-2387.

20. Ozguler, E.I., Sunol, S.G. and Sunol, A.K., *Analysis of the Stefan tube at supercritical conditions and diffusion coefficient measurements.* **Ind. Eng. Chem. Res.** 42, 2003, 4389-4397.

21. McBain, G.D., Suehrcke, H. and Harris, J.A., *Evaporation from an open cylinder*. **International Journal of Heat and Mass Transfer** 43, 2000, 2117-2128.

22. Goldstein, R.J. and Cho, H.H., *A review of mass transfer measurements using naphthalene sublimation*. **Experimental Thermal and Fluid Science** 10, 1995, 416-434.

23. Tashiro, S. and Sagawa, N., *Diffusion coefficient determination of sodium iodide vapour in rare gasses with use of ionisation sensor*. **Journal of Nuclear Science and Technology** 38(7), 2001, 551-556.

24. Slattery, J.C. and Mhetar, V.R., *Unsteady-state evaporation and the measurement of a binary diffusion coefficient.* **Chem. Eng. Science** 52(9), 1997, 1511-1515.

25. Bueno, J.L., Coca, J., Alvarez, R. and Villanueva, A.F., *Binary gaseous diffusion coefficients (Air with furan derivatives).* **J. Chem. Eng. Data** 25, 1980, 27-28.

26. Kwon, K.C., Ibrahim, T.H., YoonKook, P. and Simmons, C.M., *Pseudo-binary molecular diffusion of vapours into air*. **Advances in Environmental Research** 8, 2004, 667-678.

27. Cho, K., Irvine, T.F., Karni, J.R. and Karni, J., *Measurement of the diffusion coefficient of naphthalene into air*. **International Journal of Heat and Mass Transfer** 35, 1992, 957-966.

28. Siddiqi, M.A. and Atakan, B., *Combined experiments to measure low sublimation pressures and diffusion coefficients of organometallic compounds*. **Thermochimica Acta** 452, 2007, 128-134.

29. Da Siva, M.A.V.R., Monte, M.J.S. and Santos, L.M.N.B.F., *The design, construction and testing of a new Knudsen effusion apparatus*. **J. Chem. Thermodynamics** 38, 2006, 778-787.

30. Tesconi, M., Pikal, M.J. and Yalkowsky, S.H., *A method for the rapid estimation of sublimation rates of organic compounds at standard temperature and pressure*. **Journal of Pharmaceutical Sciences** 86, No. 11, 1997, 1299-1302.

31. Mack, E., *Average cross-sectional areas of molecules by gaseous diffusion methods.* **J. Am. Chem. Soc.** 47, 1925, 2468-2482.

32. Pieterse, N., Focke, W.W., Vuorinen, E. and Racz, I., *Estimating the gas permeability of commercial volatile corrosion inhibitors at elevated temperatures with thermo-gravimetry*. **Corrosion Science** 48, 2006, 1986-1995.

33. Pichon, C., Risoul, V., Trouve, G., Peters, W.A., Gilot, P. and Prado, G., *Study of evaporation of organic pollutants by thermo-gravimetric analysis: Experiments and modelling*. **Thermochimica Acta** 306, 1997, 143-151.

34. Marrero, T.R. and Mason, E.A., *Correlation and prediction of gaseous diffusion coefficients*. **AIChE Journal** 19, No.3, 1973, 498-503.

35. Arnold, J.H., *Studies in diffusion*. **Ind. Eng. Chem.** 22, No.10, 1930, 1091-1095.

36. Fuller, E.N., Schettler, P.D. and Giddings, J.C., *A new method for prediction of binary gas-phase diffusion coefficients*. **Ind. Eng. Chem.** 58, No.5, 1966, 19-27.

37. Geankoplis, C.J., **Transport processes and unit operations**, 3rd edition, Prentice Hall International, 1993.

38. Marrero, T.R. and Mason, E.A., *Temperature dependence of gaseous diffusion coefficients*. **Chem. Eng. Commun.** 7, 1980, 159-168.

39. Ambrose, D., Lawrenson, I.J. and Sparke, C.H.S., *The vapour pressure of naphthalene*. **J. Chem. Thermodynam.** 7, 1975, 1173-1176.

40. De Kruif, C.G., Kuipers, T., Van Miltenburg, J.C., Schaake, R.C.F. and Stevens, G., *The vapour pressure of solid and liquid naphthalene*. **J. Chem. Thermodynam.** 13, 1981, 1081-1086.

41. Salcedo-Diaz, R., Ruiz-Femenia, R., Kerkhof, P.J.A.M. and Peters, E.A.J.F., *Velocity profiles and circulation in Stefan-diffusion*. **Chem. Eng. Sc.** 2007, {article in press}.

42. Kerkhof, P.J.A.M. and Geboers, M.A.M., *Review: Analysis and extension of the theory of multicomponent fluid diffusion.* **Chem. Eng. Sc.** 60, 2005, 3129-3167.

43. Porter, K.E., *Why research is needed in distillation.* **Trans. IChemE** 73(A), 1995, 357-362.

44. Kurtz, D.P., McNulty, K.J. and Morgan, R.D., *Stretch the capacity of high-pressure distillation columns*. **Chem. Eng. Progr.** 87(2), 1991, 43-49.

45. Bravo, J.L., *Select structured packing or trays?* **Chem. Eng. Progr.** 93(7), 1997, 36-41.

46. Raynal, L., Ballaguet, J.P. and Barrere-Tricca, C., *Determination of mass transfer characteristics of co-current two-phase flow within structured packing.* **Chem. Eng. Science** 59, 2004, 5395-5402.

47. Sieres, J. and Fernandez-Seara, J., *Mass transfer characteristics of a structured packing for ammonia rectification in ammonia-water absorption refrigeration systems.* **Int. J. Refrigeration** 2006, 1-10 (article in press).

48. Basmadjian, D., **Mass transfer and separation processes: Principles and applications**, 2nd Edition, CRC Press, Taylor & Francis Group, 2007, Chapter 8.

49. Fair, J.R. and Bravo, J.L., *Distillation columns containing structured packing.* **Chem. Eng. Progr.** 86(1), 1990, 19-29.

50. Taylor, R. and Krishna, R., **Multicomponent mass transfer**, John Wiley & Sons, Inc., 1993, Chapter 7.

51. Rao, K.R., *Prediction of liquid film mass transfer coefficients in packed columns using liquid holdup.* **Can. J. Chem. Eng.** 71, 1993, 685-688.

52. Shulman, H.L., Ullrich, C.F., Proulx, A.Z. and Zimmerman, J.O., *Performance of packed columns. 2. Wetted and effective interfacial areas, gas- and liquid-phase mass transfer rates.* **AIChE J.** 1(2), 1955, 253-258.

53. Bravo, J.L. and Fair, J.R., *Generalised correlation for mass transfer in packed distillation columns.* **Ind. Eng. Chem. Process Des. Dev.** 21, 1982, 162-170.

54. Shi, M.G. and Mersmann, A., *Effective interfacial area in packed columns.* **Ger. Chem. Eng.** 8, 1985, 87-96.

55. Wagner, I., Stichlmair, J. and Fair, J.R., *Mass transfer in beds of modern, high-efficiency random packings.* **Ind. Eng. Chem. Res.** 36, 1997, 227-237.

56. Pichè, S., Grandjean, B.P.A. and Larachi, F., *Reconciliation procedure for gas-liquid interfacial area and mass-transfer coefficient in randomly packed towers.* **Ind. Eng. Chem. Res.** 41, 2002, 4911-4920.

57. Nawrocki, P.A., Xu, Z.P. and Chuang, K.T., *Mass transfer in structured corrugated packing.* **Can. J. Chem. Eng.** 69, 1991, 1336-1343.

58. Olujic, Z., Kamerbeek, A.B. and de Graauw, J., *A corrugation geometry based model for efficiency of structured distillation packing.* **Chem. Eng. Processing** 38, 1999, 683-695.

59. Brunazzi, E. and Paglianti, A., *Liquid-film mass-transfer coefficient in a column equipped with structured packings.* **Ind. Eng. Chem. Res.** 36, 1997, 3792-3799.

60. Shetty, S. and Cerro, R.L., *Fundamental liquid flow correlations for the computation of design parameters for ordered packings.* **Ind. Eng. Chem. Res.** 36, 1997, 771-783.

61. Laso, M., de Brito, M.H., Bomio, P. and von Stockar, U., *Liquid-side mass transfer characteristics of a structured packing.* **Chem. Eng. J.** 58, 1995, 251-258.

62. Murrieta, C.R., Seibert, A.F., Fair, J.R. and Rocha, J.A., *Liquid-side mass-transfer resistance of structured packings.* **Ind. Eng. Chem. Res.** 43, 2004, 7113-7120.

63. Billet, R. and Schultes, M., *Predictions of mass transfer columns with dumped and arranged packings: Updated summary of the calculation method of Billet and Schultes.* **Trans IChemE** 77(A), 1999, 498-504.

64. Rocha, J.A., Bravo, J.L. and Fair, J.R., *Distillation columns containing structured packings: A comprehensive model for their performance. 1. Hydraulic models.* **Ind. Eng. Chem. Res.** 32, 1993, 641-651.

65. Xu, Z.P., Afacan, A. and Chuang, K.T., *Predicting mass transfer in packed columns containing structured packings.* **Trans. IChemE** 78, 2000, 91-98.

66. Olujic, Z., *Development of a complete simulation model for predicting the hydraulic and separation performance of distillation columns equipped with structured packings.* **Chem. Biochem. Eng.** 11, 1997, 31.

67. Olujic, Z., Seibert, A.F., Kaibel, B., Jansen, H., Rietfort, T. and Zich, E., *Performance characteristics of a new high capacity structured packing.* **Chem. Eng. Processing** 42, 2003, 55-60.

68. Olujic, Z., Seibert, A.F. and Fair, J.R., *Influence of corrugation geometry on the performance of structured packings: an experimental study*. **Chem. Eng. Processing** 39, 2000, 335-342.

69. Verschoof, H.J. and Olujic, Z., *A general correlation for predicting the loading point of corrugated sheet structured packings.* **Ind. Eng. Chem. Res.** 38, 1999, 3663-3669.

70. Fair, J.R. Seibert, A.F., Behrens, M., Saraber, P.P. and Olujic, Z., *Structured packing performance – Experimental evaluation of two predictive models.* **Ind. Eng. Chem. Res.** 39, 2000, 1788-1796.

71. Rejl, J.F., Linek, V., Moucha, T., Prokopova, E., Valenz, L. and Hovorka, F., *Vapour- and liquid-side volumetric mass transfer coefficients measured in distillation column. Comparison with data calculated from absorption correlations.* **Chem. Eng. Science** 61, 2006, 6096-6108.

72. Coulson, J.M. and Richardson, J.F., **Coulson & Richardson's Chemical Engineering**, Vol 1, 6th Ed., Butterworth Heinemann, 1999, Chapter 10.

Appendix 1. Stefan Tube Experimental Setup

A1.1 Gas Flow Chamber Design

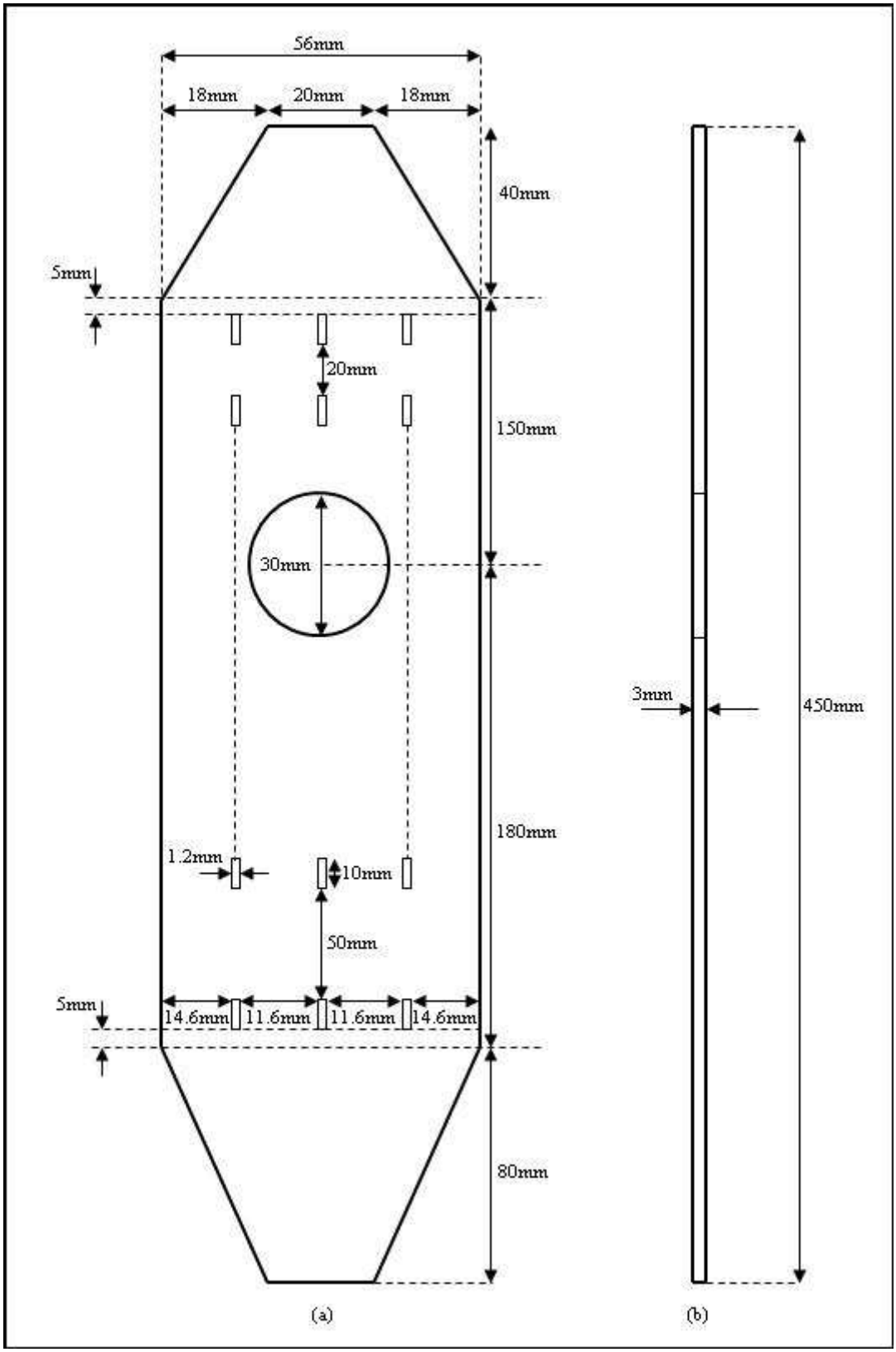

Figure A1.1: *Chamber Top and Bottom Plates (a) Top view, (b) Side view*

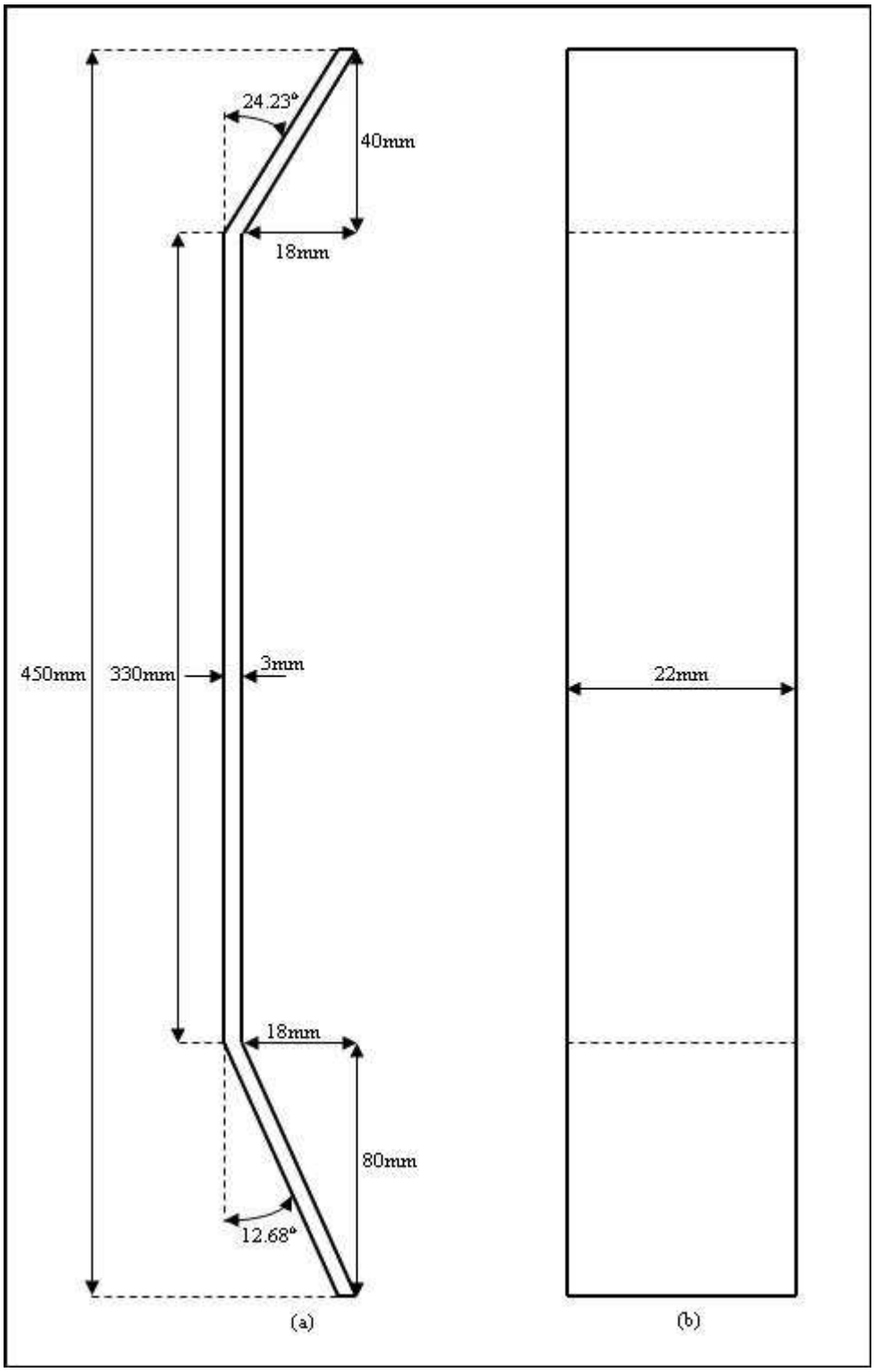

Figure A1.2: *Chamber Side Plates (a) Top view, (b) Side view*

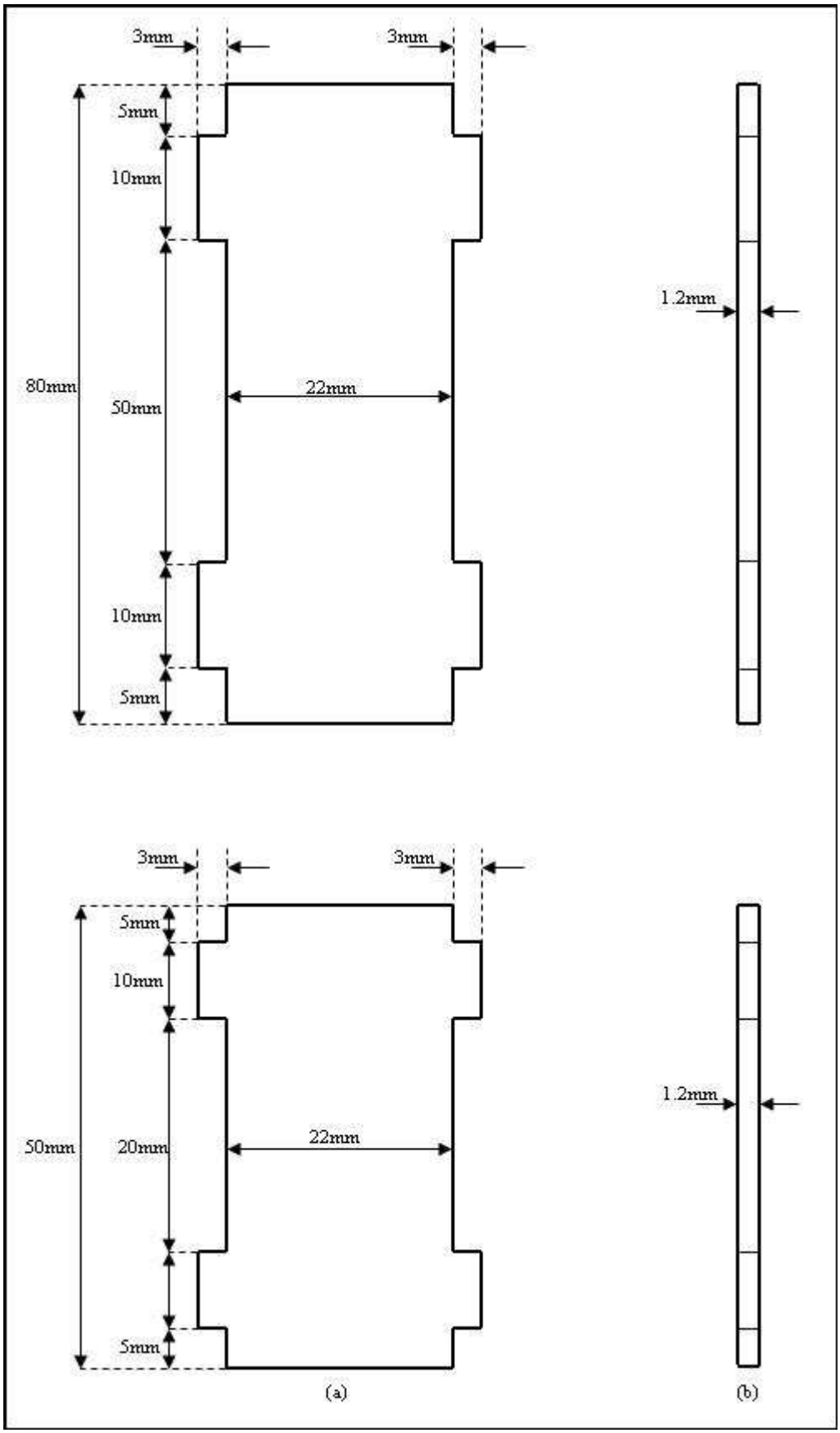

Figure A1.3: *Chamber Straightening Vanes (a) Side view, (b) Top view*

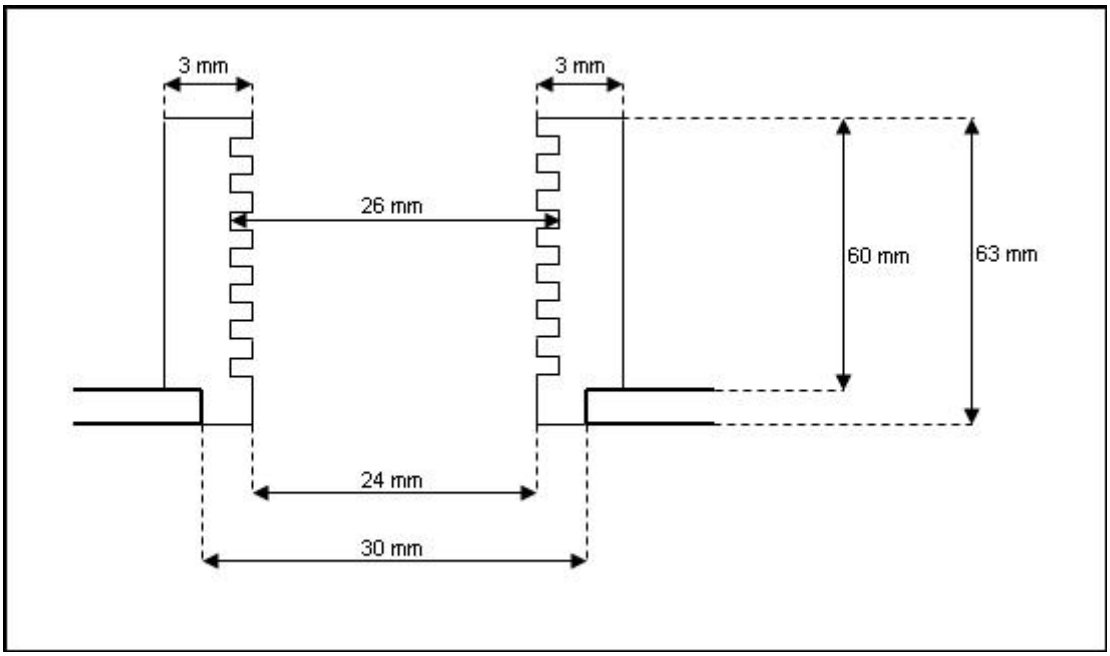

Figure A1.4: *Dimensions of the Stainless Steel Buss for the Topside Circular Opening in the Gas Flow Chamber*

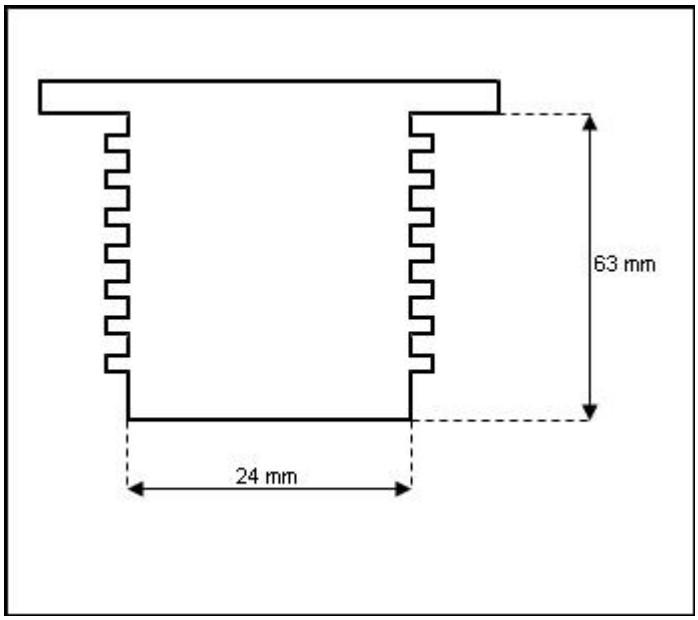

Figure A1.5: *Stainless Steel Screw Lid to fit into the Buss Illustrated in Figure A1.4*

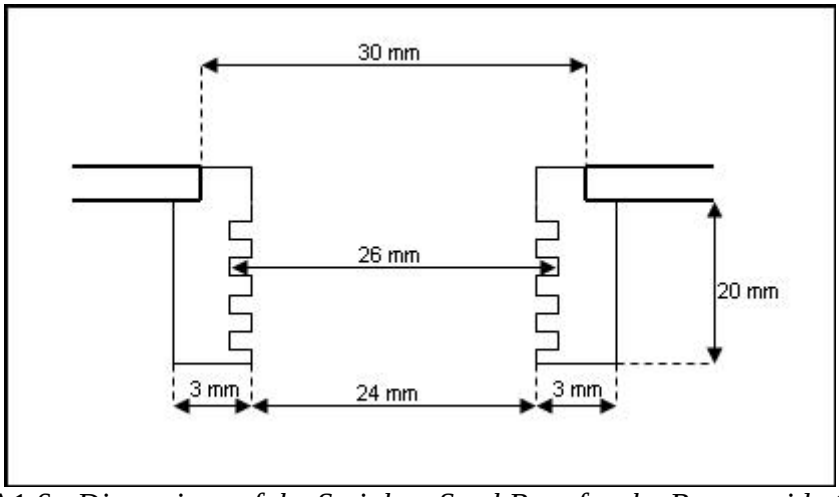

Figure A1.6: *Dimensions of the Stainless Steel Buss for the Bottom-side Circular Opening in the Gas Flow Chamber*

A1.2 Piping and Instrumentation Specification

Table A1.1: *Instrumentation for Stefan tube experiment*

Symbol	Description	Type	Pressure (atm)		Temperature (^oC)		Flow Rate (m^3/h)		Material of Construction
			Min	Max	Min	Max	Min	Max	
PI01	Pressure Indicator	Mechanical pressure gauge	0	4	15	30	-	-	304 SS (glycerin filled)
TI01	Temperature Indicator	Bimetal mechanical temperature sensor	0	1.5	15	30	-	-	304 SS
PI02	Pressure Indicator	Manometer	0	6	20	90	-	-	-
TI02	Temperature Indicator	PT100	-	-	20	90	-	-	-
FI	Flow Indicator	Rotameter	0	5	15	30	0	0.3	-
TIT	Temperature Indicator and Transmitter	Alcohol Thermometer	-	-	0	150	-	-	304 SS (wetted material)
CV01	Control Valve	Needle Valve	0	5	0	60	0	0.3	304 SS
V01	Water Bath Drain Valve	Plug/Ball Valve	-	-	-	-	-	-	304 SS

Table A1.2: *Piping specification for Stefan tube experiment*

Line NO.	**Material of Construction**	**Nominal OD, in. (mm)**	**Nominal ID, in. (mm)**	**Approximate Length, m**	**Allowable Working Pressure, atm**
1	Copper	0.5 (12.7)	0.451 (10.2)	0.5	3
2	Copper	0.5 (12.7)	0.451 (10.2)	1.5	3
3	Copper	0.5 (12.7)	0.451 (10.2)	0.5	3
4	Copper	0.5 (12.7)	0.451 (10.2)	0.2	3

A1.3 Experimental Setup within Fume Cabinet

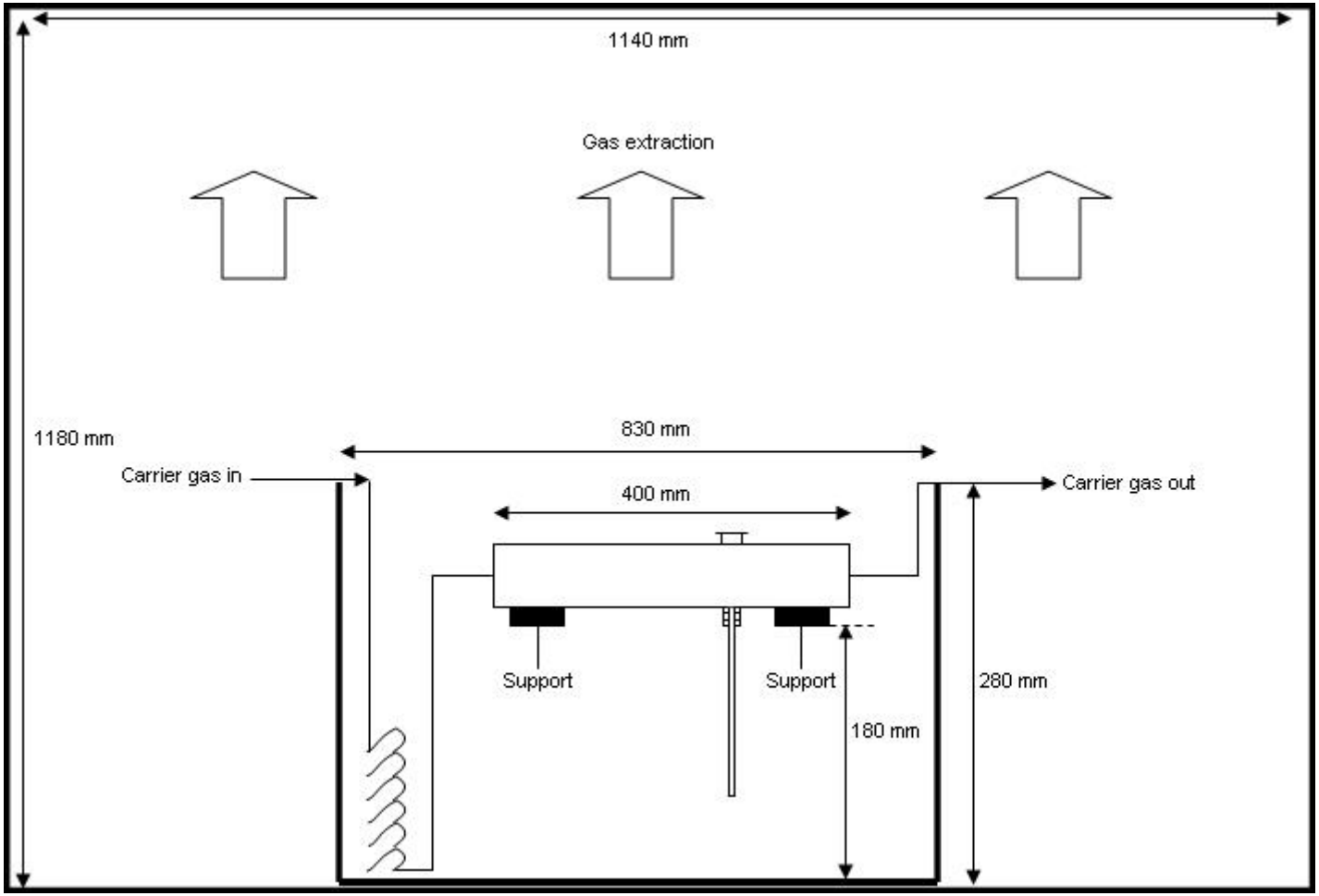

Figure A1.7: *Illustration of the experimental setup within the fume cabinet (dimensions included)*

Appendix 2. Experimental Results for the Diffusion Coefficient Measurements

A2.1 Experimental Results for the Naphthalene/Air System

Table A2.1: *Experimental results for the naphthalene/air system at various gas flow rates (tests for turbulence)*

Temperature	Gas Flow Rate	Mass Loss	Experiment Duration	Molecular Mass	Vapour Pressure	Barometric Pressure	Diff. Path Length	Tube Diameter	Diffusion Flux	Diffusion Coefficient	Diffusion Coefficient
T (K)	Q (m3/h)	Δm (g)	t_{exp} (hr)	M_{napht} (g/mol)	p_{napht} [Pa]	P_{system} (Pa)	(z_2-z_1) (m)	d_{tube} (m)	N_{napht} (mol/m^2.s)	D_{napht} (m^2/s)	D_{napht} (cm^2/s)
299.15	0.0425	0.00121	22.50	128.16	12.353	99800	0.062	0.0152	6.423E-07	8.019E-06	0.0790
299.15	0.0425	0.00136	25.25	128.16	12.353	99800	0.062	0.0152	6.433E-07	8.031E-06	0.0791
299.15	0.0850	0.00129	24.00	128.16	12.353	99500	0.062	0.0152	6.420E-07	8.014E-06	0.0787
299.15	0.0850	0.00154	28.50	128.16	12.353	99300	0.062	0.0152	6.454E-07	8.057E-06	0.0790
299.15	0.1274	0.00142	26.33	128.16	12.353	99500	0.062	0.0152	6.441E-07	8.040E-06	0.0790
299.15	0.1274	0.00120	22.25	128.16	12.353	99400	0.062	0.0152	6.442E-07	8.042E-06	0.0789
299.15	0.1699	0.00131	23.67	128.16	12.353	99400	0.062	0.0152	6.612E-07	8.253E-06	0.0810
299.15	0.1699	0.00135	24.50	128.16	12.353	99800	0.062	0.0152	6.582E-07	8.216E-06	0.0809
299.15	0.2124	0.00131	22.17	128.16	12.353	99400	0.062	0.0152	7.059E-07	8.812E-06	0.0864
299.15	0.2124	0.00150	25.25	128.16	12.353	99300	0.062	0.0152	7.096E-07	8.858E-06	0.0868
299.15	0.2549	0.00172	26.33	128.16	12.353	99300	0.062	0.0152	7.802E-07	9.739E-06	0.0954
299.15	0.2549	0.00151	23.42	128.16	12.353	99500	0.062	0.0152	7.702E-07	9.615E-06	0.0944
346.15	0.0456	0.03641	11.50	128.16	601.281	99500	0.062	0.0152	3.782E-05	1.119E-05	0.1099
346.15	0.0456	0.03215	10.25	128.16	601.281	99500	0.062	0.0152	3.746E-05	1.108E-05	0.1089
346.15	0.1367	0.03151	10.00	128.16	601.281	99500	0.062	0.0152	3.764E-05	1.114E-05	0.1094
346.15	0.1367	0.03577	11.42	128.16	601.281	99500	0.062	0.0152	3.742E-05	1.107E-05	0.1087

Table A2.2: *Experimental results for the naphthalene/air system at various tube diameters (tests for wall adsorption)*

T (K)	Q (m3/h)	Δm (g)	t_{exp} (hr)	M_{napht} (g/mol)	p_{napht} [Pa]	P_{system} (Pa)	(z_2-z_1) (m)	d_{tube} (m)	N_{napht} (mol/m^2.s)	D_{napht} (m^2/s)	D_{napht} (cm^2/s)
317.45	0.0425	0.00085	13.37	128.16	65.447	99500	0.061	0.0050	7.020E-06	1.726E-05	0.1695
320.55	0.0425	0.00165	19.92	128.16	84.990	101000	0.061	0.0050	9.145E-06	1.749E-05	0.1743
331.15	0.0425	0.00340	17.25	128.16	199.209	101000	0.061	0.0050	2.176E-05	1.833E-05	0.1827
299.15	0.0425	0.00065	55.00	128.16	12.353	101000	0.061	0.0050	1.305E-06	1.602E-05	0.1597
336.45	0.0425	0.00280	5.00	128.16	298.122	99900	0.061	0.0082	2.298E-05	1.314E-05	0.1295
321.05	0.0425	0.00199	12.60	128.16	88.602	99900	0.061	0.0082	6.482E-06	1.191E-05	0.1174
308.55	0.0425	0.00133	25.87	128.16	29.907	99900	0.061	0.0082	2.110E-06	1.104E-05	0.1089
321.05	0.0425	0.00112	5.32	128.16	88.602	99700	0.061	0.0102	5.588E-06	1.026E-05	0.1010
326.45	0.0425	0.00397	11.88	128.16	137.605	99800	0.061	0.0102	8.861E-06	1.066E-05	0.1049
303.35	0.0425	0.00111	27.88	128.16	18.477	99800	0.061	0.0102	1.056E-06	8.792E-06	0.0866
326.75	0.0425	0.00270	6.00	128.16	140.944	99400	0.061	0.0122	8.343E-06	9.803E-06	0.0962
308.55	0.0425	0.00199	22.25	128.16	29.907	99400	0.061	0.0122	1.658E-06	8.676E-06	0.0851
320.25	0.0425	0.00610	23.45	128.16	82.889	99400	0.061	0.0122	4.823E-06	9.447E-06	0.0927

Table A2.3: *Experimental results for the naphthalene/air system at various diffusion path lengths (tests for wall adsorption)*

T (K)	Q (m3/h)	Δm (g)	t_{exp} (hr)	M_{napht} (g/mol)	p_{napht} [Pa]	P_{system} (Pa)	(z_2-z_1) (m)	d_{tube} (m)	N_{napht} (mol/m^2.s)	D_{napht} (m^2/s)	D_{napht} (cm^2/s)
321.35	0.0425	0.00586	21.42	128.16	90.835	99400	0.105	0.0152	3.268E-06	1.009E-05	0.0990
306.95	0.0425	0.00141	19.25	128.16	25.839	99400	0.105	0.0152	8.749E-07	9.072E-06	0.0890
306.85	0.0425	0.00138	19.00	128.16	25.602	99500	0.105	0.0152	8.675E-07	9.076E-06	0.0891
321.15	0.0425	0.00451	17.00	128.16	89.341	99800	0.105	0.0152	3.169E-06	9.940E-06	0.0979
335.55	0.0425	0.01094	12.50	128.16	278.680	99400	0.105	0.0152	1.045E-05	1.097E-05	0.1076
335.15	0.0425	0.01293	15.33	128.16	270.415	99300	0.105	0.0152	1.007E-05	1.088E-05	0.1067
299.15	0.0425	0.00104	24.88	128.16	12.353	99500	0.080	0.0152	4.992E-07	8.041E-06	0.0790
313.15	0.0425	0.00331	20.00	128.16	45.111	99500	0.080	0.0152	1.977E-06	9.126E-06	0.0896
334.15	0.0425	0.01241	12.50	128.16	250.720	99800	0.080	0.0152	1.186E-05	1.050E-05	0.1034
328.15	0.0425	0.00869	14.33	128.16	157.526	99900	0.080	0.0152	7.242E-06	1.003E-05	0.0989

Table A2.4: *Experimental results for the naphthalene/air system at the optimal parameters*

T (K)	Q (m3/h)	Δm (g)	t_{exp} (hr)	M_{napht} (g/mol)	p_{napht} [Pa]	P_{system} (Pa)	(z_2-z_1) (m)	d_{tube} (m)	N_{napht} (mol/m^2.s)	D_{napht} (m^2/s)	D_{napht} (cm^2/s)
299.15	0.0425	0.00117	21.67	128.16	12.353	99300	0.062	0.0152	6.450E-07	8.052E-06	0.0789
299.15	0.0425	0.00116	21.50	128.16	12.353	99300	0.062	0.0152	6.444E-07	8.045E-06	0.0788
299.15	0.0425	0.00114	21.00	128.16	12.353	99300	0.062	0.0152	6.484E-07	8.094E-06	0.0793
300.45	0.0425	0.00143	23.23	128.16	14.011	99500	0.062	0.0152	7.352E-07	8.126E-06	0.0798
304.35	0.0425	0.00183	20.17	128.16	20.299	99600	0.062	0.0152	1.084E-06	8.376E-06	0.0823
304.35	0.0425	0.00184	20.15	128.16	20.299	99400	0.062	0.0152	1.091E-06	8.429E-06	0.0827
309.45	0.0425	0.00296	19.87	128.16	32.446	99500	0.062	0.0152	1.780E-06	8.748E-06	0.0859
309.45	0.0425	0.00302	20.17	128.16	32.446	99500	0.062	0.0152	1.789E-06	8.793E-06	0.0863
309.45	0.0425	0.00321	21.58	128.16	32.446	99500	0.062	0.0152	1.776E-06	8.732E-06	0.0858
319.85	0.0425	0.00779	20.12	128.16	80.161	99500	0.062	0.0152	4.625E-06	9.510E-06	0.0934
319.85	0.0425	0.00753	19.50	128.16	80.161	99500	0.062	0.0152	4.612E-06	9.483E-06	0.0931
331.15	0.0425	0.00846	8.50	128.16	199.209	100500	0.062	0.0152	1.189E-05	1.018E-05	0.1009
331.15	0.0425	0.01040	10.50	128.16	199.209	100500	0.062	0.0152	1.183E-05	1.013E-05	0.1005
346.15	0.0425	0.03575	11.42	128.16	601.281	100600	0.062	0.0152	3.740E-05	1.107E-05	0.1099
346.15	0.0425	0.03482	11.17	128.16	601.281	100200	0.062	0.0152	3.725E-05	1.102E-05	0.1090

A2.2 Experimental Results for the Naphthalene/CO_2 System

Table A2.5: *Experimental results for the naphthalene/CO_2 system (includes variations of gas flow rate, tube diameter and diffusion path length)*

T (K)	Q (m3/h)	Δm (g)	t_{exp} (hr)	M_{napht} (g/mol)	p_{napht} [Pa]	P_{system} (Pa)	(z_2-z_1) (m)	d_{tube} (m)	N_{napht} (mol/m^2.s)	D_{napht} (m^2/s)	D_{napht} (cm^2/s)
313.95	0.0348	0.00432	26.05	128.16	48.386	99700	0.062	0.0152	1.981E-06	6.624E-06	0.0652
313.95	0.0348	0.00322	19.07	128.16	48.386	100100	0.062	0.0152	2.017E-06	6.745E-06	0.0666
329.65	0.0348	0.01223	19.30	128.16	177.253	99700	0.062	0.0152	7.569E-06	7.250E-06	0.0713
329.65	0.0348	0.01465	23.27	128.16	177.253	100100	0.062	0.0152	7.521E-06	7.204E-06	0.0712
346.25	0.0348	0.03500	15.80	128.16	605.505	100200	0.062	0.0152	2.646E-05	7.776E-06	0.0769
346.25	0.0348	0.02220	9.93	128.16	605.505	99800	0.062	0.0152	2.669E-05	7.845E-06	0.0773
298.55	0.0348	0.00092	23.65	128.16	11.650	100600	0.062	0.0152	4.646E-07	6.138E-06	0.0609
298.55	0.0348	0.00117	30.07	128.16	11.650	100100	0.062	0.0152	4.648E-07	6.140E-06	0.0607
303.85	0.0348	0.00107	16.25	128.16	19.369	99700	0.062	0.0152	7.865E-07	6.360E-06	0.0626
321.15	0.0348	0.00391	19.00	128.16	89.341	99600	0.061	0.0122	3.816E-06	6.953E-06	0.0683
332.75	0.0348	0.00959	17.83	128.16	225.337	99100	0.061	0.0122	9.971E-06	7.459E-06	0.0730
303.35	0.0348	0.00088	22.53	128.16	18.477	99300	0.105	0.0152	4.665E-07	6.685E-06	0.0655
321.35	0.0348	0.00431	21.50	128.16	90.835	99300	0.105	0.0152	2.394E-06	7.392E-06	0.0724
306.35	0.0348	0.00165	25.50	128.16	24.449	99700	0.080	0.0152	7.729E-07	6.441E-06	0.0634
329.35	0.0348	0.00761	15.83	128.16	173.136	99800	0.080	0.0152	5.741E-06	7.258E-06	0.0715
313.25	0.0696	0.00296	18.83	128.16	45.509	99800	0.062	0.0152	1.877E-06	6.660E-06	0.0656
341.15	0.0696	0.01147	7.50	128.16	421.203	99800	0.062	0.0152	1.827E-05	7.611E-06	0.0750
298.85	0.0248	0.00106	50.55	128.16	11.997	200000	0.062	0.0152	2.505E-07	3.216E-06	0.0322
298.85	0.0248	0.00111	54.27	128.16	11.997	200000	0.062	0.0152	2.443E-07	3.137E-06	0.0314
314.15	0.0248	0.00193	22.10	128.16	49.239	200000	0.062	0.0152	1.043E-06	3.430E-06	0.0343
329.95	0.0248	0.00741	21.85	128.16	181.459	200000	0.062	0.0152	4.051E-06	3.795E-06	0.0380
329.95	0.0248	0.00339	9.93	128.16	181.459	200000	0.062	0.0152	4.076E-06	3.819E-06	0.0382
345.45	0.0248	0.01980	18.02	128.16	572.457	200000	0.062	0.0152	1.313E-05	4.078E-06	0.0408
345.85	0.0248	0.01102	9.90	128.16	588.771	200000	0.062	0.0152	1.330E-05	4.020E-06	0.0402
303.55	0.0248	0.00160	48.17	128.16	18.829	200000	0.062	0.0152	3.968E-07	3.297E-06	0.0330

A2.3 Experimental Results for the Naphthalene/Helium System

Table A2.6: *Experimental results for the naphthalene/helium system (includes variations of gas flow rate, tube diameter and diffusion path length)*

T (K)	Q (m3/h)	Δm (g)	t_{exp} (hr)	M_{napht} (g/mol)	p_{napht} [Pa]	P_{system} (Pa)	(z_2-z_1) (m)	d_{tube} (m)	N_{napht} (mol/m^2.s)	D_{napht} (m^2/s)	D_{napht} (cm^2/s)
313.75	0.0961	0.02367	30.42	128.16	47.548	99800	0.062	0.0152	9.295E-06	3.161E-05	0.3113
313.75	0.0961	0.01375	17.63	128.16	47.548	99300	0.062	0.0152	9.314E-06	3.167E-05	0.3104
313.75	0.0961	0.01497	19.27	128.16	47.548	99400	0.062	0.0152	9.281E-06	3.156E-05	0.3096
328.95	0.0961	0.06040	21.02	128.16	167.783	99500	0.062	0.0152	3.433E-05	3.466E-05	0.3404
329.15	0.0961	0.07203	24.25	128.16	170.440	99500	0.062	0.0152	3.548E-05	3.529E-05	0.3465
298.35	0.0961	0.00436	23.78	128.16	11.424	99500	0.062	0.0152	2.190E-06	2.948E-05	0.2895
298.35	0.0961	0.00432	23.75	128.16	11.424	99400	0.062	0.0152	2.173E-06	2.925E-05	0.2869
344.45	0.0961	0.10118	10.78	128.16	533.449	99700	0.062	0.0152	1.121E-04	3.721E-05	0.3661
344.55	0.0961	0.08013	8.37	128.16	537.239	99500	0.062	0.0152	1.144E-04	3.772E-05	0.3704
319.85	0.0961	0.01652	12.23	128.16	80.161	99300	0.062	0.0152	1.613E-05	3.316E-05	0.3250
300.25	0.0961	0.00259	18.25	128.16	13.743	99500	0.061	0.0122	2.631E-06	2.915E-05	0.2863
333.45	0.0961	0.02462	9.23	128.16	237.720	99800	0.061	0.0122	4.944E-05	3.513E-05	0.3460
306.15	0.0961	0.00585	19.50	128.16	24.002	99900	0.080	0.0152	3.583E-06	3.040E-05	0.2997
339.15	0.0961	0.04822	9.78	128.16	364.082	99300	0.080	0.0152	5.887E-05	3.641E-05	0.3568
299.25	0.1442	0.00365	18.50	128.16	12.474	99300	0.062	0.0152	2.358E-06	2.916E-05	0.2858
326.15	0.1442	0.02138	9.37	128.16	134.339	99300	0.062	0.0152	2.726E-05	3.410E-05	0.3342

Table A2.6: *Continues*

T (K)	Q (m3/h)	Δm (g)	t_{exp} (hr)	M_{napht} (g/mol)	p_{napht} [Pa]	P_{system} (Pa)	(z_2-z_1) (m)	d_{tube} (m)	N_{napht} (mol/m^2.s)	D_{napht} (m^2/s)	D_{napht} (cm^2/s)
298.35	0.0684	0.00161	18.82	128.16	11.424	200000	0.062	0.0152	1.022E-06	1.376E-05	0.1376
298.35	0.0684	0.00202	22.50	128.16	11.424	200000	0.062	0.0152	1.072E-06	1.444E-05	0.1444
303.15	0.0684	0.00273	18.82	128.16	18.132	200000	0.062	0.0152	1.733E-06	1.494E-05	0.1494
303.15	0.0684	0.00291	19.25	128.16	18.132	200000	0.062	0.0152	1.806E-06	1.556E-05	0.1556
313.45	0.0684	0.00345	9.32	128.16	46.314	200000	0.062	0.0152	4.423E-06	1.543E-05	0.1543
313.45	0.0684	0.00585	15.33	128.16	46.314	200000	0.062	0.0152	4.557E-06	1.590E-05	0.1590
319.45	0.0684	0.01075	16.47	128.16	77.515	200000	0.062	0.0152	7.798E-06	1.656E-05	0.1656
319.45	0.0684	0.00965	14.50	128.16	77.515	200000	0.062	0.0152	7.949E-06	1.688E-05	0.1688
328.75	0.0684	0.01882	13.75	128.16	165.163	200000	0.062	0.0152	1.635E-05	1.677E-05	0.1677
328.75	0.0684	0.01582	11.00	128.16	165.163	200000	0.062	0.0152	1.718E-05	1.762E-05	0.1762
344.15	0.0684	0.04386	9.23	128.16	522.226	200000	0.062	0.0152	5.674E-05	1.925E-05	0.1925
344.15	0.0684	0.05326	10.82	128.16	522.226	200000	0.062	0.0152	5.881E-05	1.995E-05	0.1995

A2.4 Sample Calculations

The following sample calculations relates to the first experimental run depicted in Table A2.1.

Calculation of the vapour pressure of naphthalene:

The correlation by Ambrose et al [39] is used and is represented by equation 2.31.

$$T.\log p = \frac{1}{2}a_0 + \sum a_s.E_s\left(x\right) \tag{2.31}$$

$$\frac{301.6247}{2} + \left(791.4937\right)\left(\frac{\left(2\times 299.15\right)-574}{114}\right) +$$

$$= \left(-8.2536\right)\left[2\left(\frac{\left(2\times 299.15\right)-574}{114}\right)^2 - 1\right] +$$

$$\left(0.4043\right)\left[4\left(\frac{\left(2\times 299.15\right)-574}{114}\right)^3 - 3\left(\frac{\left(2\times 299.15\right)-574}{114}\right)\right]$$

$$= 326.7862$$

$$\log p = 1.0924$$

$$p = 12.353 \text{ Pa}$$

Calculation of the diffusion flux:

The diffusion flux is calculated through equation 2.28:

$$N_A = \frac{\Delta m}{M_A.t_{\exp}.\left(\frac{\pi}{4}\right).d_{tube}^2} \tag{2.28}$$

$$= \frac{0.00121}{\left(128.16\right)\left(22.5\times 3600\right)\left(\frac{\pi}{4}\times 0.0152^2\right)}$$

$$= 6.423\times 10^{-7} \text{ mol/m}^2\text{.s}$$

Calculation of the diffusion coefficient:

The diffusion coefficient is calculated through equation 2.27:

$$N_A = \frac{D_{AB}P}{RT(z_2 - z_1)} \ln\left(\frac{P - p_{A2}}{P - p_{A1}}\right) \tag{2.27}$$

$$6.423\times10^{-7} = \frac{D_{AB}\times 99800}{(8.3145)(299.15)(0.062)} \ln\left(\frac{99800-0}{99800-12.353}\right)$$

$$D_{AB} = 8.019\times10^{-6}\ \text{m}^2/\text{s}$$

$$= 0.08019\ \text{cm}^2/\text{s}$$

In order to obtain the diffusion coefficient for atmospheric pressure, the diffusion coefficient needs to be adjusted, giving the final diffusion coefficient (at a pressure of 101325 Pa) as follows:

$$D_{AB,1atm} = D_{AB,P} \times \frac{P}{101325}$$

$$= 0.08019 \times \frac{99800}{101325}$$

$$= 0.0790\ \text{cm}^2/\text{s}$$

A2.5 Account of Error Analysis

The error analysis performed on the experimental results for the diffusion coefficient experiments were approached as follows:

The main input variables for the calculation of the diffusion coefficient were first identified and are as follows:

- System temperature
- Mass loss
- Experimental duration
- Diffusion path length
- Diffusion tube diameter

The system temperature was measured with a calibrated PT100 temperature probe with an accuracy 0.1 ^{o}C. The mass loss was determined with a calibrated semi-micro analytical balance that exhibits a maximum measurement uncertainty of 0.04 mg. Due to the long duration of each experimental run, the uncertainties in the experimental duration were found to have a negligible effect on the diffusion coefficient calculation. Uncertainties in the experimental duration were therefore not included in the error analysis. Uncertainties in the determination of the diffusion path length and tube diameter were solely due to the physical measurement of the two parameters in question. The measurement of the diffusion path length and tube diameter was accurate to within 0.01 mm and the maximum error in the measurement of the two parameters was therefore assumed to be 0.01 mm.

The maximum positive deviation from the experimentally obtained diffusion coefficient was determined by establishing the effect that an increase, or decrease, of the uncertainty in each variable would have on the value of the diffusion coefficient. It was found that the maximum *positive* deviation from the experimental results is obtained by:

1. *Increasing* the measured mass loss by the measurement uncertainty.
2. *Decreasing* the measured system temperature by the measurement uncertainty.
3. *Increasing* the measured diffusion path length by the measurement uncertainty.
4. *Decreasing* the measured tube diameter by the measurement uncertainty.

The maximum *negative* deviation is obtained by following the steps outlined above in the opposite manner. In order to demonstrate the error analysis, the sample calculations performed in A2.4 is repeated with the measurement uncertainties included to obtain the maximum positive deviation:

Calculation of the vapour pressure of naphthalene (T = 299.05 K):

$$T.\log p = \frac{1}{2}a_0 + \sum a_s.E_s(x) \tag{2.31}$$

$$\frac{301.6247}{2} + (791.4937)\left(\frac{(2\times 299.05)-574}{114}\right) +$$

$$= (-8.2536)\left[2\left(\frac{(2\times 299.05)-574}{114}\right)^2 - 1\right] +$$

$$(0.4043)\left[4\left(\frac{(2\times 299.05)-574}{114}\right)^3 - 3\left(\frac{(2\times 299.05)-574}{114}\right)\right]$$

$$= 325.412$$

$$\log p = 1.0882$$

$$p = 12.233 \text{ Pa}$$

Calculation of the diffusion flux (Δm = 0.00125 g, d = 0.01519):

$$N_A = \frac{\Delta m}{M_A.t_{\exp}.\left(\frac{\pi}{4}\right).d_{tube}^2} \tag{2.28}$$

$$= \frac{0.00125}{(128.16)(22.5\times 3600)\left(\frac{\pi}{4}\times 0.01519^2\right)}$$

$$= 6.645\times 10^{-7}\ \text{mol/m}^2\text{.s}$$

Calculation of the diffusion coefficient:

$$N_A = \frac{D_{AB}P}{RT(z_2 - z_1)}\ln\left(\frac{P - p_{A2}}{P - p_{A1}}\right) \tag{2.27}$$

$$6.645\times 10^{-7} = \frac{D_{AB}\times 99800}{(8.3145)(299.05)(0.06201)}\ln\left(\frac{99800-0}{99800-12.233}\right)$$

$$D_{AB} = 8.374\times 10^{-6}\ \text{m}^2\text{/s}$$

$$= 0.08374\ \text{cm}^2\text{/s}$$

Adjusting the diffusion coefficient to atmospheric pressure:

$$D_{AB,1atm} = D_{AB,P}\times\frac{P}{101325}$$

$$= 0.08374\times\frac{99800}{101325}$$

$$= 0.0825\ \text{cm}^2\text{/s}$$

Calculation of the maximum deviation (%):

$$Deviation = \frac{D_{adjusted} - D_{experimental}}{D_{experimental}}\times 100$$

$$= \frac{0.0825 - 0.079}{0.079}\times 100$$

$$= 4.43\ \%$$

Appendix 3. Test Column Experimental Setup

A3.1 Test Column Design

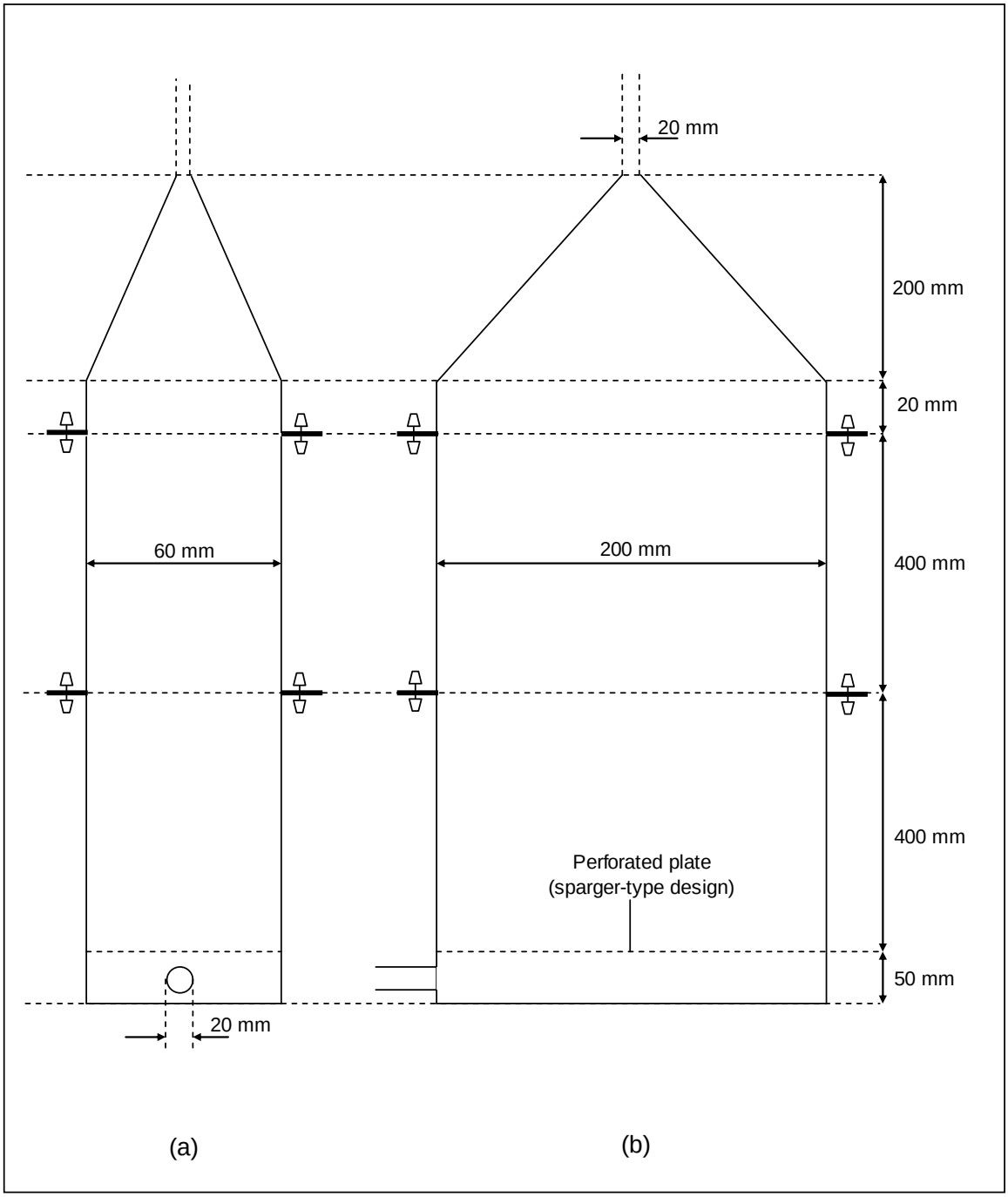

Figure A3.1: *Schematic representation of the test column (a) Side view and (b) Front view*

A3.2 Piping and Instrumentation Specification

Table A3.1: *Instrumentation for the test column*

Symbol	Description	Type	Pressure (atm)		Temperature (^oC)		Flow Rate (kg/h)		Material of Construction
			Min	Max	Min	Max	Min	Max	
MFC	Mass Flow Controller	Model 8626 (Serial no. 001000)	2	10	15	30	0	51.45	-
TI01	Temperature Indicator	PT100	-	-	-20	100	-	-	-
TI02	Temperature Indicator	PT100	-	-	-20	100	-	-	-
PI01	Pressure Indicator	Mechanical pressure gauge	0	4	0	90	-	-	304 SS (glycerin filled)
GV01	Globe Valve	-	0	4	0	60	-	-	304 SS
NV01	Needle Valve	-	0	4	0	60	-	-	304 SS

Table A3.2: *Piping specification for the test column*

Line NO.	**Material of Construction**	**Nominal OD, in. (mm)**	**Nominal ID, in. (mm)**	**Approximate Length, m**	**Allowable Working Pressure, atm**
1	Copper	0.8 (20.32)	0.75 (19.05)	1	5
2	Copper	0.8 (20.32)	0.75 (19.05)	0.5	5
3	Copper	0.8 (20.32)	0.75 (19.05)	0.3	5
4	Copper	0.8 (20.32)	0.75 (19.05)	0.3	5

A3.3 Calibration Certificate for the PT100 Temperature Probes

unitemp®

Calibration and Services

calibration • validation • training

Calibration certificate

130508T-03

certificate number

	INSTRUMENT	PROBE
Type	DT4848R0	PT100 Class A
Manufacturer	Delta	Unitemp
Bar Code Nr.	DTA44R06W7440130	PY082002
Serial Nr.	N/A	N/A

Hereby we confirm that the beside mentioned measuring system was calibrated in compliance with an accredited quality assurance system, which has been certified according to: DIN EN ISO 9001 : 2000 as an authorised calibration lab of Testo Industrial services. The measuring installations used for calibration are regularly calibrated and traceable to the national standards of the German Federal Physical Technical Institute (PTB) or other national standards exists, the measuring procedure corresponds with the technical regulations and norms valid at the time of the measurement. The documents established for this procedure are available for viewing. All the necessary measured data can be found on the following page(s) of this calibration certificate.

Location **Unitemp cc.**
47 Flamingo Crescent
Lansdowne
7780

Customer **University of Stellenbosch**

Address **Kamer 225-Processing Dep**
Chemiese Ingenieurs

Order Nr. 236033

Date of calibration 13/05/2008

Date of next calibration 13/05/2009

The instrument has been adjusted:

☐ yes ☑ no

Conformity

☑ Measured values within range of the specification[1]

☐ Measured values beyond range of the specification[1]

[1]The measurement uncertainty was calculated according to the regulations of GUM with the coverage factor k=2 and contains the uncertainty of the measuring system. The statement of conformity was made in the style of the DIN EN ISO 14253-1according to calibration instruction(**QAJI number**).

This calibration certificate may not be reproduced other than in full except the permission of the issuing laboratory.
Calibration certificates without signature and seal are not valid.

Person Responsible: Charnay Maart

page 1 of 2

CALIBRATION LABORATORY unitemp 13 MAY 2008 CAPE TOWN

Gauteng Tel: ++27-11-392-5989 www.unitemp.com
Cape Tel: ++27-21-762-8995 sales@unitemp.com

unitemp®

Calibration and Services

calibration · validation · training

Calibration certificate

130508T-03
certificate number

Measuring equipment.

Description	DKD Nr.	EQ. No
Testo 400 with probe	T16539/08-01	10288564

Ambient conditions.

Temperature: 20.5 °C
Humidity: 68.7 %RH

Measuring procedure.

Measured in a circulated liquid bath.

Measuring results.

Indication reference	Indication Measuring instrument	Deviation	Allowed tolerance	Total uncertainty of measuring	Confirmation	Measuring EQ-no.
in °C	in °C	in °C	in °C	in °C		
-20.28	-20.20	0.08	0.95	± 0.11	O.K.	10288564
99.94	98.40	-1.54	2.75	± 0.11	O.K.	10288564

Special remarks:

The measuring result is an indication of an average of three readings taken at intervals of 1 minute each. This certificate is only valid for the calibrated instrument.

CALIBRATION LABORATORY unitemp 13 MAY 2008 CAPE TOWN

page 2 of 2

Gauteng Tel: ++27-11-392-5989 www.unitemp.com
Cape Tel: ++27-21-762-8995 sales@unitemp.com

A3.4 Calibration Certificate for the Mass Flow Controller

bürkert
Fluid Control Systems

Bürkert Fluid Control Systems
Bürkert Werke GmbH & Co. KG
Christian-Bürkert-Strasse 13 - 17
D-74653 Ingelfingen
Info-Center: +49 79 40/10-111
info@de.buerkert.com
www.buerkert.com

Calibration Protocol
Mass Flow Controller Type 8626

Device Ident No.:	00185213
Nominal Flow Rate:	51.00 kg/h Air
Input Signal:	4...20 mA
Output Signal:	4...20 mA
Serial No.:	001000
Software Revision:	A.00.79
Calibration Standard:	Mass Flow Meter 8006 ID153913, SN010077
Calibration Gas:	Air
Inlet Pressure:	2.00 bar (g) referred to operating gas
Leak-Tight Pressure:	> 5.80 bar (g)
Temperature:	21.6 °C
Installation Position:	horizontal, upright

Calibration Data:

Setpoint [%]	Flow Rate [kg/h]	Deviation [% F.S.]	Allowed Dev. [% F.S.]
0.00	0.000	0.00	0.30
25.00	12.980	-0.45	0.68
50.00	25.531	-0.06	1.05
75.00	38.240	0.02	1.43
100.00	51.454	-0.89	1.80

Calibration Date: 04.10.2007 *Calibrator:* Sidered

These data refer to the time and conditions of calibration.
Reference conditions (Nl/min): 273.15 K, 1013.25 mbar (a).

Appendix 4. Experimental Results for the Mass Transfer Coefficient Determination on Structured Packing

A4.1 Experimental Results for the Naphthalene/Air System (Atmospheric pressure)

Table A4.1: *Experimental results for the naphthalene/air system at atmospheric pressure*

System temperature	Atmospheric pressure	Mass loss	Duration	ε	$u_{G,s}$	$u_{G,e}$	$Re_{G,e}$	Sc_G	k_G
^oC	Pa	g	s	-	m/s	m/s	-	-	m/s
54.6	99800	5.54	600	0.795	4.35	7.73	4542	1.90	0.0472
41.5	99900	4	1200	0.768	4.17	7.67	4855	1.94	0.0461
41.7	99900	3.43	1200	0.747	3.34	6.32	3993	1.94	0.0412
26.2	99900	3.85	4380	0.766	3.97	7.32	5058	2.00	0.0474
26.1	99900	3.32	3840	0.786	3.96	7.14	4934	2.00	0.0471
26.3	99900	3.09	3960	0.772	3.17	5.81	4015	2.00	0.0420
26.8	99900	2.96	4500	0.781	2.38	4.32	2973	2.00	0.0339
26.9	99900	2.7	5400	0.777	1.59	2.89	1992	2.00	0.0258
26.7	99900	2.39	7200	0.760	0.79	1.48	1018	2.00	0.0180
41.1	99900	3.53	1500	0.767	2.50	4.60	2919	1.94	0.0341
41.2	99900	4.14	2280	0.748	1.67	3.15	1996	1.94	0.0264
41.7	99900	4.31	3600	0.754	0.83	1.56	988	1.94	0.0170
55.1	99900	5.38	600	0.785	3.48	6.27	3678	1.90	0.0421
54.7	99900	4.31	600	0.773	2.61	4.77	2803	1.90	0.0350
55.4	99900	5.03	840	0.763	1.74	3.23	1890	1.90	0.0280
55.1	99900	4.76	1320	0.772	0.87	1.59	935	1.90	0.0176
41.2	99500	3.58	1270	0.864	4.14	6.78	4278	1.95	0.0428
41.2	99500	3.35	1163	0.864	4.14	6.78	4278	1.95	0.0438
31.8	99800	2.97	2723	0.864	3.23	5.30	3539	1.98	0.0377
31.6	99800	3.2	2453	0.844	4.04	6.77	4528	1.98	0.0458
31.6	99800	2.45	3058	0.854	2.02	3.35	2238	1.98	0.0285
31.5	99800	2.34	4243	0.864	1.21	1.98	1328	1.98	0.0200
18.0	100300	1.14	3000	0.883	3.80	6.09	4437	2.03	0.0432
15.0	100300	1.15	90000	0.883	0.05	0.07	54	2.05	0.0024
26.3	100300	1.6	3600	0.883	1.50	2.40	1667	1.99	0.0231
26.3	100300	1.57	3600	0.883	1.50	2.40	1667	1.99	0.0226
26.3	100300	1.65	3600	0.883	1.50	2.40	1667	1.99	0.0239

A4.2 Experimental Results for the Naphthalene/Air System (System pressure above atmospheric pressure)

Table A4.2: *Experimental results for the naphthalene/air system for a system pressure of above atmospheric pressure*

System temperature	Atmospheric pressure	Mass loss	Duration	ε	$u_{G,s}$	$u_{G,e}$	$Re_{G,e}$	Sc_G	k_G
^oC	Pa	g	s	-	m/s	m/s	-	-	m/s
12.0	160000	1.07	25200	0.864	0.47	0.77	931	2.08	0.0093
12.0	160000	1.27	25200	0.864	0.61	1.00	1211	2.08	0.0109
12.0	160000	1.55	25200	0.864	0.83	1.35	1630	2.08	0.0132
12.0	160000	1.79	25200	0.864	1.01	1.66	2002	2.08	0.0152
12.0	160000	1.95	25200	0.864	1.18	1.93	2328	2.08	0.0165
12.0	160000	2.3	25200	0.864	1.53	2.51	3027	2.08	0.0193
15.0	160000	1.49	25200	0.864	0.48	0.78	924	2.06	0.0095
15.0	160000	1.69	25200	0.864	0.64	1.05	1247	2.06	0.0106
15.0	160000	2.02	25200	0.864	0.83	1.37	1617	2.06	0.0126
15.0	160000	2.37	25200	0.864	1.02	1.68	1986	2.06	0.0147
15.0	160000	2.6	25200	0.864	1.19	1.95	2310	2.06	0.0161
15.0	160000	3.16	25200	0.864	1.55	2.54	3003	2.06	0.0194
18.0	160000	2.02	25200	0.864	0.48	0.79	917	2.04	0.0095
18.0	160000	2.32	25200	0.864	0.65	1.06	1238	2.04	0.0107
18.0	160000	2.79	25200	0.864	0.84	1.38	1604	2.04	0.0128
18.0	160000	3.24	25200	0.864	1.04	1.70	1971	2.04	0.0148
18.0	160000	3.69	25200	0.864	1.20	1.97	2292	2.04	0.0169
18.0	160000	4.33	25200	0.864	1.57	2.56	2979	2.04	0.0197
30.0	160000	2.63	10800	0.864	0.50	0.82	889	1.98	0.0091
30.0	160000	3.33	10800	0.864	0.75	1.23	1333	1.98	0.0114
30.0	160000	3.72	10800	0.864	0.88	1.44	1555	1.98	0.0126
30.0	160000	4.42	10800	0.864	1.08	1.77	1911	1.98	0.0150
30.0	160000	4.03	9000	0.864	1.25	2.05	2222	1.98	0.0163
30.0	160000	3.79	7200	0.864	1.63	2.67	2889	1.98	0.0191

A4.3 Experimental Results for the Naphthalene/CO_2 System (Atmospheric pressure)

Table A4.3: *Experimental results for the naphthalene/CO_2 system at atmospheric pressure*

System temperature	Atmospheric pressure	Mass loss	Duration	ε	$u_{G,s}$	$u_{G,e}$	$Re_{G,e}$	Sc_G	k_G
°C	Pa	g	s	-	m/s	m/s	-	-	m/s
45	99200	0.86	1500	0.795	0.21	0.38	437	1.40	0.0062
45	99200	1.60	1200	0.805	0.64	1.12	1294	1.40	0.0139
45	100000	0.50	1800	0.825	0.26	0.45	527	1.39	0.0076
45	100000	0.83	1800	0.805	0.53	0.92	1079	1.39	0.0123
45	100000	0.70	1200	0.805	0.79	1.38	1618	1.39	0.0152
45	100000	0.88	1200	0.805	1.05	1.84	2157	1.39	0.0190
45	100000	1.00	1200	0.805	1.31	2.31	2696	1.39	0.0214
45	100000	1.20	1200	0.805	1.58	2.77	3236	1.39	0.0257
45	100000	0.84	2400	0.805	0.39	0.69	809	1.39	0.0093
45	100000	0.60	1800	0.805	0.39	0.69	809	1.39	0.0088
45	100000	0.57	1800	0.805	0.39	0.69	809	1.39	0.0083
45	100000	0.76	1800	0.805	0.53	0.92	1079	1.39	0.0111
45	100000	0.85	1500	0.805	0.66	1.15	1348	1.39	0.0151
45	100000	0.77	1500	0.805	0.66	1.15	1348	1.39	0.0135
45	100000	0.75	1200	0.805	0.79	1.38	1618	1.39	0.0164
45	100000	0.83	1200	0.805	0.92	1.61	1887	1.39	0.0181
45	100000	0.79	1200	0.805	0.92	1.61	1887	1.39	0.0171
45	100000	0.91	1200	0.805	1.05	1.84	2157	1.39	0.0197
45	100000	0.94	1200	0.805	1.18	2.08	2427	1.39	0.0202
50	100400	2.04	1200	0.805	1.48	2.60	2971	1.39	0.0236
45	100400	1.44	1200	0.805	1.46	2.56	3010	1.38	0.0251
45	100400	1.49	1500	0.805	1.17	2.05	2408	1.38	0.0208
45	100400	1.58	1500	0.805	1.34	2.35	2759	1.38	0.0219
45	100400	1.41	1200	0.805	1.56	2.73	3210	1.38	0.0243
50	100300	1.74	1800	0.805	0.74	1.30	1485	1.39	0.0136
40	100300	0.99	1200	0.805	1.68	2.95	3558	1.38	0.0259

A4.4 Experimental Results for the Naphthalene/Helium System (Atmospheric pressure)

Table A4.4: *Experimental results for the naphthalene/helium system at atmospheric pressure*

System temperature	Atmospheric pressure	Mass loss	Duration	ε	$u_{G,s}$	$u_{G,e}$	$Re_{G,e}$	Sc_G	k_G
°C	Pa	g	s	-	m/s	m/s	-	-	m/s
15.4	100000	0.29	3600	0.795	0.296	0.527	49.79	4.32	0.0142
15.2	100000	0.37	4800	0.805	0.296	0.520	49.21	4.32	0.0138
16.0	100000	0.35	5400	0.805	0.223	0.391	36.84	4.32	0.0108
15.8	100700	0.45	5520	0.805	0.227	0.399	37.84	4.29	0.0118
15.8	100700	0.54	7620	0.805	0.182	0.319	30.27	4.29	0.0103

A4.5 Sample Calculations

The following sample calculations relates to the first experimental run depicted in Table A4.1.

Packing specific dimensions:

- corrugation base (B) = 17.4 mm
- the corrugation side (S) = 11.2 mm
- the crimp height (h) = 7.05 mm
- Corrugation angle (θ) = 45 ^{o}

Gas properties relating to this experimental run:

- Density of air (ρ_G) = 1.061 kg/m^3
- Viscosity of air (μ_G) = 1.977 x 10^{-5} N.s/m^2
- Vapour pressure of naphthalene (p_{Naph}) = 152.6 Pa

Experimental readings:

- System pressure = 99 800 Pa
- System temperature = 54.6 ^{o}C
- Naphthalene mass loss = 5.54 g
- Experimental duration = 600 s
- $y_{A,i} = 1.53\times10^{-3}$ (-)
- $y_{A,b} = 1.46\times10^{-4}$ (-)
- $c_T = 36.6$ mol/m^3
- $A_C = 2.86\times10^{-2}$ m^2

Calculation of the hydraulic diameter (d_h):

The hydraulic diameter is calculated through equation 3.23:

$$d_h = \frac{Bh}{S} \tag{3.23}$$
$$= \frac{17.4 \times 7.05}{11.2}$$
$$= 10.95 \text{ mm}$$
$$= 0.01095 \text{ m}$$

Calculation of the effective gas velocity ($u_{G,e}$):

The effective gas velocity is calculated through equation 3.22:

$$u_{G,e} = \frac{u_{G,s}}{\varepsilon \sin\theta} \tag{3.22}$$
$$= \frac{4.35}{0.795 \times \sin 45}$$
$$= 7.73 \text{ m/s}$$

Calculation of the effective Reynolds number ($\mathrm{Re}_{G,e}$):

The effective Reynolds number is calculated through equation 3.21:

$$\mathrm{Re}_{G,e} = \frac{\rho_G u_{G,e} d_h}{\mu_G} \tag{3.21}$$
$$= \frac{1.061 \times 7.73 \times 0.01095}{1.977 \times 10^{-5}}$$
$$= 4541$$

Calculation of the mass transfer rate of the sublimating specie (n_A):

$$n_A = \frac{\left(naphthalene\ mass\ loss \big/ naphthalene\ molar\ mass \right)}{\exp erimental\ duration}$$

$$= \frac{\left(5.54 \big/ 128.16 \right)}{600}$$

$$= 7.205 \times 10^{-5}\ \text{mol/s}$$

Calculation of the logarithmic mean driving force ($\Delta y_{A,Lm}$):

The logarithmic mean driving force is calculated through equation 3.19 ($y_{A,b}$ at $h = 0$ is assumed to be equal to zero):

$$\Delta y_{A,Lm} = \frac{\left(y_{A,i} - y_{A,b} \right)_h - \left(y_{A,i} - y_{A,b} \right)_0}{\ln\left(\dfrac{\left(y_{A,i} - y_{A,b} \right)_h}{\left(y_{A,i} - y_{A,b} \right)_0} \right)} \tag{3.19}$$

$$= \frac{1.46 \times 10^{-4}}{\ln\left(\dfrac{1.53 \times 10^{-3} - 1.46 \times 10^{-4}}{1.53 \times 10^{-3}} \right)}$$

$$= 1.45 \times 10^{-3}$$

Calculation of the vapour phase mass transfer coefficient (k_G):

The mass transfer coefficient is calculated through equation 3.20:

$$k_G = \frac{n_A}{c_T A_C \Delta y_A} \tag{3.20}$$

$$= \frac{7.205 \times 10^{-5}}{(36.6) \times \left(2.86 \times 10^{-2} \right) \times \left(1.45 \times 10^{-3} \right)}$$

$$= 0.0472\ \text{m/s}$$

Nomenclature

Symbol	Description	Units
	Roman	
A_C	Specific area of coated packing	m^2
a	Area	m^2
B	Corrugation base	m
C_G	Packing specific constant	-
C	Sutherland constant	-
c	Concentration	mol/m^3
D	Diffusion coefficient	cm^2/s
d	Diameter	m
F_t	Liquid holdup correction factor	-
f	Fraction of liquid filled channels	-
f_C	Incipient percolation threshold	-
g	Gravitational acceleration	m/s^2
HETP	Height equivalent to a theoretical plate	m
HTU	Height of a transfer unit	m
h	Packing crimp height	m
h_L	Fractional liquid holdup	-
J	Molar Flux	$mol/s.m^2$
k	Mass transfer coefficient	m/s
l	Packing characteristic length	m
M	Molar mass	g/mol
m	Mass	g
N	Convective flux	$mol/s.m^2$
n	Mass transfer rate	mol/s
P	Pressure	Pa
p	Vapour pressure	Pa
Re	Reynolds number	-

R	Ideal gas constant	J/mol.K
Sh	Sherwood number	-
Sc	Schmidt number	-
S	Corrugation side	m
T	Temperature	K
t	Duration	s
u	Velocity	m/s
V	Molar volume	m^3/mol
v	Special atomic diffusion volume	m^3/mol
W	Width	m
x	Mol fraction	-
y	Mol fraction	-
z	Length	m

Greek

α	Angle between packing and horizontal axis	^{o}
ε	Void fraction	-
λ	Stripping factor	-
θ	Corrugation angle	^{o}
ξ	Friction factor	-
Ω	Empirical collision integral	-
μ	Viscosity	Pa.s
ρ	Density	kg/m^3

Subscripts

A, B	Components A and B
e	Effective
exp	Experimental
G	Gas phase
h	Hydraulic
L	Liquid phase
Lm	Log mean
lam	Laminar

s	Superficial
T	Total
turb	Turbulent

List of Relevant Correlations from Literature

Reference	Correlation
	Chapter 2
Arnold [35]	$D_{AB} = \dfrac{0.00837\sqrt{\dfrac{1}{M_A}+\dfrac{1}{M_B}}}{\left(V_A^{1/3}+V_B^{1/3}\right)^2}.\left(\dfrac{T^{5/2}}{T+C}\right)$
Chapman-Enskog [37]	$D_{AB} = \dfrac{1.8583\times10^{-7}T^{3/2}}{P\sigma^2\Omega}\left(\dfrac{1}{M_A}+\dfrac{1}{M_B}\right)^{\frac{1}{2}}$
Chen *et al.* [22]	$D_{AB} = 1.495\times10^{-6}T^{1.888}$
Cho *et al.* [27]	$D_{AB} = 8.1771\times10^{-7}T^{1.983}$
Fuller *et al.* [36]	$D_{AB} = \dfrac{1.00\times10^{-3}.T^{1.75}\left(1/M_A + 1/M_B\right)^{1/2}}{P\left[\left(\sum_A v_i\right)^{1/3}+\left(\sum_B v_i\right)^{1/3}\right]^2}$
Gustafson *et al.* [15]	$D_{AB} = \dfrac{\left(0.186\times10^{0.00283T}\right)}{V^{0.213}}$
	Chapter 3
Bravo *et al.* [7]	$Sh_G = 0.0338\left(\dfrac{u_{G,e}\rho_G d_{eq}}{\mu_G}\right)^{0.8} Sc_G^{0.333}$
Rocha *et al.* [9]	$Sh_G = 0.054\left(\dfrac{\left(u_{G,e}+u_{L,e}\right)\rho_G S}{\mu_G}\right)^{0.8} Sc_G^{0.33}$
Olujic *et al.* [58, 66-68]	$k_G = \sqrt{\left(\dfrac{Sh_{G,lam}D_G}{d_{hG}}\right)^2+\left(\dfrac{Sh_{G,turb}D_G}{d_{hG}}\right)^2}$
Erasmus [3]	$Sh_G = 0.2641\,\mathrm{Re}_{G,e}^{0.62}\,Sc_G^{0.5}$